



室蘭工業大学

学術資源アーカイブ

Muroran Institute of Technology Academic Resources Archive



核融合炉用W-SiC/SiCハイブリッド材料の耐熱流束特性の研究

メタデータ	言語: eng 出版者: 公開日: 2013-11-15 キーワード (Ja): キーワード (En): 作成者: ワリード, アルサイド モレス モハメッド アブダラ メールアドレス: 所属:
URL	https://doi.org/10.15118/00005105

"High Heat Flux Durability of W-SiC/SiC Hybrid Component for the Nuclear Fusion Applications"

By

Waleed Alsayed Mohrez Mohammad Abdalla

A dissertation submitted for the degree of Doctor of Philosophy at the Division of Chemical and Materials Engineering.

At

Muroran Institute of Technology



室蘭工業大学

Muroran Institute of Technology

September 2013

Dedicated to My Parents, Wife and My Children

Contents

PREFACE.....	i
Acknowledgements	ii
Abstract.....	iii
List of Abbreviation and Nomenclature	v
Chapter-1-Introduction	1
Chapter-2- <u>Fusion power and Materials - literature survey</u>	4
2.1 Plasma and fusion energy	6
2.1.1 Fusion reaction and fusion power.....	8
2.2-Fusion Materials.....	12
2-2-1–low activation Ferritics:	12
2-2-2-mechanical behavior of ferritic steels:	13
2-2-3 Current and future concerns of ferritic steels.....	16
2-2-4- Tungsten alloy	18
2-2-5-SiC _f /SiC	21
2-2-5-1 manufacturing history and trade marks of SiC _f /SiC.....	21
2-2-5-2 Development of SiC _f /SiC composites	23
2-3-High heat flux components (HHFC _s) of fusion reactors.....	25
2-3-1 ITER plasma facing materials and operating conditions.....	26
2-3-2- Design aspects of divertor in ITER.	29
References	32
Chapter- 3- Experimental work and achievements	38
3-1-Introduction.....	39
3-2-Experimental work and methodology	39
3-3-Fabrication of tile (NITE-W/SiC-S2)	40
3-4-Microstructure investigation of the tile (NITE-W/SiC-S2)	45
3-5-Fabrication of tile (NITE-W/SiC-Dh1).....	47
3-6-Microstructure investigation of the tile (NITE-W/SiC-Dh1).....	50
3-7-Fabrication of tile (NITE-W/SiC-Dv1).....	52

3-8-Microstructure investigation of the tile (NITE-W/SiC-Dv1).....	55
3-9-Results and Discussion	57
3.10-Conclusion.....	58
References.	59
Chapter-4- Divertor Plasma Exposure Test of W-SiC/SiC dual layer tiles Inside the Large Helical Device (LHD)	60
4-1-Overview of the Large Helical Device (LHD).....	62
4-2-Experimental work.....	66
4-2-1-Preparation of W-SiC/SiC dual layer tiles for plasma exposure in LHD.....	67
4-2-2-Tiles mounting inside LHD.....	68
4-3- Results.....	70
4-3-1-Conditions of the Plasma Exposure.....	70
4-3-2-Cooling conditions during plasma exposure.....	74
4-3-3-Pick up the irradiated tiles outside the LHD.....	74
4-4-Discussion.....	75
4-5-Conclusion.....	75
References.....	76
Chapter-5-Damage Analysis of Plasma Exposed W-SiC/SiC tiles By Means of Ultra Sonic Testing Method	77
5-1-Overview and background of ultra sonic testing.....	78
5-2-Sound wave propagation in materials.....	80
5-3-Wavelength and Defect Detection.....	81
5-4-Introduction :.....	82
5-5-Experimental work and achievements.....	82
5-6-Scanning conditions and sensitivity calibration:.....	84
5-7-Results and discussion.....	85
5-7-1-C-scanning of the tile (NITE-W/SiC-S2).....	87
5-7-2-C-scanning of the tile (NITE-W/SiC-Dh1).....	88
5-7-3-C-scanning of the tile (NITE-W/SiC-Dv1).....	89
5-7-4-The temperature distribution on the tiles surface.....	90
5-7-5-A&B-Scan of the irradiated tiles.....	90

5-8-Conclusion	94
References	95
Chapter-6-Macro and Microstructure evolution of W-SiC/SiC tiles after Divertor Plasma Exposure.....	96
6-1-Introduction	97
6-2- Results	97
6-3-Diffusion behavior analysis by Electron probe Micro-analyzer (EPMA).....	115
6-4-Deducing the surface and implanted temperature of the W-SiC/SiC irradiated tiles.....	119
6-4-1-Deducing the implanted temperature by: the comparison between the grain size distributions.....	120
6-4-2-Deducing the implanted temperature; utilizing the damage analysis by ultrasonic method.....	123
6-4-3-Deducing the implanted temperature by: tracking the diffusion of silicon in the interphase layer.....	124
6-4-4-Deducing the distribution of the temperature by: finite element method.....	125
6-4-4-1-Building and loading of the model.....	126
6-5-Discussion.....	129
6-6-Conclusion.....	131
References	132
Chapter-7-Future Work and promising achievements.....	133
7-1-Introduction	134
7-2-First wall exposure test inside LHD	134
7-2-1-Future investigation of plasma surface interaction.....	137
7-3-Tungsten monoblock with actively cooled SiC/SiC tube.	138
7-3-1 Challenges of fabrication technology for actively cooled mockup.	139
References.....	139
Chapter-8-Summary.....	140
List of Publications and Scientific Conferences.....	143

PREFACE

This dissertation was submitted for fulfilling the requirements of the degree of Doctor of Philosophy (PhD) in Engineering, at the division of chemical and materials engineering at Muroran Institute of Technology. It contains research carried out at the division of chemical and Materials Engineering, and collaboration with the national institute of Fusion Sciences. The research activities were commenced in October 2010, under the supervision of Professor Yutaka Kohno and Professor Akira Kohyama. Except where appropriately referenced, this work is entirely original.

Waleed Alsayed Mohrez

September 2013

Acknowledgements

First of all, I would like to thank, Professor AKIRA KOHAYAM, for welcoming me in his group for three years, and for providing me the opportunity to pursue with a PhD and his inspiration to my future research activity. I am grateful to Professor YUTAKA KONO, for his fruitful supporting, and I would like to express my deep thanks to professor KISHIMOTO for his valuable discussions and his technical support at his laboratory. Also deep thanks to all the members of FEEMA project at Muroran institute of technology for their continuous support during my research for three years, special thanks to Nagano san for her kindness.

Special thanks to the Egyptian ministry of the high education and scientific research for their financial support which had been presenting to me for two years, and great appreciation to the Egyptian cultural bureau of the Egyptian embassy in Tokyo for their professional and fruitful administrative support via their contacts and continuous follow-up of my research activity .

I would like to present my deep appreciation and special thanks to all the team of international center of Muroran institute of technology for their support and mitigation the difficulties, during my stay in Japan, special thanks to Naito san and Myshata san.

Also I would like to present my grateful to the national institute of fusion science, for their scientific guides and to their effective collaboration during my experimental work inside the large helical device, special thanks to professor Masuzaki for his guide and active support.

Abstract

Fusion power plants are a potential replacement for fission power and a promising clean source of energy for the near future, but the design of a commercial fusion reactor represents a great scientific, technical and industrial challenge. Levels of irradiation reached in plasma-facing materials (PFM) designed to absorb heat and provide neutron shielding will be a lot more intense than those reached during fission. Materials directly exposed to radiation will therefore be expected to undergo dramatic modifications of their mechanical properties, in addition to becoming radioactive through transmutation. Because the replacement of irradiated components would be expensive and time consuming, the ideal material should be able to meet the design life of 20 years under severe operating conditions.

W/SiC/SiC Hybrid component tile has many advantages as a high heat flux component (HHFC) material for fusion, in theory. However, due to insufficient data known, it's high potentiality and near term availability has not been well recognized. This work provides the recent materials R & D status and the first plasma exposure test result from the world largest helical device, Large Helical Device of National Institute for Fusion Science, Japan. Tungsten armor with SiC/SiC substrate layer survived during the LHD plasma exposure with 10 MW/m^2 maximum heat load for the 6 second operation cycle.

After divertor plasma exposure test inside the LHD; visual and non destructive tests were conducted to evaluate the damage of the exposed tiles inside LHD, where both tests provided precise damage analysis and evaluate qualitative measurement of the degradation occurred on the surface of tungsten and at the interface.

The macro and microstructure evolution, including crack and pore formation, was analyzed and an excellent high heat load resistance is demonstrated. EPMA analysis was conducted to investigate the behavior of diffusion of elements in the region of interface between W and SiC/SiC.

Deducing of the implanted temperature to the interface region of the irradiated tiles was conducted by Four techniques, utilizing the microstructure evolution and Finite elements

method, where the investigated and deduced data provided an evidence of the implanted temperature during the divertor plasma exposure test, these data was reliable to determine the heat flux durability of the W-SiC/SiC hybrid component as future structure materials for divertor in the future.

this study also previewed suggestions and promising achievements, for future work, where five tiles were fabricated and exposed to a long time of exposure inside the first wall of LHD, to investigate in the near future the effect of plasma contamination to the surface of the exposed tiles, where the purpose of the future study will investigate the effect of hydrogen absorption into the surface of hybrid component of W-SiC/SiC. Also the fabrication of tungsten monoblock with actively cooled SiC/SiC tube was fabricated to investigate in the future the effect of larger heat flux durability up to 30 Mw/m^2 of tungsten monoblock, with a simultaneous cooling system, but the fabrication faced a difficulty related to the poor bonding between tungsten and SiC/SiC actively cooled tube, where the modification of hot isostatic press technology is being processes to make direct solid state diffusion bonding between tungsten and SiC/SiC tube.

List of Abbreviation and Nomenclature

C

- **CFC:** Carbon Fibers reinforcement Carbon Matrix.
- **CVD:** Chemical Vapor Deposition.
- **CVI:** Chemical Vapor Infiltration.

D

- **DBTT:** Ductile –Brittle Transfer Temperature.
- **D-D:** Deuterium-Deuterium Fuel Cycle.
- **DEMO:** The Demonstration Reactor.
- **DOE:** Department of Energy of USA.
- **dpa:** Displacement –Per Atom .
- **D-T:** Deuterium-Tritium Fuel Cycle.

E

- **ELM:** Edge Localized Mode.
- **EPMA:** Electron Probe Micro Analyzer.
- **EUROFER:** European Ferritic.

F

- **FFTF:** Fast Flux Test Facility.

G

- **GDOES:** Glow Discharge optical Emission Spectroscopy
- **GFR:** Gas Cooled Fast Reactors.

H

- **HEMJ:** Helium Cooled Modular Divertor with Multiple Jets cooling.
- **HFIR:** High Flux Isotope Reactor.

V

- **HHFCs:** High Heat Flux Components.

I

- **IFMIF:** International Fusion Materials Irradiation Facility.
- **ITER:** International Thermo Experimental Reactor.

J

- **JLF:** Japan Low Ferritic.

L

- **LAFM:** Low Active/Martensitic Steels.
- **LAMs:** Low Active Materials.
- **LPS:** Liquid Phase Sintering.

M

- **MeV:** Milli Electron Volt.
- **MOTA:** Material Open Test Assembly.
- **Mw/m²:** Mega Watt per Meter Square.

N

- **NFA:** Nano structured Ferritic Alloy.
- **NITE:** Nano Infiltration and Transient Eutectic Phase.

O

- **ODS:** Oxidized Dispersion Strength Ferritic Steel.
- **ORNL:** Oak Ridge National Laboratories.

P

- **PFC:** Plasma Facing Component.

- **PFM:** Plasma Facing Materials.
- **PFM:** Plasma Facing Materials.
- **PIP:** Polymer Infiltration and pyrolysis.
- **PSIs:** Plasma Surface Interactions.

R

- **RS/MI:** Reaction Sintering/Melting Infiltration.

T

- **T-He:** Tritium-Helium Fuel Cycle.

U

- **UCSP:** University of California, Santa Barbra.

V

- **VDE:** Vertical Displacement Event.
- **VHR:** Very High Temperature Reactor.
- **VT:** Vertical Target.

Chapter-1

Introduction

1-Introduction

The objectives of the presented dissertation is to investigate the high heat flux durability of the hybrid W-SiC/SiC component, after the divertor plasma exposure test inside the largest helical device in the world, (LHD).

The experimental work included; the fabrication of the hybrid tiles of W-SiC/SiC, where three tiles were fabricated successfully, by three different fabrication methods and starting materials, utilizing NITE process.

Two tiles were fabricated by solid state diffusion bonding, where one tile used horizontal rolled tungsten plate and SiC/SiC composite, with ID (NITE-W/SiC-Dh1), the second tile was fabricated by vertical rolled tungsten plate and SiC/SiC composite, with ID (NITE-W/SiC-Dv1), the third tile was fabricated by liquid sintering of tungsten powder and pliable preform of SiC/SiC, with ID (NITE-W/SiC-S2). Hot press technology was used for fabrication, where both tiles (NITE-W/SiC-Dh1)&(NITE-W/SiC-Dv1) were fabricated under pressure up to 16 Mpa and temperature up to 1600 °C at argon atmosphere, where the tile (NITE-W/SiC-S2) was fabricated under pressure up to 20MPa and temperature up to 1800 °C at argon atmosphere.

The main purpose to use different tungsten materials; powder, vertical and horizontal rolled plates, could be argued due to the different thermal conductivity of each tungsten armor, where it had been investigated that the different oriented grains of tungsten has anisotropic thermal conductivity, thus the heat flux durability of each tile will be versatile due to these anisotropic thermal conductivities.

Macro and micro structure analysis of the tiles fabricated was conducted; by optical microscope and SEM, where analyses showed coherent structure of SiC fibers and SiC matrix, showed also sufficient bonding between W and SiC/SiC along each tile fabricated.

After fabrication and analysis of each fabricated tiles; the three tiles were prepared for the high heat flux test inside the large helical device at national institute of fusion science, where each tile was cut and polished to appropriate size of the sample holder and manipulator of the experiment conditions, where three tiles arranged and mounted inside the helical divertor, where plasma exposure time was up to 5.6 second and the heat flux

load was tentatively calculated to be 10 Mw/m^2 . Investigation of the irradiated tiles after divertor plasma exposure.

This study included the analysis of the irradiated tiles by macro and microstructure, where the analysis evaluated the condition and the degradation of tungsten surface, as well as the diffusion bonding layer at the interface region, also SiC/SiC region were investigated and evaluated, where crack and fiber/matrix interfacial debonding, beside fiber pull out were detected.

Also EPMA study was conducted to investigate the behavior of diffusion through the interface after plasma exposure. Non destructive test by means of ultra sonic was conducted to investigate the condition of the irradiated tiles along the whole exposed surface area.

Deducing of the implanted temperature to the interface region of the irradiated tiles was conducted by Four techniques, utilizing the microstructure evolution and Finite elements method, where the investigated and deduced data provided an evidence of the implanted temperature during the divertor plasma exposure test, these data was reliable to determine the heat flux durability of the W-SiC/SiC hybrid component as future structure materials for divertor in the future.

The study also previewed suggestions and promising achievements, for future work, where five tiles were fabricated and exposed to a long time of exposure inside the first wall of LHD, to investigate in the near future the effect of plasma contamination to the surface of the exposed tiles, where the purpose of the future study will investigate the effect of hydrogen absorption into the surface of hybrid component of W-SiC/SiC. Also the fabrication of tungsten monoblock with actively cooled SiC/SiC tube was fabricated to investigate in the future the effect of larger heat flux durability up to 30 Mw/m^2 of tungsten monoblock, with a simultaneous cooling system, but the fabrication faced a difficulty related to the poor bonding between tungsten and SiC/SiC actively cooled tube, where the modification of hot isostatic press technology is being processes to make direct solid state diffusion bonding between tungsten and SiC/SiC tube.

Chapter-2
Literature Survey of Fusion Materials and
Fusion Reactors

2- Fusion power and Materials - literature survey

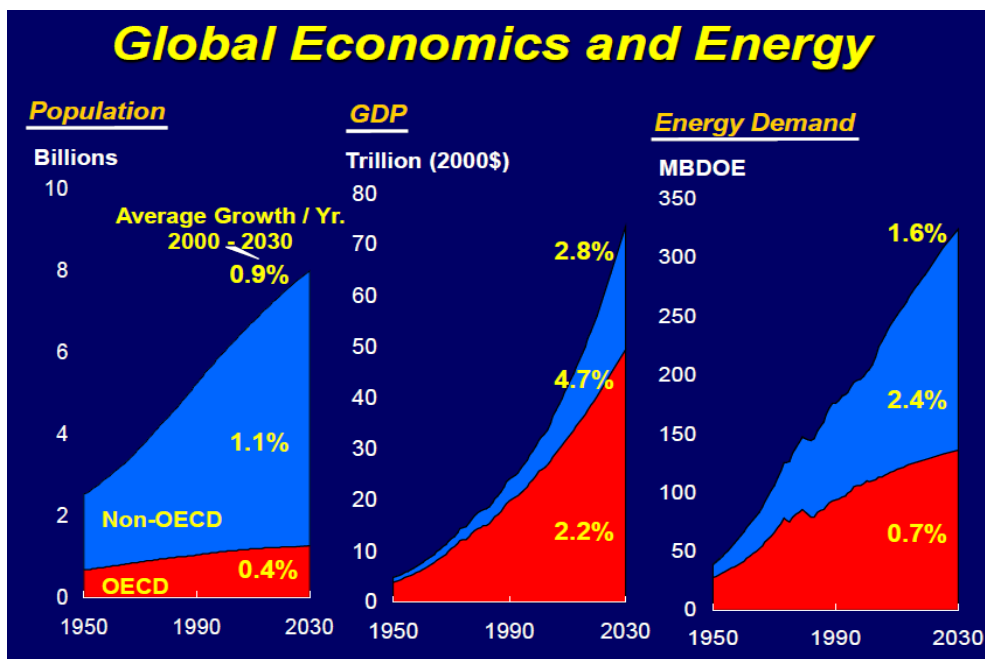
Fusion power plants are a potential replacement for fission power and a promising clean source of energy for the near future, but the design of a commercial fusion reactor represents a great scientific, technical and industrial challenge. Levels of irradiation reached in plasma-facing materials (PFM) designed to absorb heat and provide neutron shielding will be a lot more intense than those reached during fission. Materials directly exposed to radiation will therefore be expected to undergo dramatic modifications of their mechanical properties, in addition to becoming radioactive through transmutation. Because the replacement of irradiated components would be expensive and time consuming, the ideal material should be able to meet the design life of 20 years under severe operating conditions.

Several materials, such as steel, vanadium alloys and silicon carbide fibre-reinforced silicon carbide (SiCf /SiC) composites have been considered candidates and tested; so-called low-activation ferritic/martensitic steels (LAFM) developed since the 1970s, are in the most advanced stage. They are able to resist high levels of irradiation and high thermal load, and are considered the best candidates for fusion power.

Steels in fission reactors typically experience a dose of 20 displacements – per-atom (dpa) but levels of damage will be as high as 200 dpa in a fusion reactor [1]. This will cause modifications of the microstructure and production of gas via transmutation. Such severe conditions will only be achieved experimentally in three prototype facilities to be constructed in the near future: the International Fusion Materials Irradiation Facility (IFMIF), the International Thermonuclear Experimental Reactor (ITER), currently being built, and the demonstration reactor (DEMO) whose realisation will depend on results provided by the IFMIF and ITER. The time scale for these experiments is in the range 15-30 years ahead.

2.1 Plasma and fusion energy

The global economic and population demand always the development and innovation of new methods of energy supply, Nuclear power plants are nowadays a reliable source of electricity. They are all based on fission reactions and the technology is well advanced. Fusion power is expected to be a promising replacement source of energy in the future but the technology to sustain a reaction has not yet been mastered and the deployment of fusion power is not expected before 2050 [2]. The theoretical basis for a fusion reaction was originally postulated in the 1920s and the first Tokamak, a machine confining a plasma using a toroidal magnetic field, was realised in the 1950s by Kurchatov [3]. Since then, research into controlled fusion has been continuously carried out but the longest burns in experimental reactors only lasted for a couple of seconds, whereas a full-scale commercial reactor would have to sustain the plasma for much longer periods. Large scale international research programmes such as the IFMIF, ITER (Fig.2.1.) and DEMO aim at proving the scientific and technological feasibility and the economic viability of fusion energy [4].



According to Mohammad Abdou in December 2009
 Presentation at TWAS-ARO Meeting Bibliotheca Alexandria

One major concern about fusion remains the production of radioactive waste through activation of structural components and the severe life conditions of materials exposed directly to the plasma; high temperature (peak operating temperatures range from room temperature to 500-700°C), high radiation flux (the high-energy neutron wall loading is expected to be around 1 Mw/m² [5] and high displacement damage over the life of the reactor (200 dpa) [6].

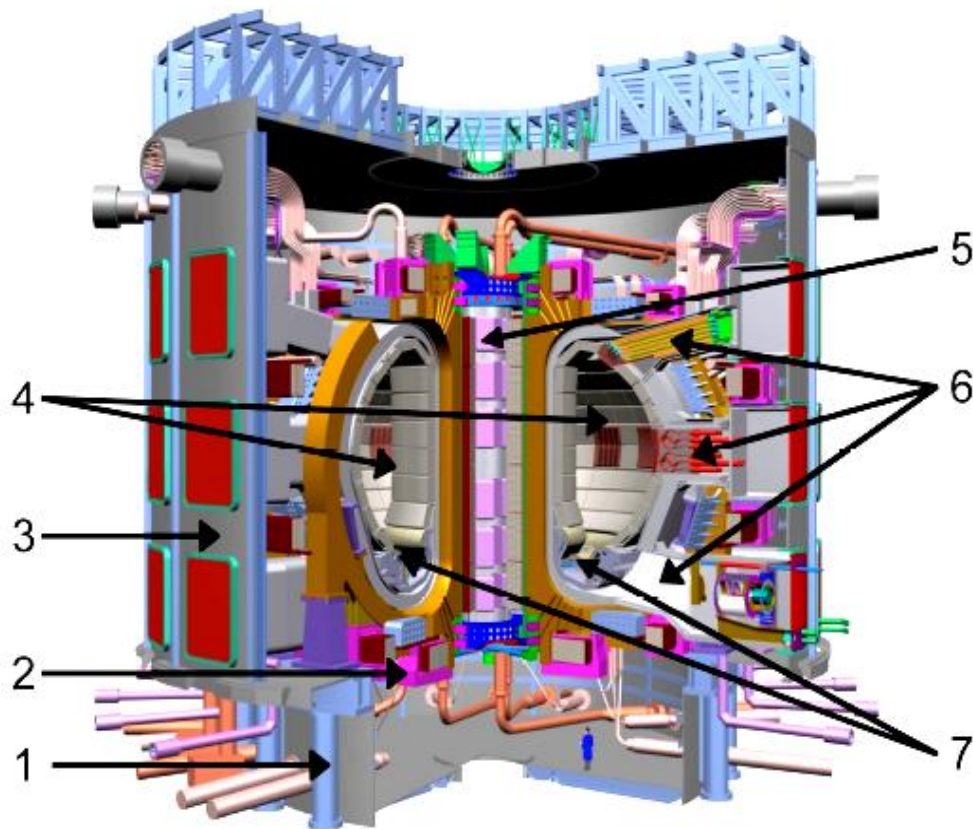


Figure 2.1: Scheme of the experimental fusion reactor ITER. 1: gravity supports; 2: cryostat; 3: bioshield; 4: Tokamak containing the plasma chamber; 5: central solenoid; 6: port plugs providing access to the plasma; 7: divertor cassettes. Blanket modules composing the plasma chamber of the Tokamak are detailed in Figure 2.3. Picture from [7].

2.1.1 Fusion reaction and fusion power

Nuclear energy is based on fission reactions, which consist of splitting heavy nuclei into smaller ones in an extremely exothermic reaction. In a fusion reaction, two small elements, usually deuterium (D), tritium (T) or helium, fuse to form a heavier atom. Amongst several possible reactions (D-D, D-T or T-He) (Fig.2.2.), that between deuterium and tritium (D-T) is the easiest one to initiate [8]. Plasma of deuterium (2H) and tritium (3H) is heated to about 100 million Kelvin. 2H and 3H fuse to form an unstable 5H which bursts into a 4He (helium ion or α particle) with 3.5 MeV of kinetic energy and a neutron (n) with a recoil energy of 14.1 MeV [9, 10](Fig.2.3.)

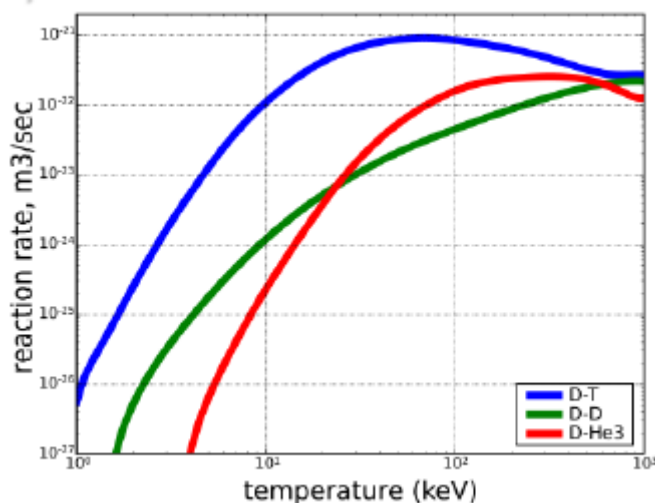


Fig.2.2 different plasma reactions, between D-T, D-D, D-He³

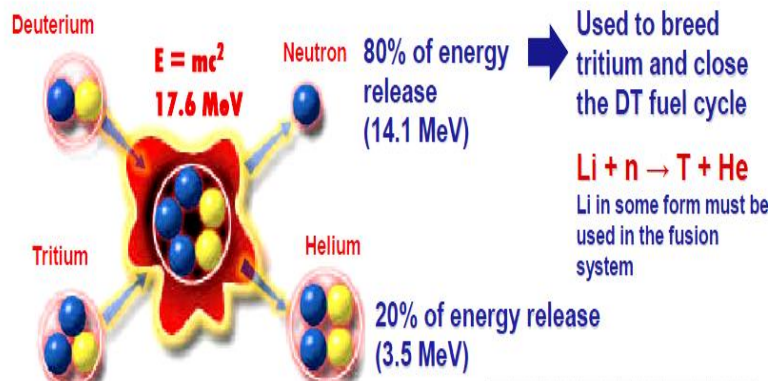


Fig.2.3.Schematic view of Deuterium and tritium reaction (Illustration from DOE brochure)

Alfa particles produced during the reaction are confined in the reactor by the magnetic field. However, neutrons are not affected and are able to escape the plasma. They move through the first wall of the vacuum chamber and, by collision, exchange energy with a coolant system (usually liquid lithium). The heat released can be used to produce steam, which generates electricity via turbines. The initial energy of neutrons created during the deuterium-tritium fusion reaction is equivalent to 14.1 MeV (large peak in Fig.2.4.) but there is also a significant flux at lower energies.

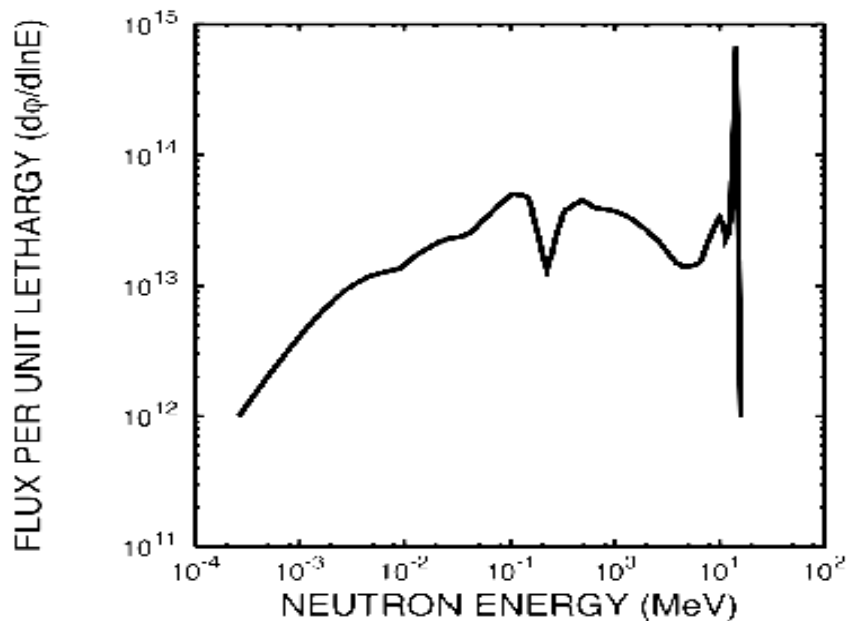


Figure 2.4.: calculated neutron energy spectrum for a fusion reactor. Graph from [11].
Calculation after [12]

The constant flux of neutrons on the first wall has three main consequences: Displacement of atoms, activation of elements and generation of gas. Neutrons directly hit atoms composing the first-wall blanket of the reactor (Fig.2.5.)[13], and produce interstitials and vacancies. The material becomes radioactive and radiation-induced gas (helium, hydrogen) is produced through transmutation. Such changes in the structure dramatically modify the mechanical properties of the material.

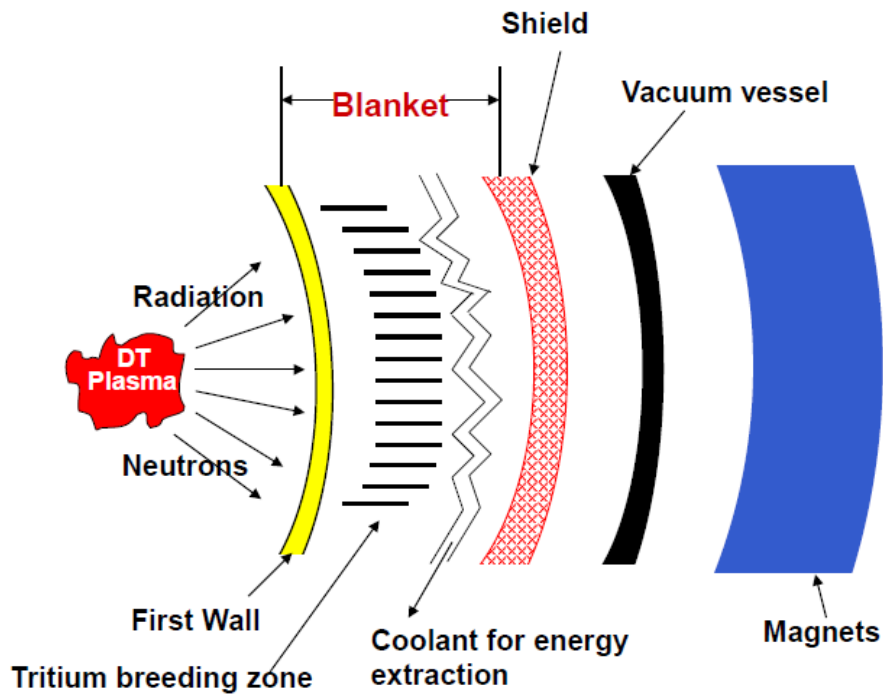


Fig.2.5: Scheme of blanket module

Many steps will be necessary to test materials and validate predictions before the first commercial fusion power plant produces electricity. For that purpose, several large-scale facilities are being built.

The IFMIF will be used for testing candidates in conditions similar to those found in a fusion reactor. It will use a source based on the deuteron-lithium stripping reaction (D-Li source) to accelerate deuterons on a liquid lithium target, producing a large flux of neutrons with an energy close to 14 MeV. The irradiation doses will be around 50 dpa per year, permitting the achievement of the expected critical dose of ≈ 200 dpa within a few years [13, 14]. The only limiting factor is the small irradiation volume (≈ 0.5 L).

In parallel with the IFMIF, ITER will be an experimental full-scale fusion reactor based on a plasma torus that should produce plasma burns for 500s and generate 400-500 MW [15]. It is being developed to prove the economic sustainability of fusion reactions as a viable energy source and will also serve as test beds for the blanket modules [16] that will be used as structural materials in DEMO.

DEMO is a larger scale prototype designed to produce electricity and demonstrate the fusion power viability [15]. It is an intermediary step between ITER and a commercial reactor, required to satisfy all the basic functions of a power plant. The size scales, energies involved, temperatures and levels of irradiation are constantly increasing with the development of new fission reactors and soon fusion reactors. Table 2.1 gives a comparison the targeted performances for ITER, DEMO and a commercial reactor.

Table 2.1: General performance goals for fusion devices (ITER, DEMO and a future commercial fusion reactor) [17-20].

Performance criteria	ITER	DEMO	Commercial Reactor
Fusion power(GW)	0.5-1	2-4	3-4
Irradiation dose(dpa)	3	30-80(5 years)	100-150(5 years)
Operation mode	Pulses	Quasi-Continuous	Continuous

2-2-Fusion Materials.

Fusion materials can be divided into two groups, structural and plasma facing materials, but one of the main design criteria of such materials is the low activity which inherent on the ability of the material to be decayed fast as possible after the nuclear exposure stop. One of the most indispensable challenges in fusion technology research and development is the development of low activation materials [21, 22]. Such low active materials including: ferritic martensitic steels [23-25], vanadium alloys [26, 27] and SiC_f/SiC materials [28, 29] are considered promising candidates.

2-2-1 –low activation Ferritics:

Efforts to develop new Fe-Cr-Mo type heat resistant steels were initiated for steam generators in the early 1970s [23]. This included attempts to replace MO with W and optimize alloy composition to improve high temperature strength, which presently is still an objective for advanced conventional power plants. In the fusion program, it was recognized that the decay of induced radioactivity produced by irradiation in a fusion environment could be accelerated by removing elements such as MO, Nb and Ni and specific impurities from the steels. This led to the concept of low activation ferritic martensitic steels with different alloys designs like F82H, JLF1, and ORNL, 9Cr-2W V Ta, Eurofer, IEA F28H, table 2-2 [30]

Table 2-2 : Typical compositions of LAFs and large IEA heat of F82H.

Element (wt %)	F82H	JLF.1	ORNL	Eurofer	IEA/F82H
Cr	8.0	9.0	8.5-9.0	8.0-9.0	7.5-8.5
C	0.1	0.1	0.1	0.10-0.12	0.08-0.12
Mn	0.5	0.45	0.45	0.4-0.6	<0.5
P	<0.02			0-0.005 max	<0.01
S	<0.01			0.005 max	<0.01
V	0.2	0.19	0.25	0.20-0.30	0.15-0.25
B	0.003			0.004-0.006	<0.001
N	< 0.01	0.05		0.02-0.04	<0.02
W	2.0	2.0	2.0	1.0-1.2	1.8-2.2
Ta	0.04	0.07	0.07	0.06-0.10	0.01-0.006
Si	0.1	< 0.1	0.2	< 0.05	<0.3
Ti	LAP	<0.015		<0.02	LAP
Fe	BAL	BAL	BAL	BAL	BAL

2-2-2-mechanical behavior of ferritic steels:

Tensile properties have been obtained on neutron irradiated F82H, JLF-1 and 9Cr-2WVTa steels, along with steels containing 2.25-12% Cr. Fig.2.6. Shows tensile results of FFTF/MOTA irradiated Japanese steel specimens for displacement damage up to 62 dpa [31]. The 7 to 9 Cr steels (JLF-1, F82H and JLF-3) showed less irradiation hardening at lower temperature, and the yield strength was fairly stable to 550°C and 62 dpa. In contrast, the 2.25Cr (JLF-4) and 12Cr (JLF-1) steels showed large irradiation hardening in the lower temperature range. Similar behavior was reported from the US and EU [32]. Fig.2-7 shows dose dependence of yield strength and total elongation after neutron irradiation in FFTF and HFIR. In agreement to the observations in Fig. 2-5, it can be seen that 7 to 9Cr steels showed less irradiation hardening. After the neutron irradiation at 683 K, rapid irradiation hardening was observed in the early stages of displacement damage [33].

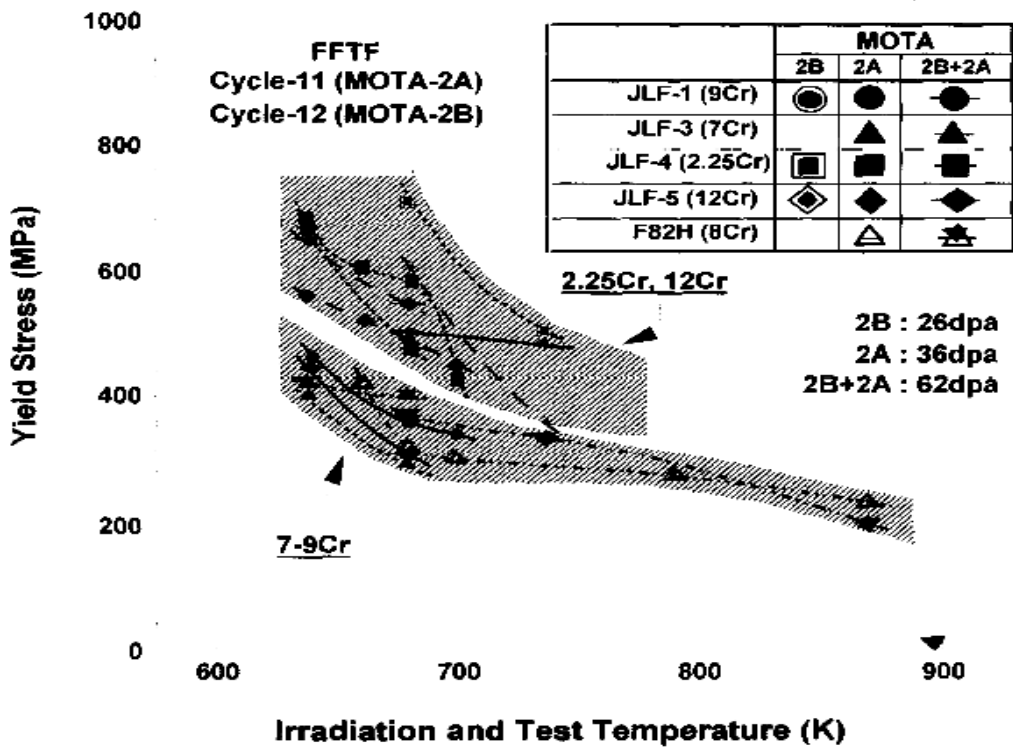


Fig 2-6 irradiation temperature and dose dependence of yield stress of JLF series of steels and F82H irradiated in FFTF/MOTA [33].

Above 20 dpa irradiation hardening decreases and then saturates at a strength level lower than the hardening observed at lower doses [33]. The figure also shows that there was more hardening after irradiation in HFIR, but the HFIR tests, which were conducted to determine a helium effect by means of the B(10) doping method, did not show significant differences to prove a clear effect of helium production on irradiation hardening[34,35].

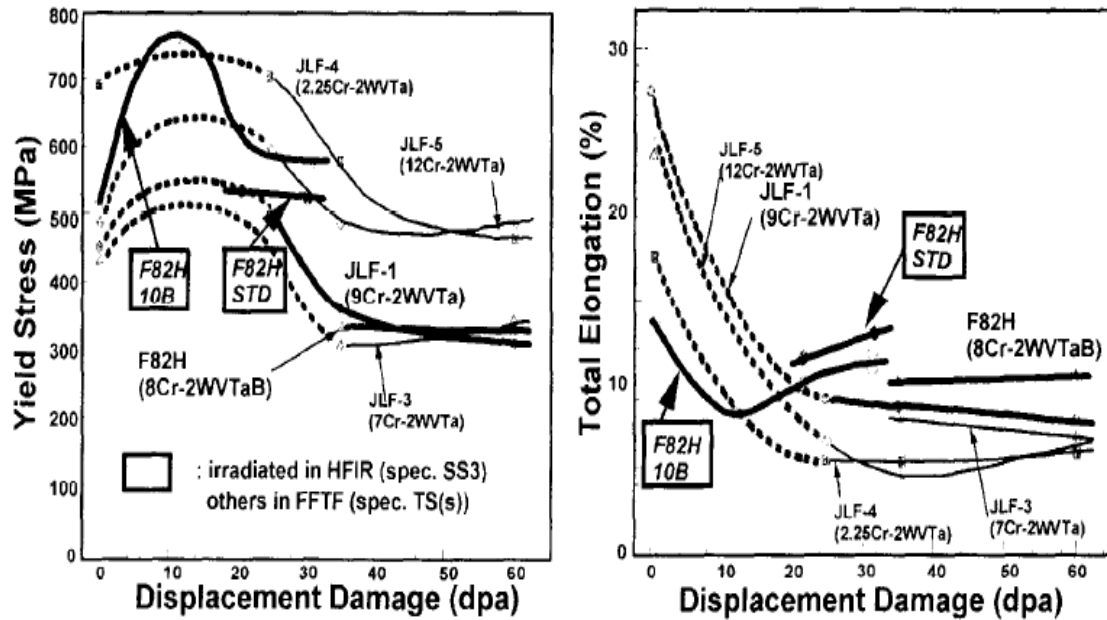


Fig.2.7. Dose dependence of yield strength following irradiation at 638 K in FFTF/MOTA and HFIR [33].

For consideration on the toughness of these steels embrittlement due to irradiation is commonly measured by the shift in DBTT in a Charpy impact [33]. Fig.2.8. shows the effect of chromium addition on the DBTT shift in LAFs due to fast neutron irradiation in FFTF. The 9Cr-2WVTa steel produced a shift in DBTT of only 4 and 15°C after irradiation in FFTF at 365°C to 7 and 10 dpa, respectively [36]. A DBTT shift of 130°C was observed for HT-9 and 50°C for modified 9Cr- 1 MO irradiated to similar conditions. The results from 365°C irradiation in FFTF showed that the 7 to 10 Cr range was the most resistant to a DBTT increase due to neutron damage. At the same time, the addition of up to 2% W and V and Ta additions were shown to effectively reduce the DBTT shift due to neutron irradiation. Likewise, irradiation to 36 dpa at 410°C indicated that the 7 to 9 Cr addition also suppressed the DBTT shift over the lower and higher Cr concentrations [33]. In Fig.2.8, the data are shown for irradiation at 365°C and for irradiation at 410°C obtained respectively, using full-sized and 1.5 mm X 1.5 mm mini-sized Charpy specimens [33].

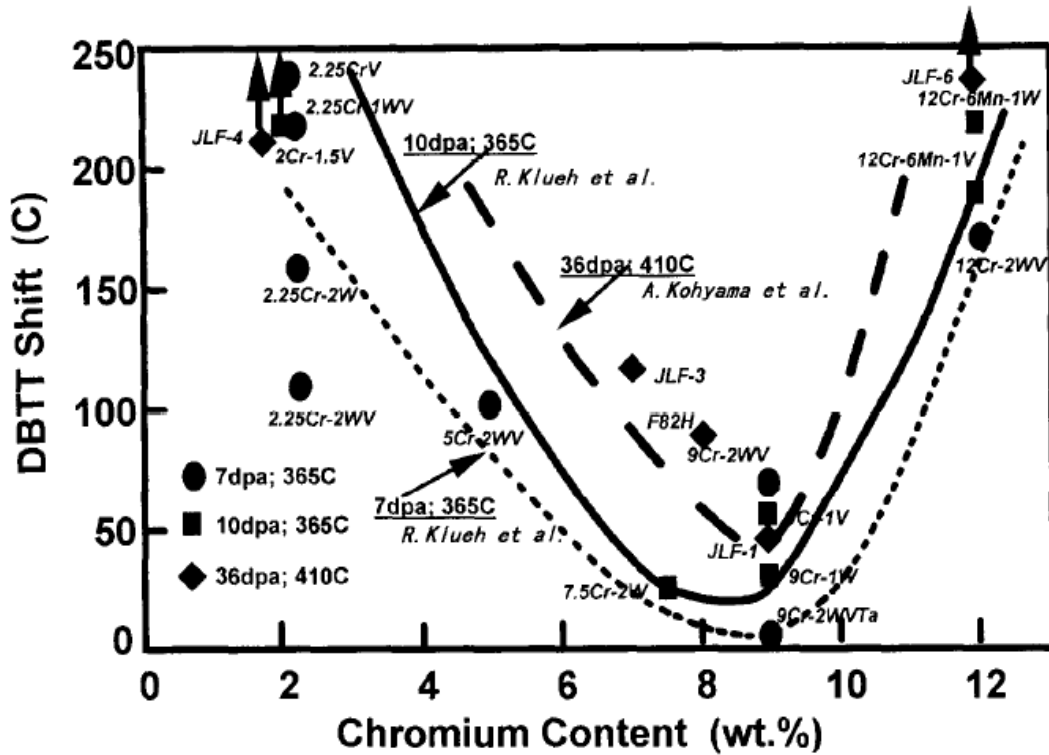


Fig.2.8.effect of chromium content on DBTT shifts to LAF_s by neutron irradiation in FFTF [33].

The influence of size effects is still not clear, and thus a quantitative comparison of the 365 and 410°C irradiation data cannot be made. The results for JLF-1 and 9Cr-2WVTa indicate that the DBTT shift saturated with fluence [31, 36].

2-2-3 Current and future concerns of ferritic steels.

Over the 15 years or so, a strong emphasis has been placed on the development of low activation ferritic /martensitic steel (with 8-12%Cr) [37].Over the last 15 years or so, a strong emphasis has been placed on the development of low activation ferritic/martensitic steel (with 8–12% Cr). The minimum operating temperature is governed by radiation hardening and ductile-to-brittle-temperature (DBTT) shift and is ~200–250 °C, while the maximum operating temperature, based on thermal creep, is about 550 °C [38]. Clearly, the latter is not sufficiently high to be joined to a W-alloy under its minimum operating temperature (~ 700 °C)[37]. Thus, development of ODS ferritic steels with higher-

temperature capabilities is a key R&D need for this application. The minimum operating temperature of ODS-FS needs to be better assessed but is about 290 °C (based on results for HT-9) [38]. The oxide dispersion significantly improves the (high-temperature) strength and thermal creep properties of ODS steels over conventional steels and increases the maximum operating temperature to ~ 700 °C or more. Nano-structured ferritic alloys (NFA) are advanced ODS steels containing high concentrations of nano-size Ti-, Y- and O-rich clusters, or nanoclusters, that provide significant (high-temperature) strength and creep resistance to these alloys (as illustrated in Fig. 2.10. [39,40]).

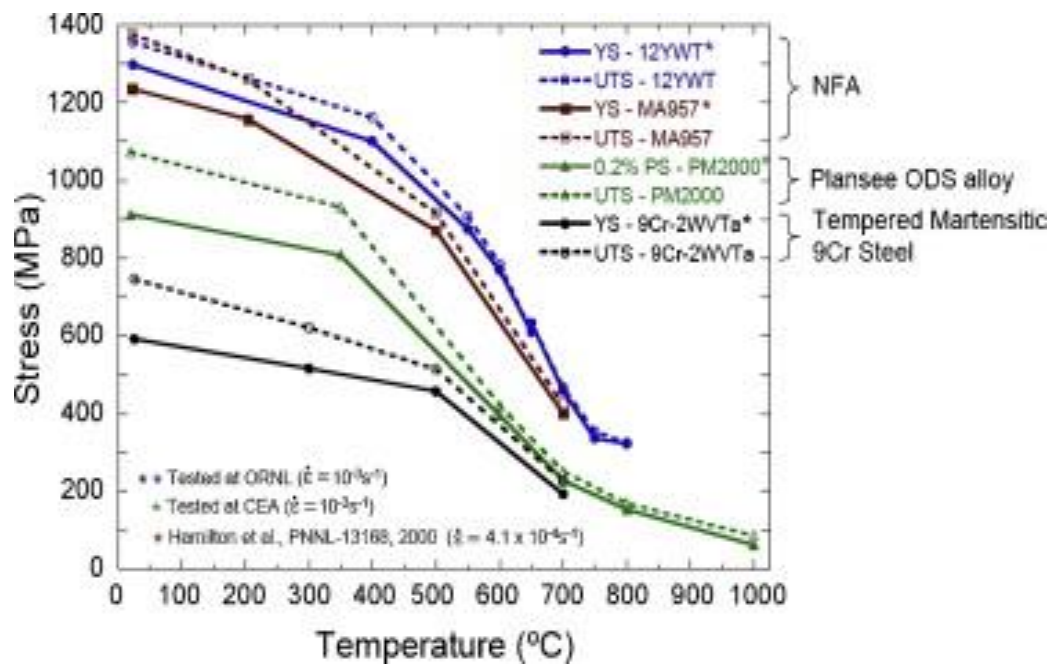


Fig.2-9. comparison of the –temperature strength of 3 nanostructured ferritic alloys (12YWT.MA957 and Plansee ODS alloy) and of a tempered martensitic 9Cr steel

The nanoclusters were initially discovered in the 12YWT NFA that was developed in Japan during the 1990s [41] and subsequently in MA957, which was developed and patented by INCO in 1978 [42]. However, these two NFA are not commercially available. Recent R&D programs conducted in the US (ORNL and UCSB) have led to the development of 14YWT [43]. The 14YWT NFA produced at ORNL in numerous small (<1.2 kg) heats contains ultra-fine grain size and nanocluster dispersions that are responsible for the exceptional

combination of high-temperature strength ($\sigma_y \sim 300$ MPa at 800 °C) and low temperature fracture toughness (transition temperature of -150 °C) [44,45]. The nano-size features of NFA improve the radiation damage resistance by trapping point defects, including He, causing enhanced recombination and suppression of He bubble formation on grain boundaries that is responsible for embrittlement of structural materials in fusion reactors [46]. Therefore, nano-structured ferritic alloys offer the potential to extend the operating limit of ferritic steels from ~ 550 °C to ~ 800 °C for application in advanced nuclear energy systems [37].

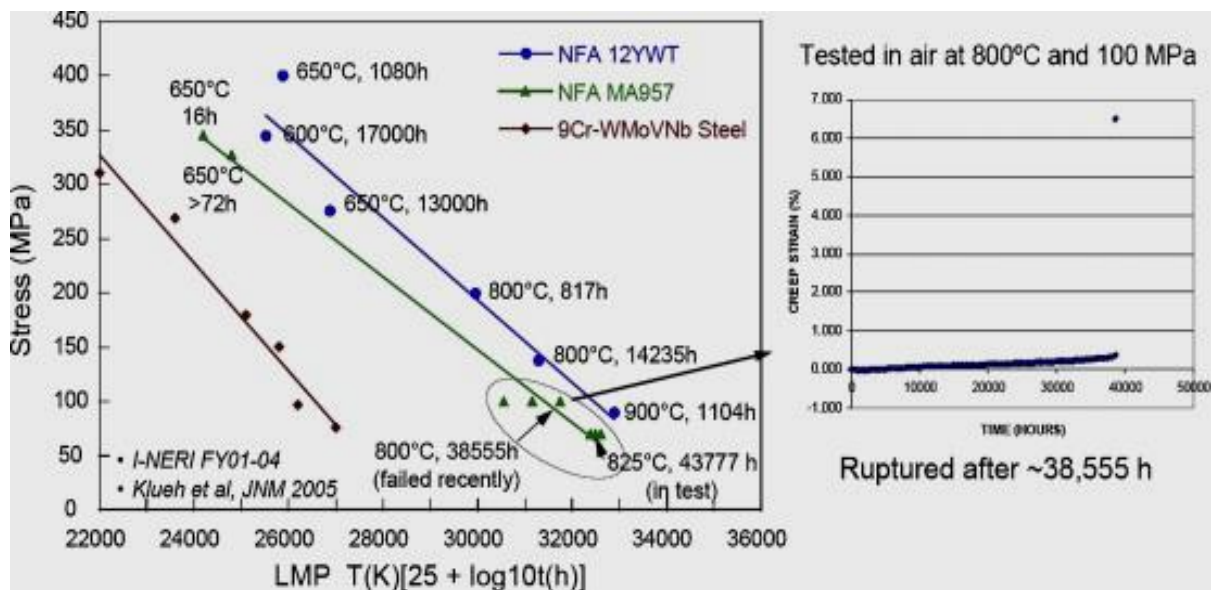


Fig.2-10. creep properties of two nanostructured alloys (12YWT and MA957) compared to tempered martensitic 9Cr steel

2-2-4- Tungsten alloy

Tungsten alloy is considering as promising candidate material as structural alloy, where the tungsten alloy showed high-temperature strength and good heat conductivity, in the present time helium cooled DEMO divertor using the tungsten alloy of W-1%La₂O₃ (WL10) which is being operated at temperatures between 600°C and 1300 °C in the EU HEMJ concept, the lower temperatures refers to the minimum temperature to transfer the

heat to the steel and the maximum temperature refers to the recrystallization and to loss of the strength [37]. The difficulty of connection tungsten materials with structural applications representing on the rather high ductile-to-brittle transition temperature (DBTT) [37]. A study of impact bending characteristics of standard tungsten materials has been accomplished (in vacuum) to illustrate the influence of microstructure characteristics like grain size, anisotropy, and texture or the influence of chemical composition [47, 48].

The design criteria for the divertor applications include creep strength (55MPa for time to rupture of minimum 20,000 h at 1200°C), thermal conductivity (100W/m*K at 1200 °C), and DBTT (300°C in the unirradiated condition, measured by EU standard mini-Charpy tests) [37]. The creep strength and thermal conductivity design aspects are satisfied by the unirradiated WL10 materials as illustrated in Figs.2.11 and 2-12[49].

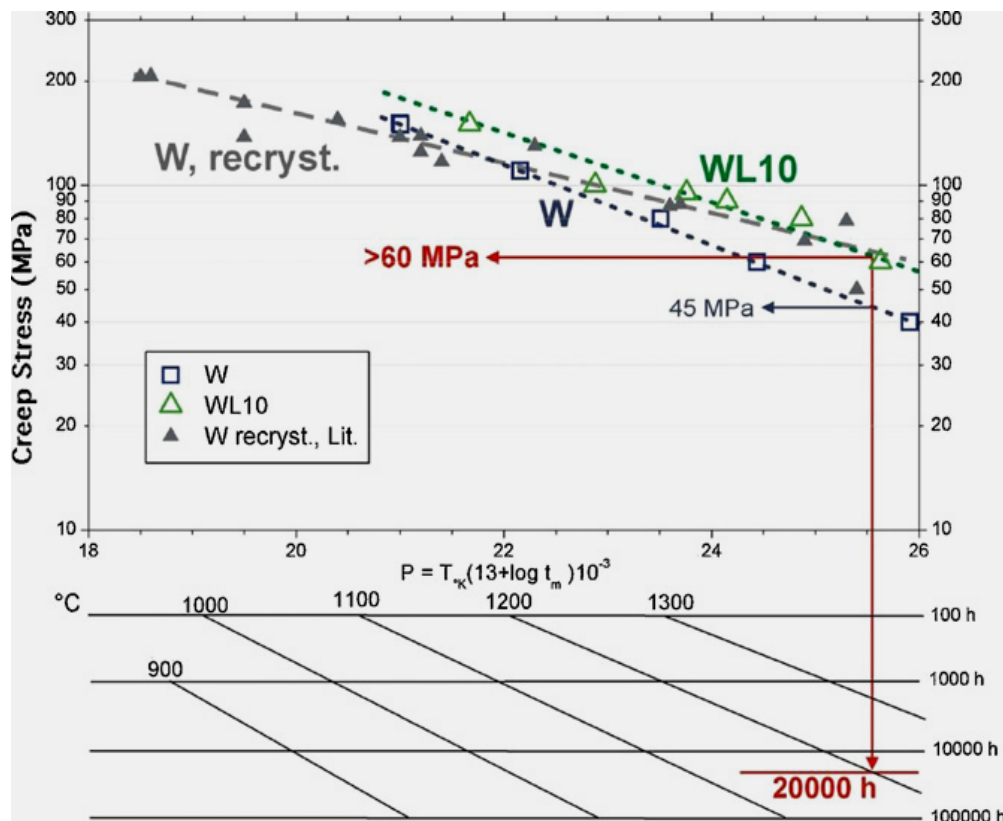


Fig. 2.11. Creep strength of tungsten in form of a Larson–Miller plot for times to rupture (desirable design value is shown)

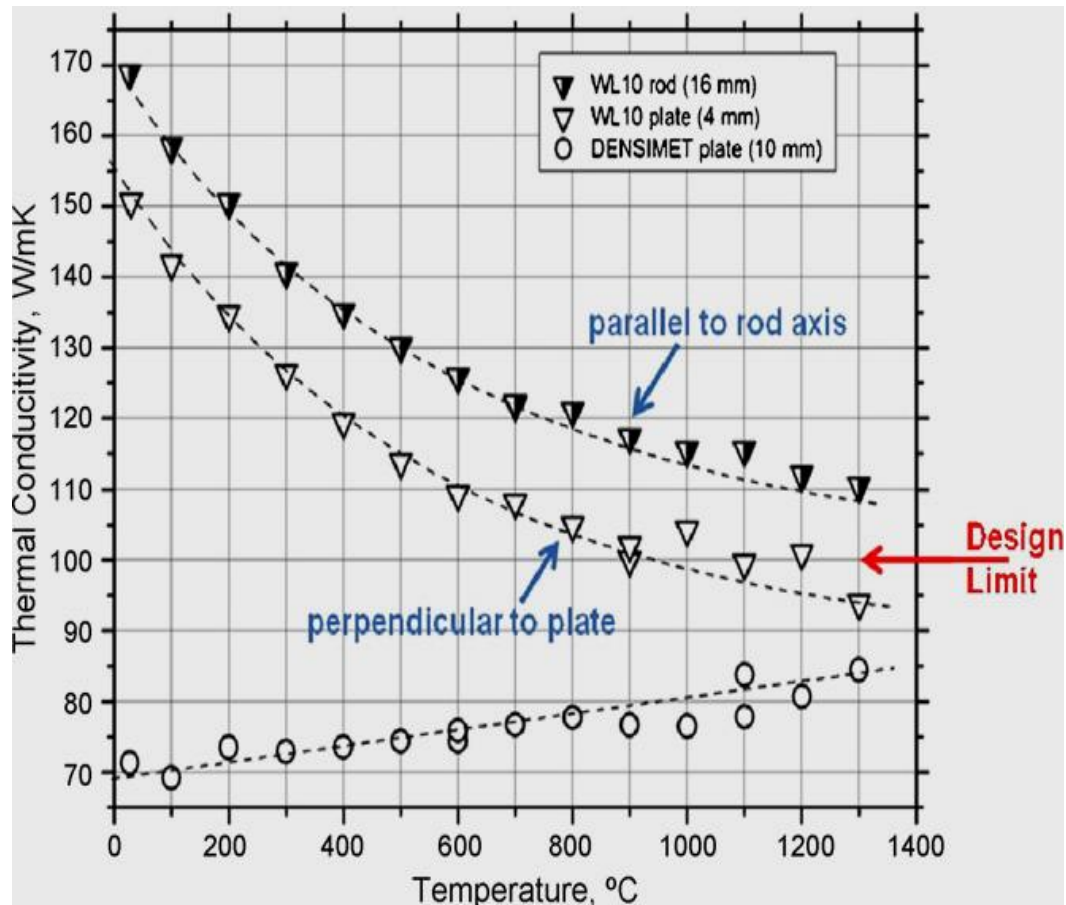


Fig. 2.12. Thermal conductivity of W measured by laser flash analysis (desirable design value is shown)

Where there is no data available for the recrystallization behavior of tungsten alloy, so the design aspects depend on an operating time of about 20,000 h and hence such operating time can be considered as the minimum recrystallization time of the structural materials [37]. Results for pure tungsten showed material recrystallization at 1300°C, however during other studies at the same temperature with WL10, recrystallization was not observed even after nearly 2000h [37]. Such study showed the benefits of the addition of lanthanum-oxide particles in tungsten where lanthanum oxide-particles improved the materials processing, make suppression of the recrystallization, and slight creep strengthening [37].

2-2-5- SiC_f/SiC

The final goal of the Fusion Technology Programme is power generation under attractive economical and environmental conditions. In this pursuit the use of structural low activation materials (LAM) is fundamental as their use will reduce the risk related to accidents, will facilitate maintenance operations and will simplify decommissioning and waste management. Among LAMs, the SiC_f/SiC composites are the leading candidates as structural material for fusion reactors, due to their good mechanical properties at high temperature, low chemical sputtering, good resistance to oxidation at high temperature ($\leq 1000^{\circ}\text{C}$) and very low short and medium term activation. [50].

2-2-5-1 manufacturing history and trade marks of SiC_f/SiC

Industry has a large installed capacity for full scale production of SiC_f/SiC composites parts. Moreover the industry is capable of ‘engineerability’ of such materials by optimizing a specific component with fibre architecture. The most widely studied and used fibres are the NICALON™. Since the beginning of 1990s the SEP Division of SNECMA™ has been involved with the manufacturing of SiC_f/SiC composites for fusion power reactors [51].

A standard 2-D composite named CERASEP® N2-1 was used to carry out the initial evaluation work at the start of the European programme and demonstrate the capability of such material. One of the characteristics of this particular SiC_f/SiC composite was its two dimensional strengthening feature, achieved using a fabric of NICALON™ CG fibre (with about 12% oxygen) and by increasing the density of the preform by a SiC CVI matrix. Due to the geometric complexity of the parts making up the TAURO blanket and in order to improve the material’s shear related properties, CERASEP® N3-1 was subsequently developed. This material, also produced with NICALON™ CG fibres, offered an innovative 3-D strengthening feature: the GUIPEX® texture. CERASEP® N2-1 and N3-1 materials offered fairly similar mechanical and thermal properties (Table 2-3) but the main advantages of the 3-D material are as follows: improved thermal conductivity in the Z direction, increased and more consistent interlaminar shear failure stress with the absence of interlaminar delamination during manufacturing and use, and lower dispersion of the

shear strength. CERASEP® N3-1 features can be improved by using high purity SiC fibres virtually stoichiometric and ‘oxygen free’ and with thermal conductivity intrinsically higher than that of the NICALON™ CG. Benefits with respect neutron irradiation induced change in the fibre properties are expected. Other positive aspects related to the use of such fibres are: an increasing in the maximum operating temperature from 1100 to 1300°C and improvements in mechanical properties. In parallel with SiC_f/SiC composite manufacturing by the CVI technique, alternative matrix processing routes are going to be investigated, in particular polymer infiltration and pyrolysis (PIP) [52]. This technology is less expensive than CVI, can be carried out at lower temperature and allows the manufacturing of more complex shapes. ENEA™ has extensively used Preceramic polymers with SiC nanopowders. This composites exhibited interesting mechanical properties in particular high strain to failure and toughness. As all composites produced by PIP, the material exhibits lower thermal conductivity, poor crystallinity and high residual oxygen content. The availability of more advanced fibres allowing higher pyrolysis temperature will permit the reduction of free oxygen and the increase of the matrix crystallinity and properties. Recently, the use of an hybrid process combining CVI and PIP processes allowed the fabrication of composites with relevant thicknesses (6 and 10 mm) with an intermediate matrix structure [53]. Flat panels were produced with different duration of CVI process and number of PIP cycles. The maximum density for 10 mm thick panels was reached at 60 h of CVI and seven PIP cycles (2.05 g.cm⁻²) [53].

Table (2-3) [52]

SEP SiC_f/SiC composites main properties

Property	Temperature (°C)	CERASEP [®] N2-1 (2-D)	CERASEP [®] N3-1 (3-D)
Density (g/cm ³)	20	2.5	>2.4
Porosity (%)	20	10	10 ± 2
Fibre content (%)	–	40	40
Tensile strength (in plane) (MPa)	20	285	300 ± 20
Tensile strain (in plane) (%)	20	0.75	0.8 ± 0.25
Young modulus (in plane) (GPa)	20	200	200 ± 20
Trans-laminar shear strength	20	200 MPa	200 ± 20 GPa
Inter-laminar shear strength (MPa)	20	–	44
Thermal conductivity (in plane) (W m ⁻¹ K ⁻¹)	1000	15	15
Thermal conductivity (through the thickness) (W m ⁻¹ K ⁻¹)	20	9	13 ± 2
Thermal conductivity (through the thickness) (W m ⁻¹ K ⁻¹)	800	5.8	7.6
Thermal conductivity (through the thickness) (W m ⁻¹ K ⁻¹)	1000	5.7	7.5
Thermal expansion coefficient (in plane) (K ⁻¹)	20	4.0 × 10 ⁻⁶	4.0 × 10 ⁻⁶
Thermal expansion coefficient (through the thickness) (K ⁻¹)	20	2.5 × 10 ⁻⁶	–

2-2-5-2 Development of SiC_f/SiC composites

SiC fiber reinforced SiC matrix (SiC_f/SiC) composites are promising structural candidates for advanced nuclear energy systems, such as gas cooled fast reactor (GFR), very high temperature reactor (VHTR) and fusion reactor due to their potentiality for providing excellent mechanical properties at high-temperature and low induced radioactivity [54-57]. There have been many efforts to develop high-performance SiC/SiC composites, using chemical vapor infiltration (CVI), polymer infiltration and pyrolysis (PIP), reaction sintering/melting infiltration (RS/MI) and their combined processes [58-61]. However, the low porosity, high-crystallinity and near-stoichiometric composition in matrix have been recognized as key requirements for high-temperature and neutron irradiation application [62– 64]. From these aspects, a newly innovative process called Nano-Infiltration and Transient Eutectic-phase (NITE) process has been extensively developed at Kyoto University. NITE process, which is first successful application of liquid phase sintering (LPS) process to matrix densification for SiC/SiC composites, enabled a production of well-crystallized SiC matrix with low porosity by incorporating both SiC nano-powder infiltration and the advanced SiC fibers with well-crystallized microstructure and near-stoichiometric composition like TyrannoTM-SA fibers [65–69]. General properties and issues for advanced SiC/SiC and comparison with (NITE) are summarized in Table 2-

4[70], the modern process of fabrication by NITE process showed a good mechanical properties with different types of fibers and different coating of fibers where the coating of fibers create interface between fibers and matrix and create gap between neighboring fibers such effect of coating makes variation of mechanical properties, as shown in Fig.2.13.[70].

Table (2-4) [70]

List of developmental SiC/SiC composites for structural materials and corresponding issues				
Category	Advanced fiber CVI	Advanced fiber MI	Crystallized PIP	NITE
Fiber	Tyranno-SA/Hi-Nicalon Type-S			
Interphase	PyC	PyC/SiC	Varied	PyC
Matrix				
Base phase	3C-SiC	3C-SiC	3C-SiC	3C-SiC
Porosity	10%~	0%	~20%	0%~
Excess Si	Occasionally	10%~	None	None
Excess C	None	Occasionally	~10%	None
Other phase (s)	None	None	None	Oxides, <10%
General issues				
Strength	Moderate	Moderate	Low	Moderate-high
Thermal conductivity	Moderate	High	Low-moderate	Moderate-high
Hermeticity	Poor	Poor	Poor	Good

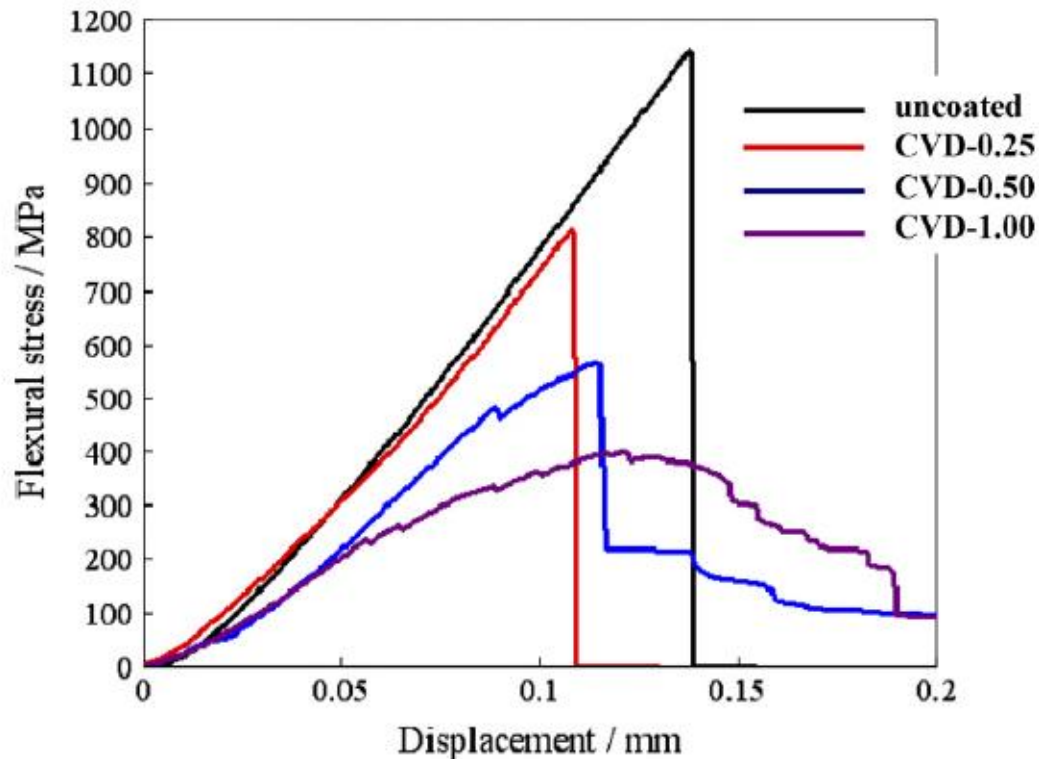


Fig.2-13.The variation of flexural stress of SiC/SiC by NITE process without fiber coating and with different thickness of pyrolytic fiber coating (pyc).

2-3-High heat flux components (HHFC_s) of fusion reactors.

The High heat flux components of fusion reactors are considering the main critical design aspects to develop the performance of fusion reactors, the term HHFC_s means that the components which can accommodate high thermal load inside the pressure vessel of the reactor; like divertor and first wall. The HHFC_s itself consists of the plasma facing materials or armor and the heat sink. The main design aspects of the HHFC_s are to select the plasma facing materials which can accommodate not only the quasi-state plasma high heat flux but also the off-normal events of plasma like plasma disruption; like edge localized mode (ELM) and vertical displacement events (VDE_s).

2-3-1- ITER plasma facing materials and operating conditions.

It is important to know the off-normal conditions of the plasma heat load as severe operating conditions of the HHFCs, where those major conditions are [71]:

1- Major disruptions:

- Peak energy density parallel to the field in the divertor at the separatrix: 100–600 MJ/m² (outer plate); 130–780 MJ/m² (inner plate).
- Projecting these values onto the target plates gives:
 - Outer plate: $\approx 4\text{--}25$ MJ/m²,
 - Inner plate: $\approx 7\text{--}40$ MJ/m².
- Deposition time: $\approx 1.5\text{--}3$ ms (rise time), 1.5–6ms (decay time).

2- Vertical displacement events (VDEs)—power deposition on upper wall blanket shield modules (upward VDE), divertor dome, baffle or lower blanket shield modules (downward VDE):

- Power flux outside divertor (mapped to outer mid-plane) parallel to field lines near the separatrix at wall/baffle/dome contact = 800MW/m².
- Energy deposition on outer wall blanket shield modules (accounting for component shaping) $\approx 20\text{--}30$ MJ/m² (upward and downward VDEs).
- Timescales $\approx 0.1/0.3$ ms (downward/upward).

3- Edge localized modes (ELM):

- Maximum energy density on divertor target for:
 - Controlled ELMs: 0.5 MJ/m² (inner plate); 0.3 MJ/m² (outer plate).
 - Uncontrolled ELMs: 10 MJ/m² (inner plate); 6MJ/m² (outer plate).
- Deposition time: $\approx 0.25\text{--}0.5$ ms.
- Frequency (controlled/uncontrolled) = 20–40/1–2 Hz.

The current ITER plans include three different plasma-facing materials (PFM) for the initial operation phase, as illustrated in Fig. 2.14: beryllium for the first wall (based on its acceptable effect on plasma performance and its high oxygen gettering characteristic); tungsten for the dome and baffle divertor regions (based on its temperature capability and low physical sputtering yield by neutral particles); carbon-fiber-composite (CFC) for the

divertor vertical targets. CFC has high thermal shock resistance, does not melt and has been widely used as a PFM in plasma experimental devices, showing good compatibility over a wide range of plasma parameters. However, a key issue with carbon is tritium co deposition and the difficulty of removing tritium in particular in colder shadowed areas. The current ITER divertor armor strategy including the following sets. [72]: (1) the first divertor set will have both carbon and tungsten armor on the vertical targets, with carbon in the highest heat load region. This is based on the proven range of compatibility of carbon with a number of plasma conditions in present devices, particularly at low densities with significant additional heating. CFC also promises to make the development of techniques for ELM control and disruption mitigation easier (as compared to W) by taking advantage of the larger tolerance of the plasma to C and of the absence of melting which may present a problem of irreparable damage to the strike point surfaces, requiring the replacement of divertor modules.

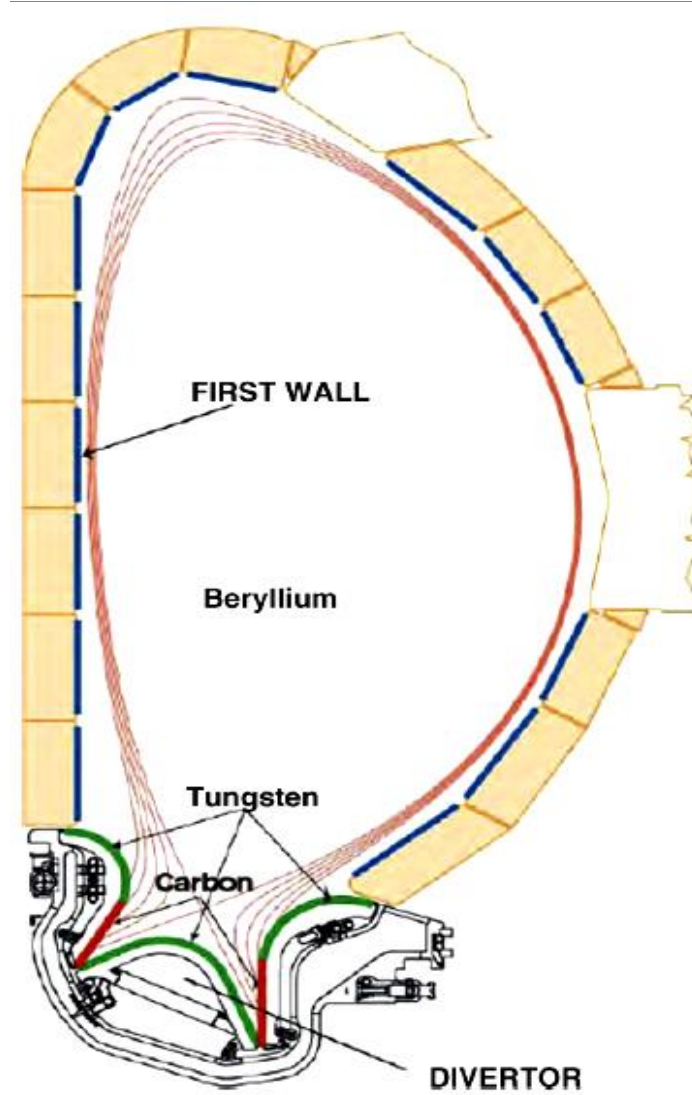


Fig.2-14. ITER plasma-facing materials for initial operation phase with hydrogen.

(2) The second divertor set will have full-tungsten armor on the vertical targets and is envisaged for later installation after the initial operational phase, and almost certainly before the tritium phase to avoid the tritium co-deposition issue with carbon. However, so as not to completely preclude the possible use of carbon early in the D–T phase, the first divertor set is designed to accommodate the heat loads foreseen in the D–T phase.

2-3-2- Design aspects of divertor in ITER.

The role of the divertor in ITER is to release the major part of the plasma thermal power and to decrease the impurities of the plasma and to decrease helium content. The design consists of 54 cassettes in a circular array [72]. The divertor cassette body is reusable to minimize activated waste; it provides neutron shielding, routes the water coolant and supports the different plasma facing components (PFCs). These consist of the dome, particle reflector plates, and inner and outer vertical targets, as illustrated in Fig.2-15[72]

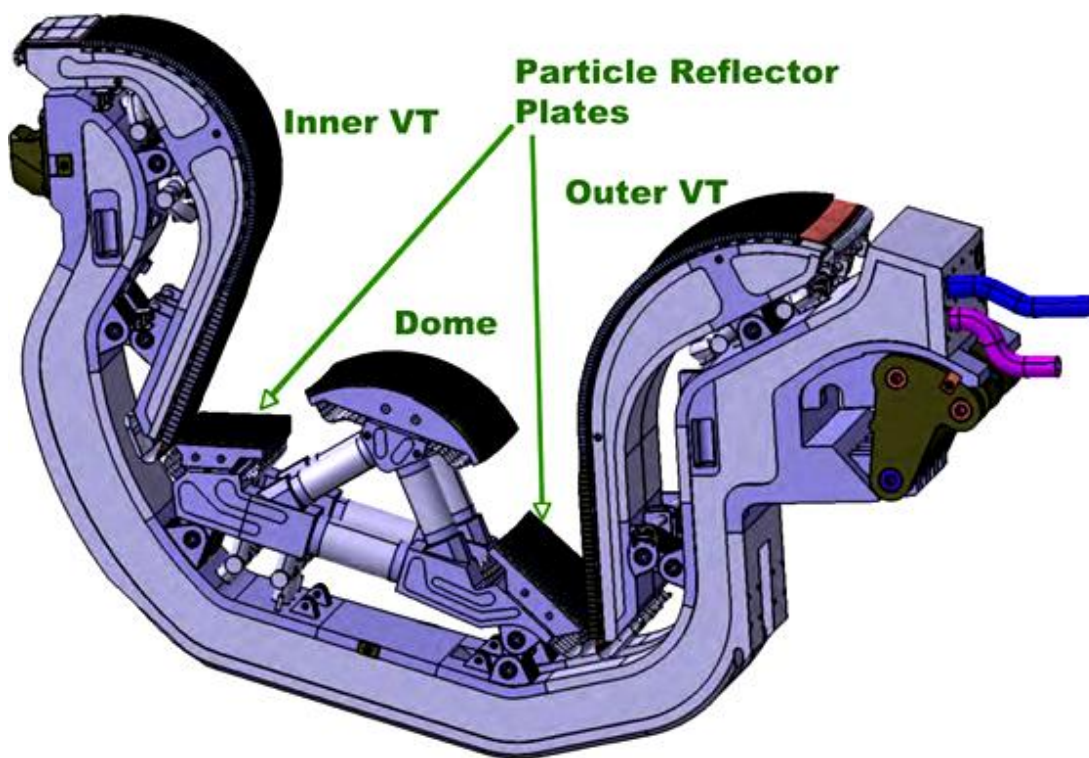


Fig.2.15. Schematic view of an ITER divertor cassette

The inner and outer vertical targets (VTs) are the PFCs that, in their lower part, intercept the magnetic field lines, and therefore remove the heat load coming from the plasma via conduction, convection and radiation[71,72]. As shown in Fig. 2.16, the lower part of the VT consists of a number of CFC monoblocks while the upper part is made up of W monoblocks. The CFC or W monoblock is bonded to the CuCrZr coolant tube via a Cu

interlayer. A swirled tape is used in the coolant tube to increase the critical heat flux. The armor thickness is based on maximizing the lifetime of the divertor while keeping the maximum armor material temperature at an acceptable level. The design requirements for the PFCs include [72]:

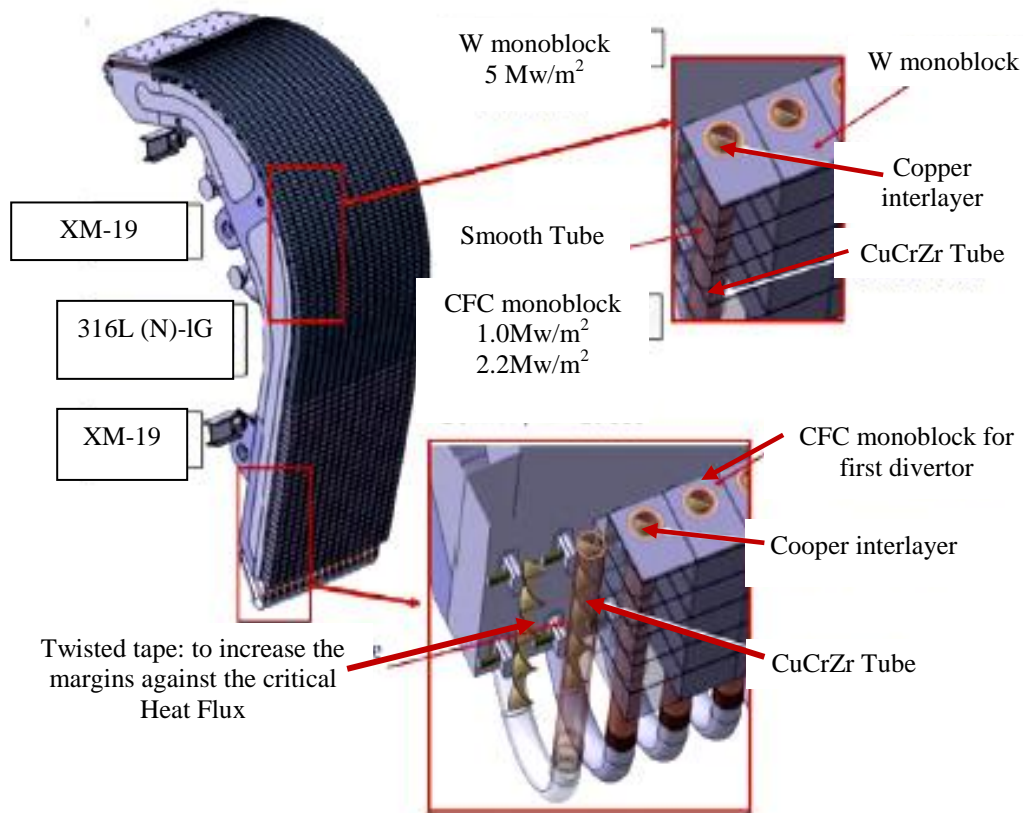


Fig.2.16. Details of the ITER divertor vertical target.

- 3000 equivalent pulses of 400 s duration at nominal parameters, Including 300 slow transients.
 - During normal operational conditions, the design surface heat flux on the vertical target is up to 10MW/m² in the strike point region and 5MW/m² in the baffle region.
 - Under slow transient thermal loading conditions, the design surface heat flux on the lower divertor vertical target geometry is up to 20MW/m² for sub-pulses of less than 10 s.
 - The dome shall sustain heat fluxes of up to 5MW/m².
 - The umbrella and the particle reflector plates shall sustain local heat flux up to 10MW/m², which can be transiently swept across the surface (about 2 s) as the plasma is returned to its correct position.
 - The maximum N-volumetric heating in the vertical target=10MW/m³.
-

References

- [1] L. J. Perkin, B. G. Logan, M. D. Rosen, M. D. Perry, T. Diaz de la Rubia, N. M. Ghoniem, T. Ditmire, P. T. Springer, and S. C. Wilks. The investigation of high intensity laser driven micro neutron sources for fusion materials research at high fluence. *Nuclear Fusion*, 40(1):1-19, 2000.
- [2] S. Konishi, S. Nishio, K. Tobita, and the DEMO design team. DEMO plant design beyond ITER. *Fusion Engineering and Design*, 63-64:11-17, 2002.
- [3] I.V. Kurchatov. On the possibility of producing thermonuclear reactions in a gas discharge. *Journal of Nuclear Materials*, 4(2):193-198, 1957.
- [4] M. Shimada, A. E. Costley, G. Federici, K. Ioki, A. S. Kukushkin, V. Mukhovatov, A. Polevoi, and M. Sugihara. Overview of goals and performance of ITER and strategy for plasma-wall interaction investigation. *Journal of Nuclear Materials*, 337-339:808-815, 2005.
- [5] R. L. Klueh and P. J. Maziasz. Effect of irradiation in HFIR on tensile properties of Cr-Mo steels. *Journal of Nuclear Materials*, 187:43-54, 1992.
- [6] Dale L. Smith, Richard F. Mattas, and Michael C. Billone. Fusion reactor materials. In Brian R.T. Frost, editor, *Materials Science and Technology*, chapter 10, pages 245-340. Wiley-VCH, 1997.
- [7] ITER official website, <http://www.iter.org/>.
- [8] Jeffrey P. Freidberg. *Plasma Physics and Fusion Energy*. Cambridge University Press, 2007.
- [9] L.K. Mansur and M.L. Grossbeck. Mechanical property changes induced in structural alloys by neutron irradiations with different helium-to-displacement ratios. *Journal of Nuclear Materials*, 155-157:130-147, 1988.
- [10] R.L. Klueh and J.M. Vitek. Fluence and helium effects on the tensile properties of ferritic steels at low temperatures. *Journal of Nuclear Materials*, 161:13-23, 1989.
- [11] L.K. Mansur. Mechanics and kinetics of radiation effects in metals and alloys. In Gordon R. Freeman, editor, *Kinetics of non homogeneous processes*, chapter 8, pages 377-463. John Wiley & Sons, Inc., 1987.
- [12] L. R. Greenwood. Neutron source characterization for fusion materials studies. *Journal of Nuclear Materials*, 104:797-801, 1981.

- [13] E.Daum, K.Ehrlich, S.Jitsukawa, H.Matsui, and A.Möslang. The international fusion materials irradiation facility IFMIF-an overview of user aspects. *Fusion Engineering and Design*, 49-50:435-444, 2009.
- [14] T. Kondo. IFMIF, its facility concept and technology. *Journal of Nuclear Materials*, 258-263:47-55, 1998.
- [15] V. Mukhovatov, M.Shimada, K.Lackner, D.J.Campbell, N.A.Uckan, J.C.Wesley, T.C. Hender, B. Lipschultz, A. Loarte, R.D. Stambaugh, R.J. Goldston, Y. Shimomura, M. Fujiwara, M. Nagami, V.D. Pustovitov, H. Zohm, ITPA CC Members, ITPA Topical Group Chairs, Co-Chairs, and the ITER International Team. Chapter 9: ITER contributions for DEMO plasma development. *Nuclear Fusion*, 47(6):S404-S413, 2007.
- [16] N.Baluc, D.S.Gelles, S.Jitsukawa, A. Kimura, R.L.Klueh, G.R.Odette, B.van der Schaaf, and Jinnan Yu. Status of reduced-activation ferritic/martensitic steel development. *Journal of Nuclear Materials*, 367-370(1):33-41, 2007.
- [17] K.Ehrlich, E.E.Bloom, and T. Kondo. International strategy for fusion materials development. *Journal of Nuclear Materials*, 283-287(1):79-88, 2000.
- [18] L. Boccaccini, L.Giancarli, G.Janeschitz, S.Hermsmeyer, Y. Poitevin, A.Cardella, and E.Diegele. Materials and design of the European demo blankets. *Journal of Nuclear Materials*, 329-333:148-155, 2004.
- [19] D.Maisonnier, I.Cook, P.Sardain, L.Boccaccini, L.Di Pace, L.Giancarli, N.Prachai, A. Pizzuto, and PPCS Team. Demo and fusion power plant conceptual studies in Europe. *Fusion Engineering and Design*, 81(8-14):1123-1130, 2006.
- [20] D.Maisonnier. European demo design and maintenance strategy. *Fusion Engineering and Design*, 83(7-9):858-864, 2008.
- [21] Report of the DOE Panel on Low Activation Materials for Fusion Application, R.W. Conn, Panel Chairman, UCLA/PPG-728,June1983.
- [22] E.E.Bloom and A.Kohyama, *J.Nucl.Mater.*179-181(1991) 1221.
- [23] F.A.Garner, D.S.Gelles and F.W.Wiffen, eds., TMS-AIME (1985).
- [24] R.L.Klueh, D.S.Gelles, M.Okada and N.H Packan, eds., ASTM STP 1047(1990).
- [25] Proc. of the IEA workshop on Ferritic/Martensitic Steel (Tokyo), eds. A.Kohyama and M.Suzuki (1992).
- [26] B.A.Loomis, A.B.Hull and D.L.Smith, *J. Nucl.Mater.* 179(1991)148.

- [27] H.Matsui, K.Kuji, M.Hasegawa and A.Kimura, J.Nucl.Mater.212-215(1994)784.
- [28] Pro. Of the DOE workshop on Ceramic Matrix Composites for Structural Application in Fusion reactors, eds. R.H.Jones and G.E.Lucas CONF-9005225(1990).
- [29] R.H.Jones, A.Sharafat, Fenici and A.Kohyama, J.Nucl.fusion Eng.Design (Proc.of ISFNT-3) (1995).
- [30] M.Tamura and A.Hishinuma, In: Proc. of IEA Low Activation Ferritic/Martensitic Steel (Oak ridge), (1993).
- [31] A. Kohyama, Y. Kohno, K. Asakura and H. Kayano, J. Nucl.Mater. 212-215 (1994) 684.
- [32] Proc. of the IEA Working Group Meet. On Ferritic/Martensitic Steels; Tokyo, JAERI Report, Vol 1 and II (1992), Oak Ridge, ORNL Report, ed. R.L. Klueh (1993). Sun-Valley, ORNL/M 3777 (1994), Oak Ridge, ORNL/M-4230 (1995).
- [33] A. Kohyama, A. Hishinuma, D.S. Gelles, R.L. Klueh, W. Dietz, K. Ehrlich Journal of Nuclear Materials 233-237 (1996) 138- 147.
- [34] K.Shiba. M. Suzuki, A. Hishinuma and J.E. Pawel, ASTM STP 1270 submitted for publication.
- [35] K. Shiba and A. Hishinuma, these Proceedings, p. 309.
- [36] R.L. Klueh and G.J. Alexander, these Proceedings, p. 336.
- [37] A.R.Raffray, R.Nygren, D.G.Whyte, S.Abel.Khalik, R.Doerner, F.Escourbiac, fusion eng.Jan.85(2010),pp.93-108.
- [38] S.J.Zinkle and N.M.Ghoniem, operating temperature windows for fusion reactors structural materials, fusion eng.dec.51-52(2000), pp.55-71.
- [39] R.L.Klueh etal. Acomparison of some commercial and experimental alloys, J.Nucl.Mater. 341(2005), pp.103-114.
- [40] D.T.Hoelzer, Private communication (from unpublished results, international nuclear energy research initiative (INERI) project, 2007-001-F (2008).
- [41] S.Kim et al., Effect of Ti and W on the mechanical properties and microstructure of 12% Cr base mechanical-alloyed nano sized ODS ferritic alloys. ISIJ Int.43 (2007), pp.1640-1646.

- [42] J.J.Fisher, US patent 4, 075, 010, and 1978.
- [43] M.J.Alinger et al., the development and stability of Y-Ti-O nano clusters in mechanically alloyed Fe-Cr based ferritic alloys, *J. NUCL.Mater.*329-333(2004), pp.382-386.
- [44] D.T.Hoelzer et al., influence of particle dispersion on the high-temperature strength of ferritic alloys. *Nucl. Mater.*367-370(2007), pp.166-172.
- [45] D.A. McClintock et al., Mechanical properties of neutron irradiated nano structured ferritic alloy 14YWT, *J.Nucl.Mater.*386-388(2009), pp.307-311.
- [46] T.Yamamoto, et al., The transport and fate of helium in nano structured ferritic alloys at fusion relevant He/dpa ratios and dpa rates, *J. Nucl. Mater.*367-370 (2007) 399-410.
- [47] M.Rieth, A.Hoffmann, Fracture behavior of tungsten-based alloys depending on microstructure and notch fabrication method, *Fusion Sci. Technol* 56 (2009) 1018-1022.
- [48] M.Rieth, A. Hoffmann, Impact bending tests on selected refractory materials, *Adv. Mater. Res.* 59 (2009) 101-104.
- [49] M.Rieth, A.Hoffmann, B.Dafferner, S.Heger, U. Jäntschi, M.Klimenkov, P.Lukits, M. Rohde, H.Zimmermann, Tungsten as structural DEMO divertor material, in: *Proceedings of Annual Meeting on Nuclear Technology, Dresden, Germany, May 12-14, 2009.*
- [50] P.Fenici, H.W.Scholz, Advanced low-activation materials. Fiber-reinforced ceramic composites, *J. Nucl. Mater.* 212- 215 (1994) 60-68.
- [51] A.Caso, P.Huet, P.C.Tramier, A new SiC/SiC composite as low activation structural material. *Proc. SiC/SiC Composites Workshop JRC:Ispra (I), 28-29 October 1996.*
- [52] A.Donato, C.A.Nannetti, A.Ortona, S.Botti, G.d'Alessandro, G.Filacchioni, A.Masci, SiC/SiC fibre ceramic matrix composites for fusion application: a new manufacturing process, in: C.Varandas, F.Serra(Eds.), *Fusion Technology 1996 — 19th SOFT Lisbon, North Holland, Amsterdam, 1997.*
- [53] A.Ortona, A.Donato, G.Filacchioni, U.deAngelis, A.La Barbera, C.A.Nannetti, B. Riccardi, J.Heatman, SiC/SiCf CMC manufacturing by CVI-PIP techniques: process optimizations. *Proc. of ISFNT-S, Rome, 19-24 September 1999.*
- [54] Tressler RE. Recent developments in fibers and interphases for high temperature ceramic matrix composites. *Composites A* 1999; 30:429-37.

- [55] Naslain R. Design, preparation and properties of non-oxide CMCs for application in engines and nuclear reactors: an overview. *Compos Sci Technol* 2004; 64:155–70.
- [56] Kohyama. A, Seki.M, Abe.K, Muroga.T, Matsui. H, Jitsukawa.S, et al. Interactions between fusion materials R&D and other technologies. *J Nucl Mater* 2000; 283–28:20–7.
- [57] Snead LL, Jones R, Kohyama A, Fenici P. Status of silicon carbide composites for fusion. *J Nucl Mater* 1996; 233–237:26–36.
- [58] Araki.H, Yang.W, Suzuki.H, Hu.Q, Busabok.C, Noda.T. Fabrication and flexural properties of Tyranno-SA/SiC composites with carbon interlayer by CVI. *J Nucl Mater* 2004; 329:567–71.
- [59] Kohyama.A, Kotani.M, Katoh.Y, Nakayasu.T, Sato.M, Yamamura.T, et al. High performance SiC/SiC composites by improved PIP processing with new precursor polymers. *J Nucl Mater* 2000; 283– 287:565–9.
- [60] Sayano.A, Sutoh.C, Suyama.S, Itoh.Y, Nakagawa.S. Development of a reaction-sintered silicon carbide matrix composite. *J Nucl Mater* 1999; 271–272:467–71.
- [61] Kotani.M, Kohyama.A, Katoh.Y. Development of SiC/SiC composites by PIP in combination with RS. *J Nucl Mater* 2001; 289:37–41.
- [62] Nozawa.T, Hinoki.T, Katoh.Y, Kohyama.A. Effects of fibers and fabrication processes on mechanical properties of neutron irradiated SiC/SiC composites. *J Nucl Mater* 2002; 307–311:1173–7.
- [63] Hinoki.T, Snead.LL, Katoh.Y, Hasegawa.A, Nozawa.T, Kohyama.A. The effect of high dose/high temperature irradiation on high purity fibers and their silicon carbide composites. *J Nucl Mater* 2002; 283– 287:1157–62.
- [64] Snead.LL, Katoh.Y, Kohyama.A, Bailey.JL, Vaughn.NL, Lowden.RA. Evaluation of neutron irradiated near-stoichiometric silicon carbide fiber composites. *J Nucl Mater* 2000; 283–287:551–5.
- [65] Kohyama.A, Dong.SM, Katoh.Y. Development of SiC/SiC composites by nano infiltration and transient eutectic (NITE) process. *Ceram Eng Sci Proc* 2002; 23:311–8.
- [66] Katoh.Y, Dong.SM, Kohyama.A. A novel processing technique of silicon carbide-based ceramic composites for high temperature applications. *Ceram Trans* 2002; 144:77–86.

- [67] Katoh.Y, Kohyama.A, Dong.SM, Hinoki.T, Kai.JJ. Microstructure and properties of liquid phase sintered SiC/SiC composites. *Ceram Eng Sci Proc* 2002; 23(3):363–70.
- [68] Dong.SM, Katoh.Y, Kohyama.A. Processing optimization and mechanical evaluation of hot pressed 2D Tyranno-SA/SiC composites, *Eur Ceram Soc* 2003; 23:1223–31.
- [69] Dong.SM, Katoh.Y, Kohyama.A. Preparation of SiC/SiC composites by hotpressing, using Tyranno-SA fiber as reinforcement. *Am-Ceram Soc* 2003; 86(1):26–32.
- [70] Influence of pyrolytic carbon interface thickness on microstructure and mechanical properties of SiC/SiC composites by NITE process Kazuya.Shimoda, Joon-Soo.Park, Tatsuya. Hinoki, Akira. Kohyama
- [71] A. Loarte, et al., Power and particle fluxes at the plasma edge of ITER: Specifications and physics basis, paper IT/P6-13, 22nd IAEA Fusion Energy Conference, Geneva, Switzerland, 13–18 October, 2008.
- [72] M. Merola, ITER PFC (Divertor, First Wall) design, in: International HHFC Workshop on Readiness to Proceed from Near Term Fusion Systems to Power Plants, December 10–12, University of California, San Diego, CA, USA, 2008 (see also Project Integration Document, ITER Organization (IDM 2234RH), Cadarache, France, January 2007) <http://aries.ucsd.edu/IHHFC/index.html>.

Chapter-3

Experimental Work and Achievements.

3- Experimental work and achievements

3-1-Introduction

This chapter will preview the fabrication conditions and technology which was used to fabricate the test samples for subsequent divertor plasma exposure test, where three samples of W/SiC/SiC hybrid component were fabricated with different operating conditions and starting materials, utilizing NITE process [1-13], where NITE process has the potential to make consolidation between tungsten and SiC/SiC simultaneously, with sintering and crystallization of SiC/SiC and tungsten. The samples produces were cut and polished to the appropriate size for the divertor plasma exposure test inside the Large Helical Device (LHD).macro and micro structure investigation of samples produced also will be provided in this chapter to evaluate the samples produced.

3-2-Experimental work and methodology

The technology used for fabrication the test materials as aforementioned is the NITE process, where the potential of NITE process provided us the consolidation of Tungsten and SiC/SiC simultaneously, with sintering and crystallization of SiC/SiC and tungsten. Schematic view of NITE process flow chart is illustrating in **Fig.3.1**. Hot press machine model (FVPHP-R-5-FRET-15), the specification of the hot press machine is illustrating in **table.3.1**, schematic view of hot press mold and whole machine is illustrating in **Fig.3.2**.

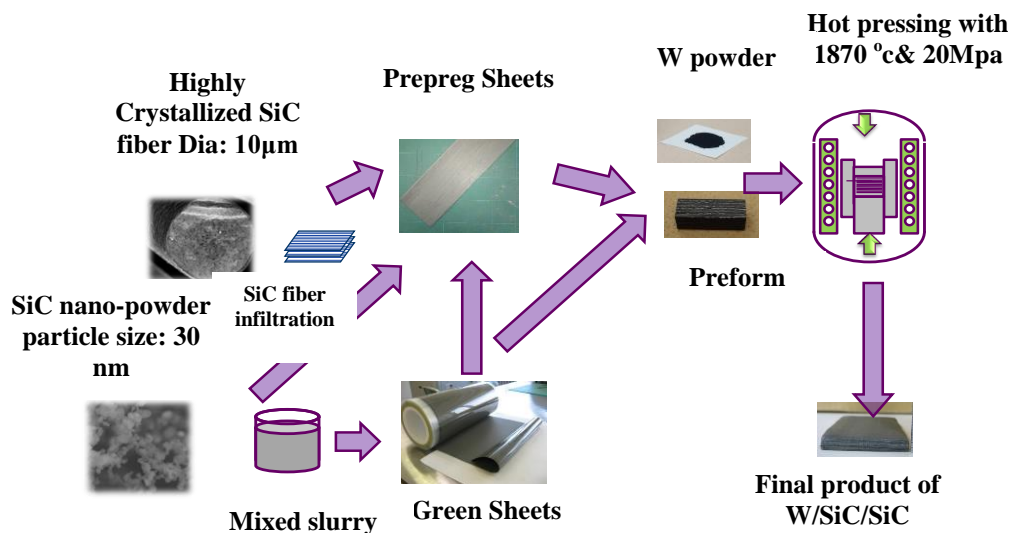


Fig.3.1. Schematic view of NITE Process flow chart

Table.3.1. Specification of the hot press machine

Model	Max temperature	Heating time	Mold dimensions	Vacuum	Atmosphere pressure	Press pressure	Electric power
FVPH P-R- 5FRE T-155	1500 ° to 1900 °c	40 minute R.T to 1500 ° c	Φ 120 mm H 110 mm	1*10 ⁻⁴ pa	0.92 M.pa N ₂ , Ar	4.9 *10 ⁴ N	220 V 15 KW

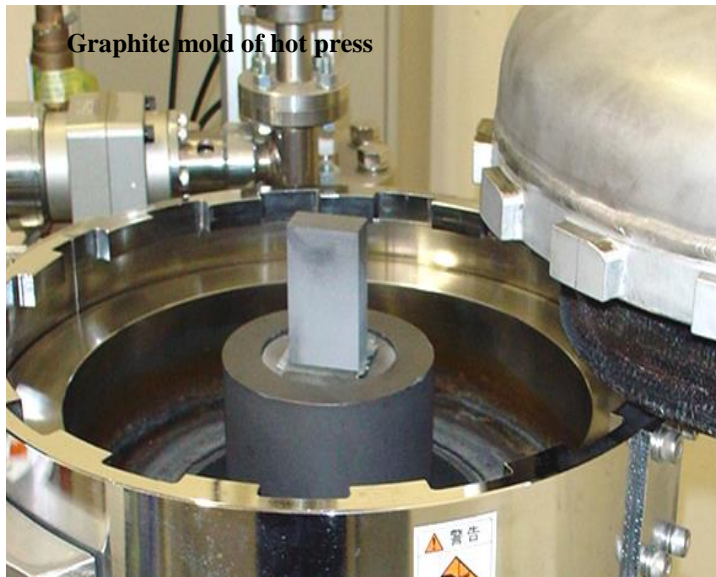


Fig .3.2.schematic view of hot press machine Model (FVPH-P-R-5-FRET-15)

3-3-Fabrication of tile (NITE-W/SiC-S2)

The fabrication of the tile (NITE-W/SiC-S2) was conducted by liquid phase sintering bonding, where the preparation of the samples included: the preparation of SiC/SiC preform, where the preform is the pliable phase of SiC/SiC before solidification, the preform consists of 8 prepreg sheets, where each prepreg sheet was prepared by infiltration the Tyranno™-SA grade-3 nano fibers into slurry of the SiC which is a mixture of SiC nano-powder and sintering additives (Al₂O₃ + Y₂O₃ = 9 wt% (Al₂O₃:Y₂O₃ = 60:40) and

SiO₂ = 3 wt%). The infiltrated fibers are stratified on the surface of pliable sheet of dried SiC called green sheet, the final stratified- infiltrated nano fibers on the green sheet called prepreg sheet. The prepreg sheets produced were arranged as (0, 90) degree cross ply to produce preform with dimension 40x40x4.5mm³. The specifications of Tyranno™-SA grade-3 nano fibers are illustrating in the **table.3.2**.

Table.3.2.Specifications of Tyranno™-SA grade-3

SiC fiber	Atomic ratio(C/Si)	Diameter(μm)	Density(mg/m ³)	Filament/yan	Tensile strength(GPa)	Elastic modulus(GPa)
Tyranno™ .SA	1.08	7.5	3.10	1600	2.51	409

After preparing the prepreg sheets, pure tungsten powder of purity 99.99% with rang size of 0.6 -0.99 μm with total weight 47.2 gm is distributed above the perform, the preform and distributed pure tungsten powder were arranged inside the graphite mold, where eventually the preform surrounded by graphite plates and carbon sheets to prevent sample to be stacked, boron nitride was sprayed between the graphite plates and preform to facilitate pickup the sample after hot pressing process. **Fig.3.3** is illustrating the arrangement of the sample inside graphite mold.

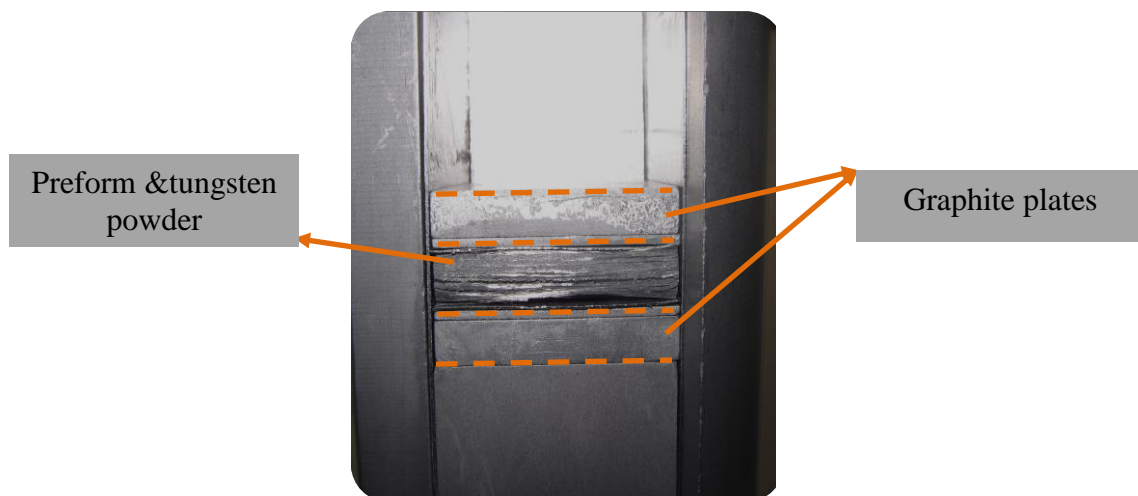


Fig.3.3. the arrangement of the sample preform inside graphite mold

The preform with tungsten powder were inserted inside the chamber of hot press, the operation of hot press was conducted with operating conditions; temperature and applied pressure, holding time, where temperature was 800° C with 10 MPa applied pressure, holding time up to 29-30 minutes, after holding time; temperature started to increase to be 1870 ° C, with applied pressure of 20 MPa, holding time of 1.5 hour. The hot press conditions chart is illustrating in **Fig.3.4**. After the operating conditions were accomplished, the sample was left to be cooled to the room temperature, when the sample cooled down; the chamber of the hot press was opened to pick up the hot pressed sample. Table.3.3 is illustrating the specification of the sample before and after hot press.

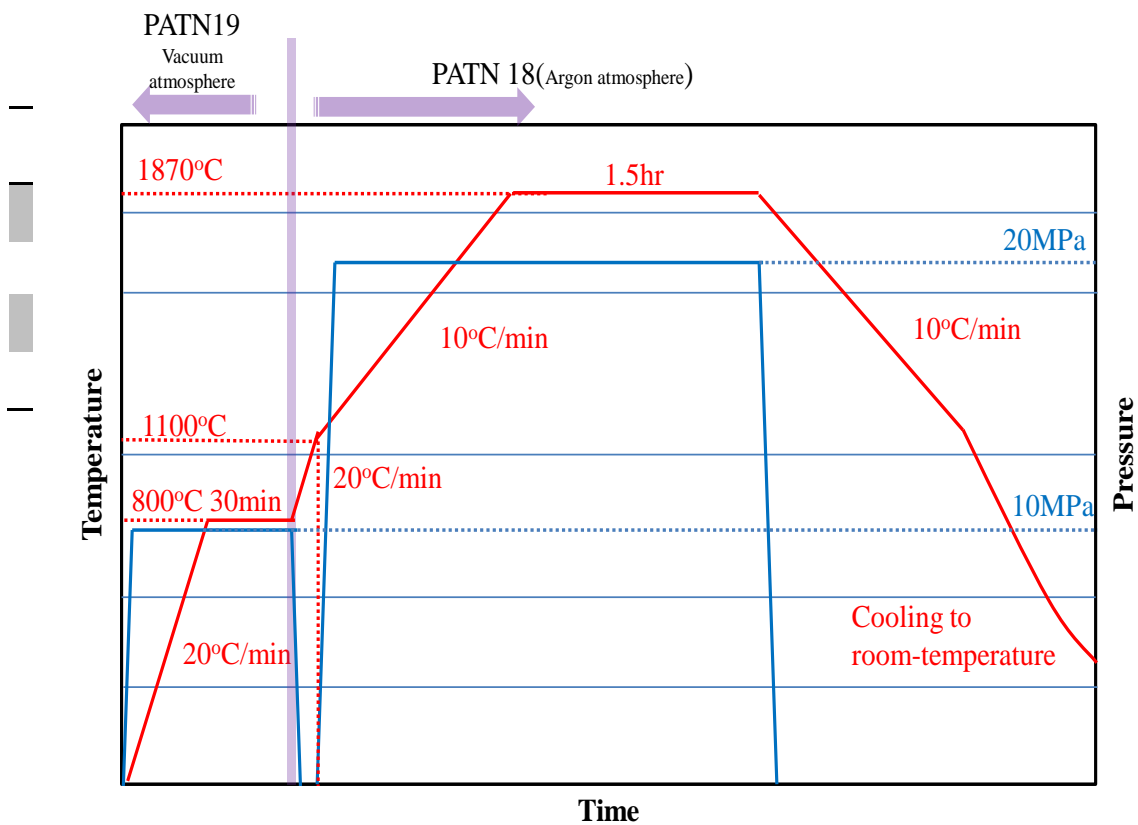


Fig.3.4. The hot press conditions chart of fabrication the tile (NITE-W/SiC-S2)

The picked sample of the tile (NITE-W/SiC-S2) was investigated after hot press by digital camera, digital microscope, the schematic photos of the hot pressed tile, where both SiC/SiC and W surfaces were captured. Fig.3.5 is showing the hot pressed tile (NITE-W/SiC-S2).

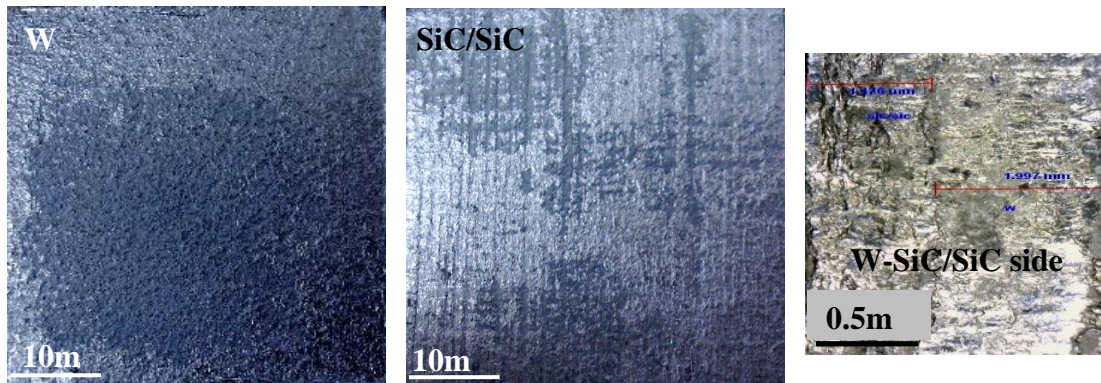


Fig.3.5.The hot pressed tile (NITE-W/SiC-S2)

Due to the traces of graphite, which covered and surrounded the sample it was very difficult to investigate tungsten and SiC/SiC surface, so the sample was cut and polished where surfaces of SiC/SiC and tungsten appeared obviously and W-SiC/SiC side view appeared and macro and micro structure could be investigated, the sample draw cut to get samples for SEM analysis beside the tile of the size appropriate for the divertor plasma exposure test ,the sample surface after polishing is illustrating in **Fig.3.6**.

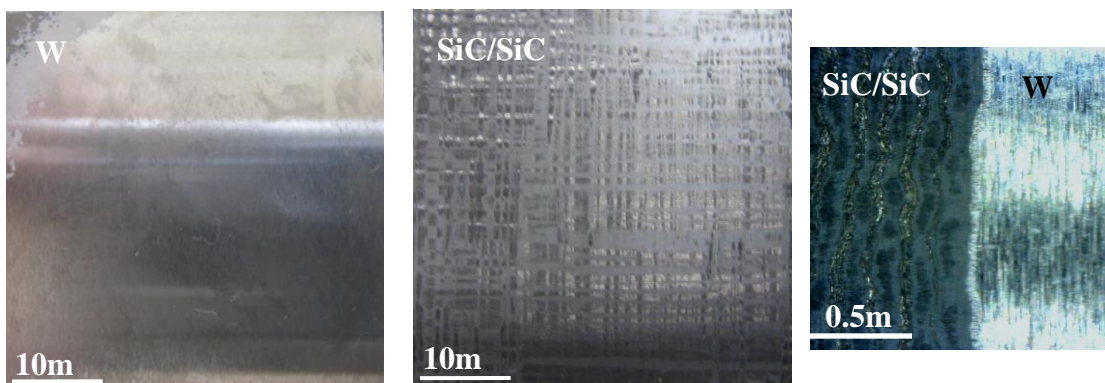


Fig.3.6.The hot pressed tile after polishing (NITE-W/SiC-S2)

After polishing the tile (NITE-W/SiC-S2) was with a total thickness of 1.5mm, where tungsten thickness was 0.7 mm and SiC/SiC thickness was 0.8mm. The polished sample was cut to get tile dimension of 30mmx10mmx1.5mm for divertor plasma exposure test, and small samples 3mmx3mmx1.5mm to investigate microstructure. The tile (NITE-W/SiC-S2) image after cutting of dimension 30x10x1.5 is illustrating in **Fig.3.7**, where the macro structure and morphology of tungsten and SiC/SiC surfaces showed smooth tungsten surface and coherent SiC fibers and matrix on SiC/SiC surface, where W-SiC/SiC side showed sufficient bonding between tungsten and SiC/SiC, and clear interphase layer, the interphase layer appeared in corrugated profile along the side view of the tile, this corrugated profile was due to the pliable form of the started material of prepreg sheets and the tungsten powder

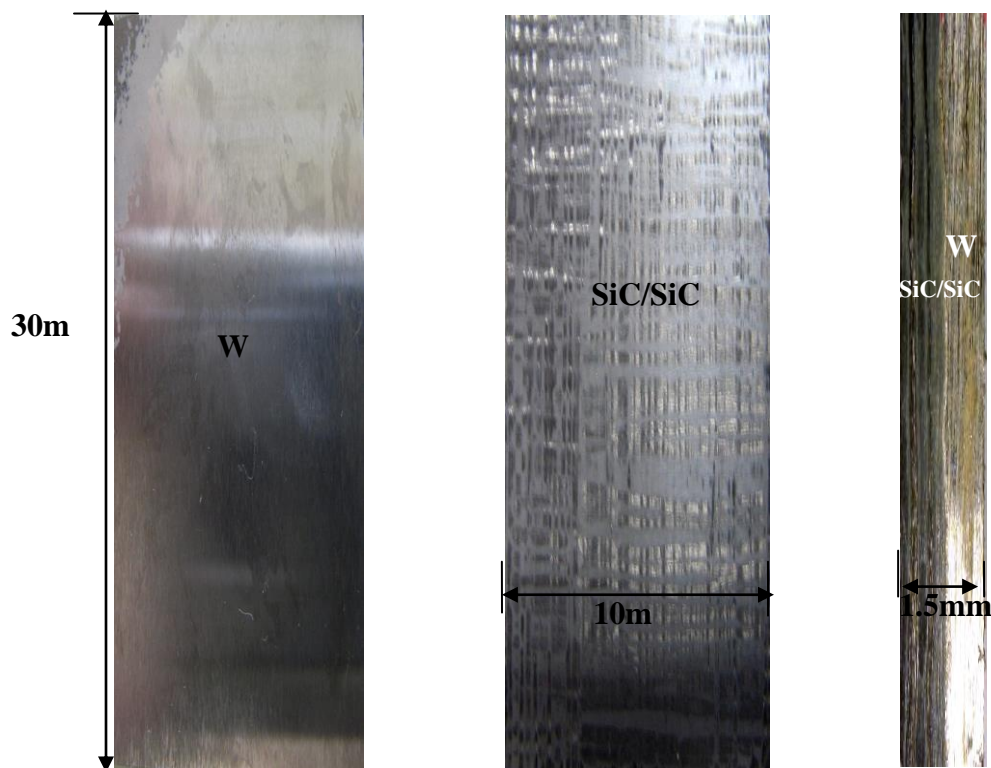


Fig.3.7.The tile (NITE-W/SiC-S2) after cutting

The following figure (**Fig.3.8**) is showing the side view of the tile (NITE-W/SiC-S2), around the circumference, where the sufficient bonding between tungsten and SiC/SiC was clear and interphase layer was coherently between tungsten and SiC/SiC.

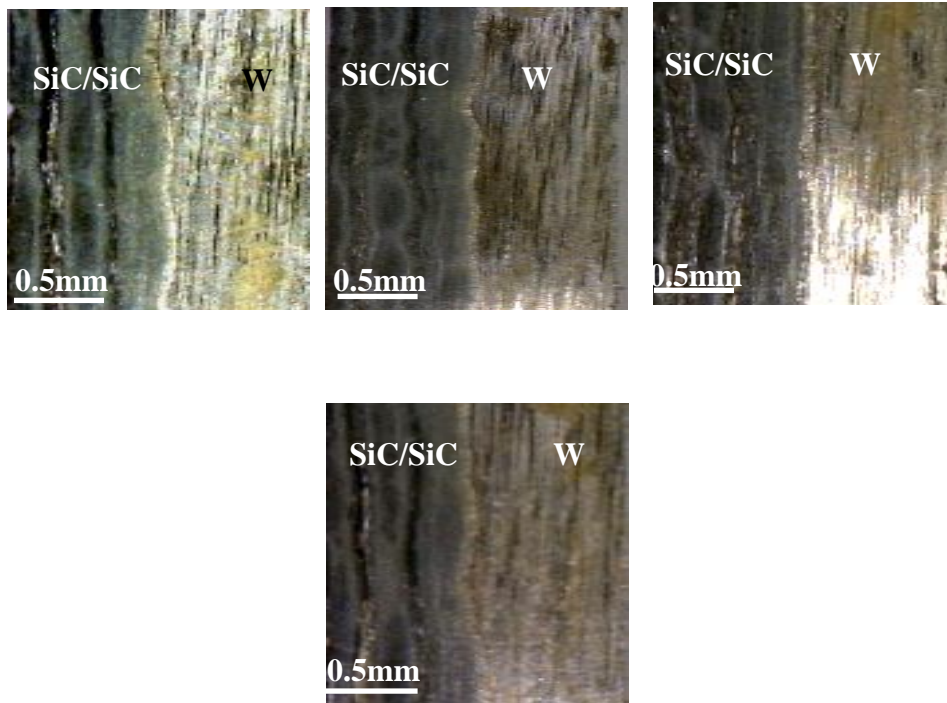


Fig.3.8.The side views of the tile (NITE-W/SiC-S2); around the circumference.

3-4-Microstructure investigation of the tile (NITE-W/SiC-S2)

SEM images of W-SiC/SiC side view showed a coherent and sufficient bonding, and interphase layer showed intermittent elements of W, C, and silicon, due to volumetric diffusion. Detailed analyses will conduct in the micro structure study.**Fig.3.9** showing SEM images of W-SiC/SiC side.

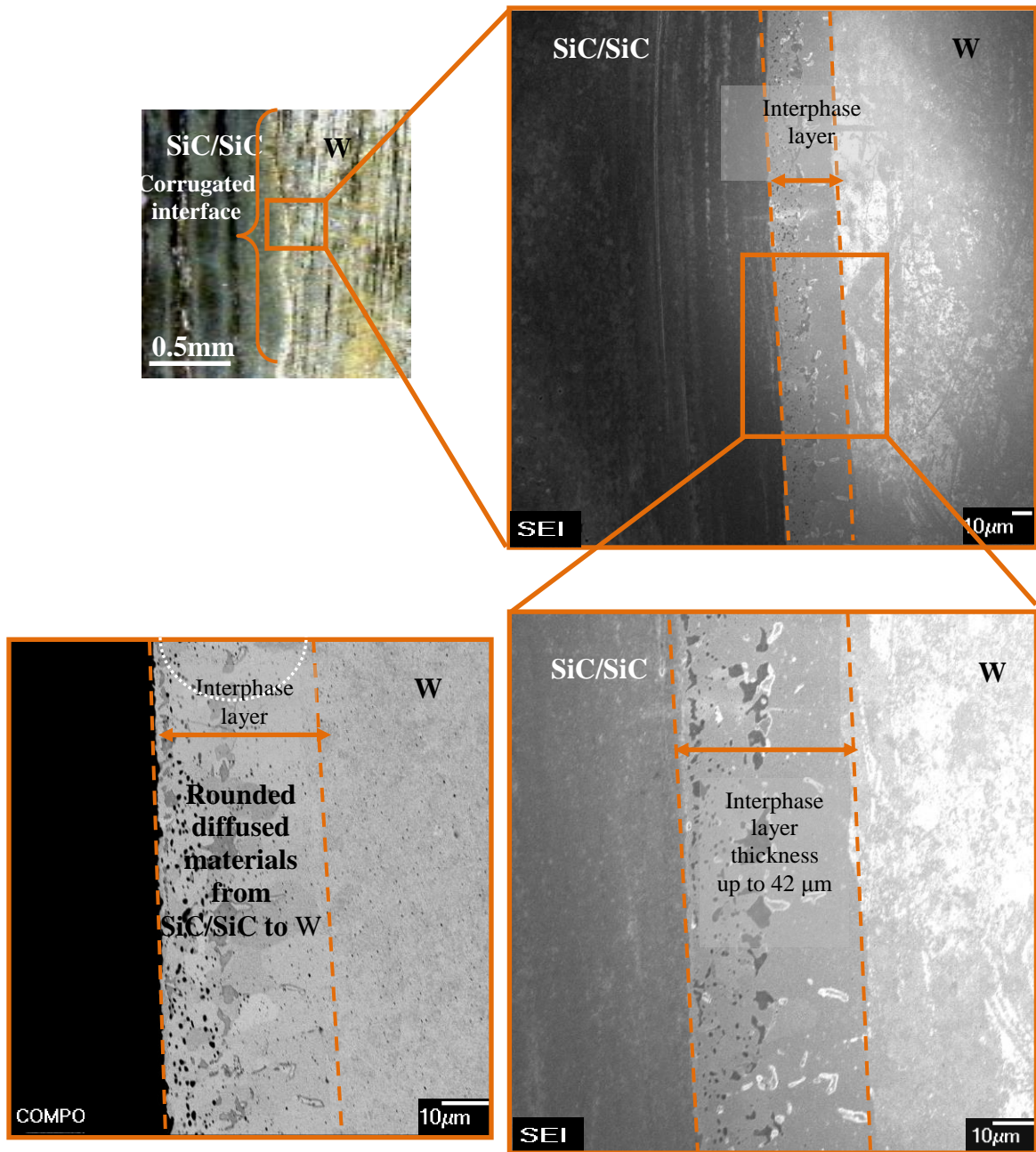


Fig.3.9. SEM images of W-SiC/SiC side of the tile (NITE-W/SiC-S2)

3-5-Fabrication of tile (NITE-W/SiC-Dh1)

The tile (NITE-W/SiC-Dh1) was fabricated, by solid state diffusion bonding, where tungsten plate and premade composite of SiC/SiC were consolidated together by hot press technology. Horizontal rolled tungsten plate was used as W armor; to study the effect of grain orientation by rolling on the heat flux durability, where anisotropic thermal conductivity of tungsten, due to different rolling direction had been investigated[14].The dimensions of SiC/SiC composite and the horizontal tungsten plate were 40.47mm x 22.03 x 1.53mm. After preparation the starting materials of tungsten plate and SiC/SiC composite, both materials was pressed under pressure up to 17.6Mpa and maximum temperature up to 1600°C.The process of hot press was commenced with gradient increase of temperature to 1100°C, with rate of 20°C /min, then the rate of temperature was increased to 10°C/min, until reached to maximum temperature of 1600°C, then the time was held; for 1 hour, after holding time the temperature started to be decreased; with the rate of 10°C to the room temperature. When the pressure reached to 17.6 Mpa, then the pressure was held for two hours and 42 minutes, after that the pressure was started to be decreased gradually to 10 Mpa. After the hot press was finished the sample was left to be cooled down, **table.3.4** is showing the specification of the starting materials and the hot pressed tile. The conditions of hot press process are showing in the **Fig.3.10**

Specification	SiC/SiC composite	W plate	Hot pressed Sample
Weight	3.4g	21.01g	24.95g→24.8g
width	22.03mm	22.03mm	22.7mm
Length	40.47mm	40.47mm	40.5mm
thickness	1.53mm	1.53mm	2.8mm

Table.3.4.The specification of the starting materials and the hot pressed tile (NITE-W/SiC-Dh1).

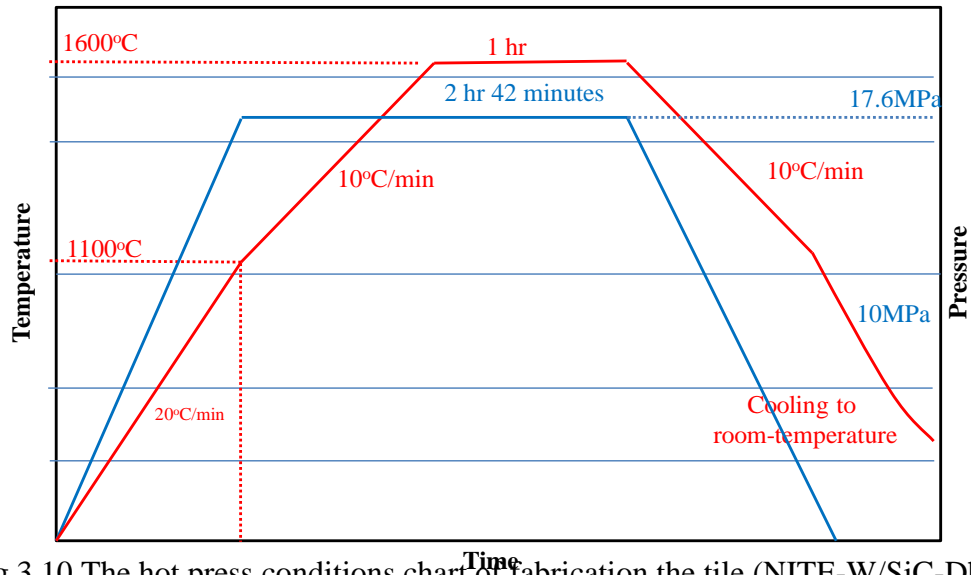


Fig.3.10.The hot press conditions chart of fabrication the tile (NITE-W/SiC-Dh1)

The picked up hot pressed tiles was investigated by digital camera and microscope, where the graphite traces was cover the tiles from all sides and both surface of tungsten and SiC/SiC. **Fig.3.11** is showing the images of the hot pressed tile (NITE-W/SiC-Dh1)

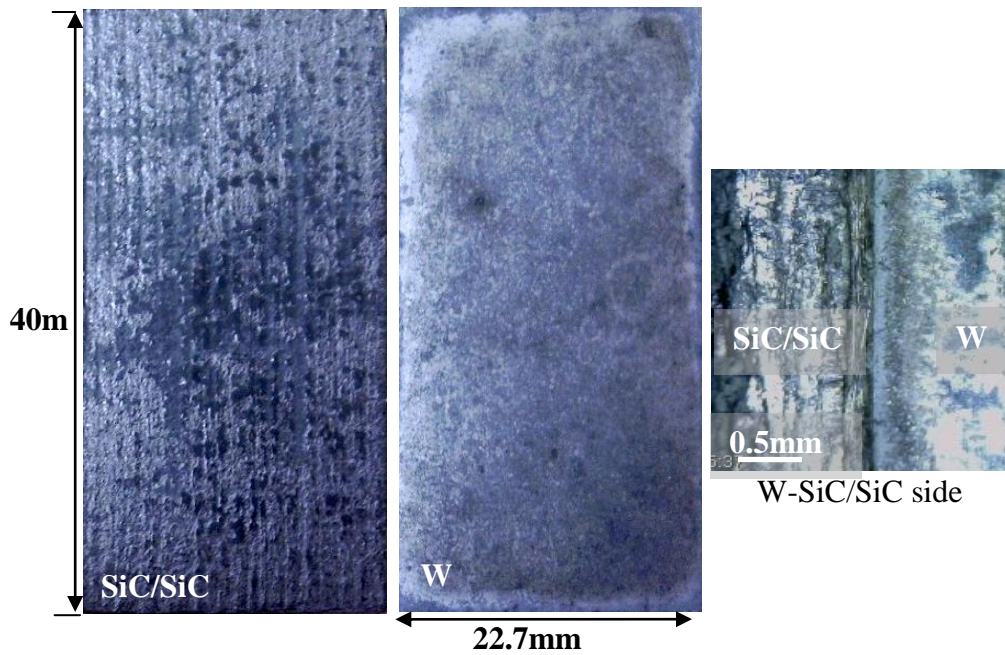


Fig.3.11.The hot pressed tile (NITE-W/SiC-Dh1)

The hot pressed tiles (NITE-W/SiC-Dh1); was polished and cut to the dimension of 30mm x 10mm x 1.5mm, to be appropriate for divertor plasma exposure test , and to receive small samples for microstructure investigation. The polished tile is illustrating in the **Fig.3.12**. The tile with dimension 30mm x 10mm x 1.5mm is illustrating in **Fig.3.13**.

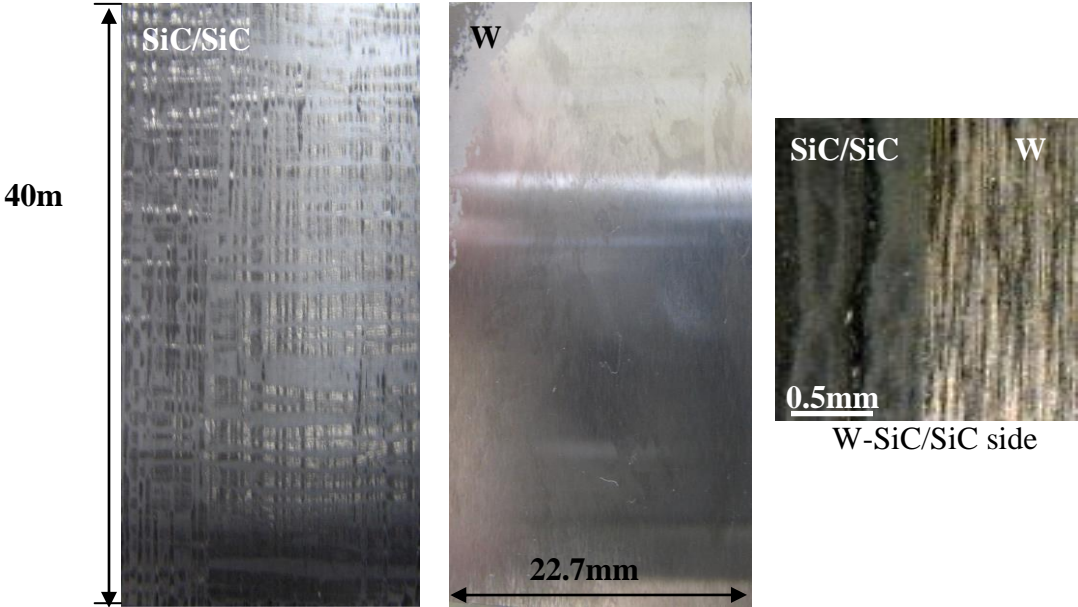


Fig.3.12.The hot pressed tile (NITE-W/SiC-Dh1) after polishing.

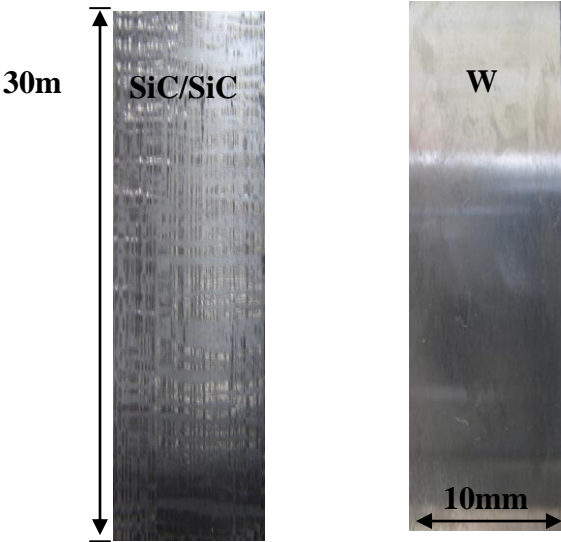


Fig.3.13.The tile (NITE-W/SiC-Dh1) after cutting

It was noticed that the side view of W-SiC/SiC side; the interphase layer appeared much thinner than the interphase layer of the tile (NITE-W/SiC-S2), the interphase layer also appeared straight and coherent between W and SiC/SiC. The side view images of the side view W-SiC/SiC around the circumference(**Fig.3.14**) showed sufficient bonding around the circumference of the tile, and showed coherent SiC fiber/SiC matrix phase, no lamination or fiber pull out.

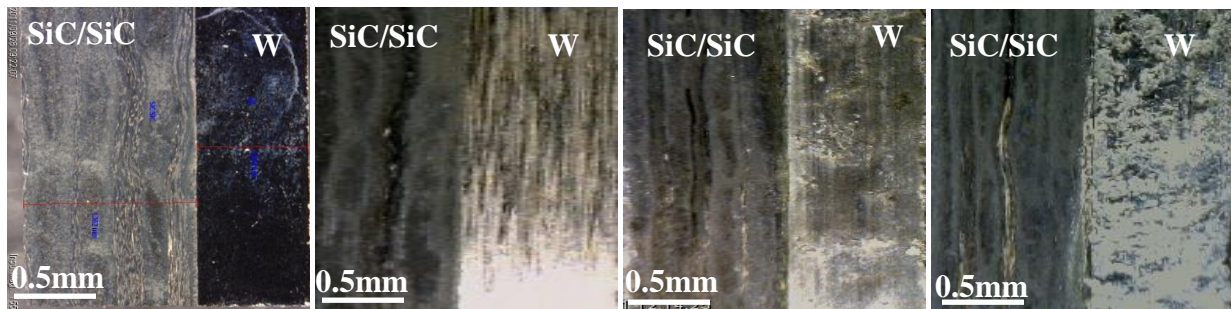


Fig.3.14.The side views of the tile (NITE-W/SiC-Dh1); around the

3-6-Microstructure investigation of the tile (NITE-W/SiC-Dh1)

SEM images of W-SiC/SiC side view showed; a coherent and sufficient bonding, and interphase layer showed intermittent elements of W, C, and silicon, due to volumetric diffusion. Detailed analyses; will conduct in the micro structure study, but the investigation showed that there was tiny bores between fibers, due to poor infiltration, beside fiber deterioration near the interface.**Fig.3.15** showing SEM images of W-SiC/SiC side. The thin and straight interphase layer was due to the solid state diffusion bonding between W& SiC/SiC.

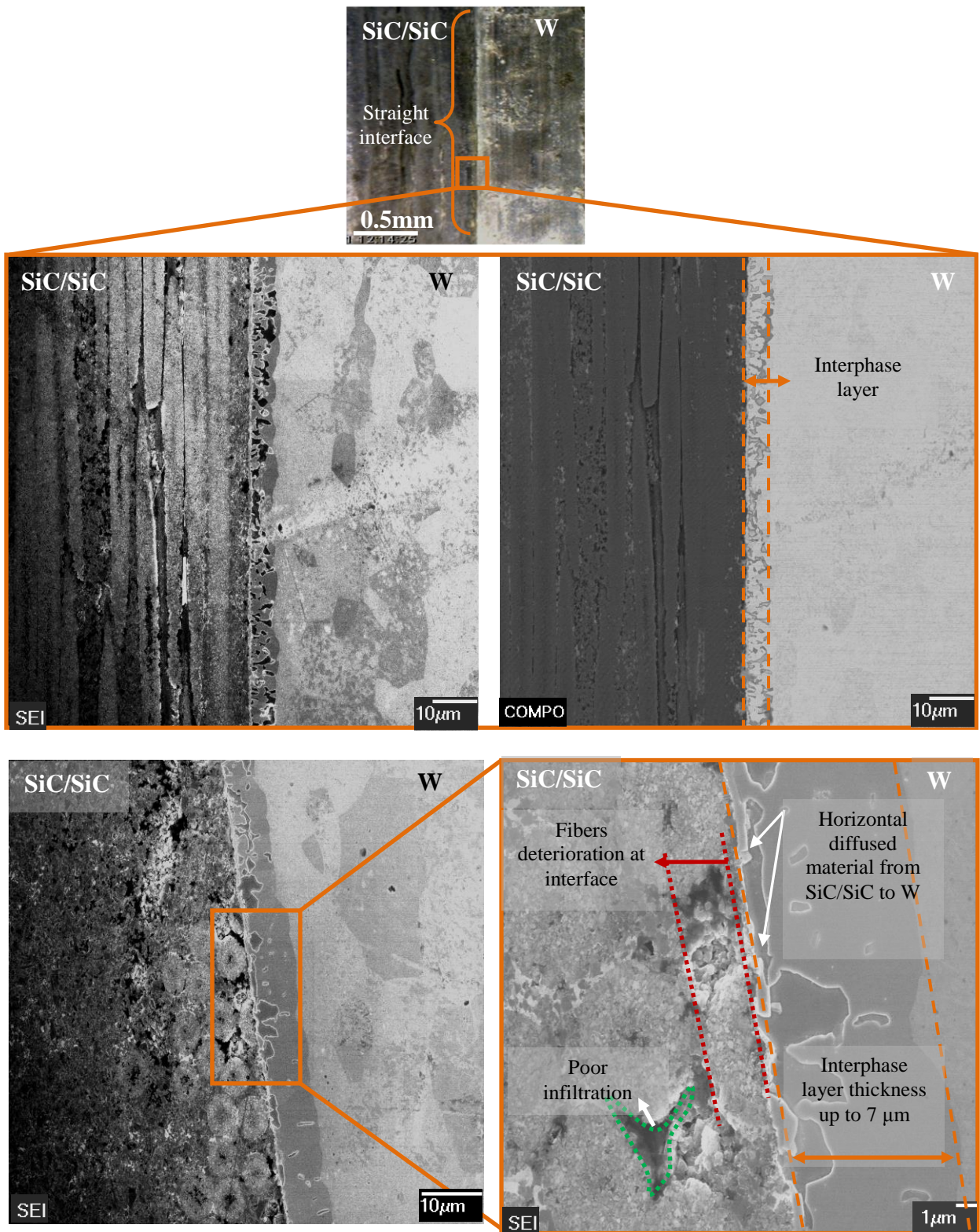


Fig.3.15. SEM images of W-SiC/SiC side of the tile (NITE-W/SiC-Dh1)

3-7-Fabrication of tile (NITE-W/SiC-Dv1)

The fabrication of the tile (NITE-W/SiC-Dv1); was conducted also by solid state diffusion bonding, where the consolidation was accomplished between vertical rolled tungsten plate, and pre-made SiC/SiC composite, where the usage of vertical rolled tungsten plate; can be argued due to the same reason in the case of the horizontal rolled tungsten plate of the tile (NITE-W/SiC-Dv1), where the anisotropic thermal conductivity of the vertical rolled tungsten plate had been investigated to be 110W/mK[14].both of tungsten tiles and SiC/SiC composite were prepared, where four vertical rolled tungsten plates were used, the dimensions of each tungsten plate were; 20mm x10.1mm x1.2mm, the dimensions of SiC/SiC composite were; 40.15mm x22mm x 2.16mm.The prepared sample was arranged inside the graphite mold as showing in **Fig.3.16**.

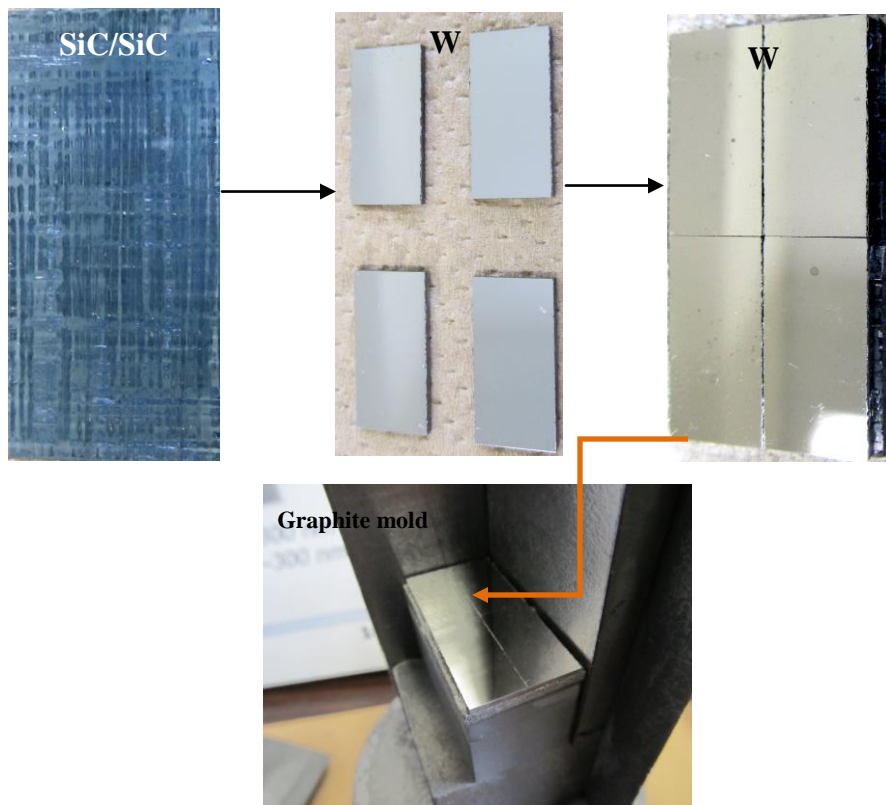


Fig.3.16.The arrangement of sample inside graphite mold to fabricate tile (NITE-W/SiC-Dv1)

After the arrangement of W plates and composite SiC/SiC, the hot press started to fabricate the tile (NITE-W/SiC-Dv1), where the starting material was pressed under pressure up to 16 Mpa and maximum temperature up to 1600 °C. The process of hot press was commenced with gradient increase of temperature to 1100 °C, with rate of 20°C /min, then the rate of temperature was increased to 10°C/min, until reached to maximum temperature of 1600°C, then the time was held; for 1 hour, after holding time the temperature started to be decreased; with the rate of 10 °C to the room temperature. When the pressure reached to 17.6 Mpa, then the pressure was held for two hours and 42 minutes, after that the pressure was started to be decreased gradually to 10 Mpa. After the hot press was finished the sample was left to be cooled down, **table.3.5** is showing the specification of the starting materials and the hot pressed tile. The conditions of hot press process are showing in the **Fig.3.17**. The hot pressed samples are also illustrating in **Fig.3.18**.

Table.3.5. The specification of the starting materials and the hot pressed tile (NITE-W/SiC-Dv1)

Specification	SiC/SiC composite	W plate	Hot pressed Sample
Weight	5.62g	4.66g	24.07g→24g
width	22mm	10.1mm	22mm
Length	40.51mm	20mm	40mm
thickness	2.16mm	1.2mm	3.37mm

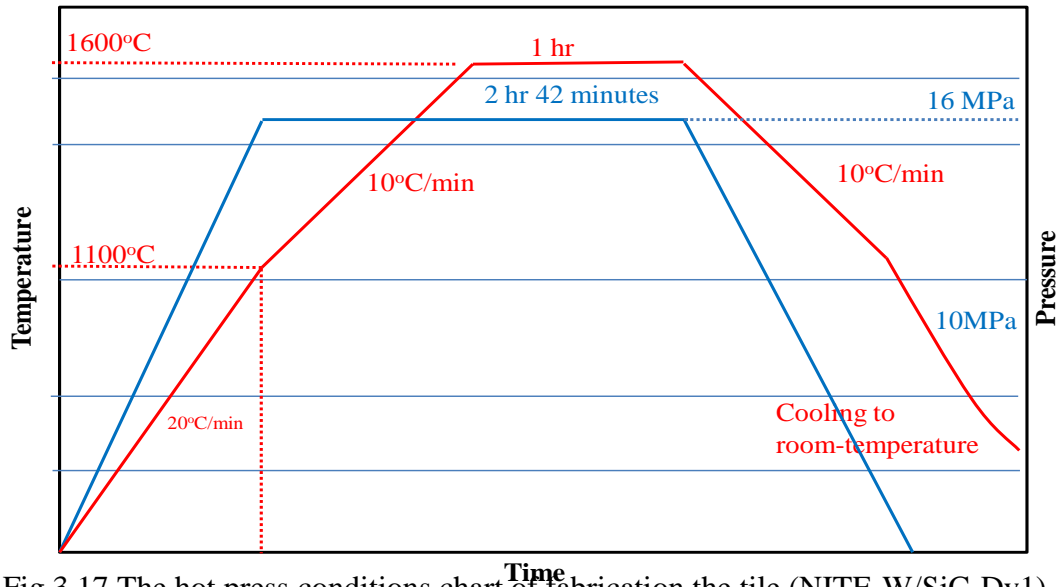


Fig.3.17.The hot press conditions chart of fabrication the tile (NITE-W/SiC-Dv1)

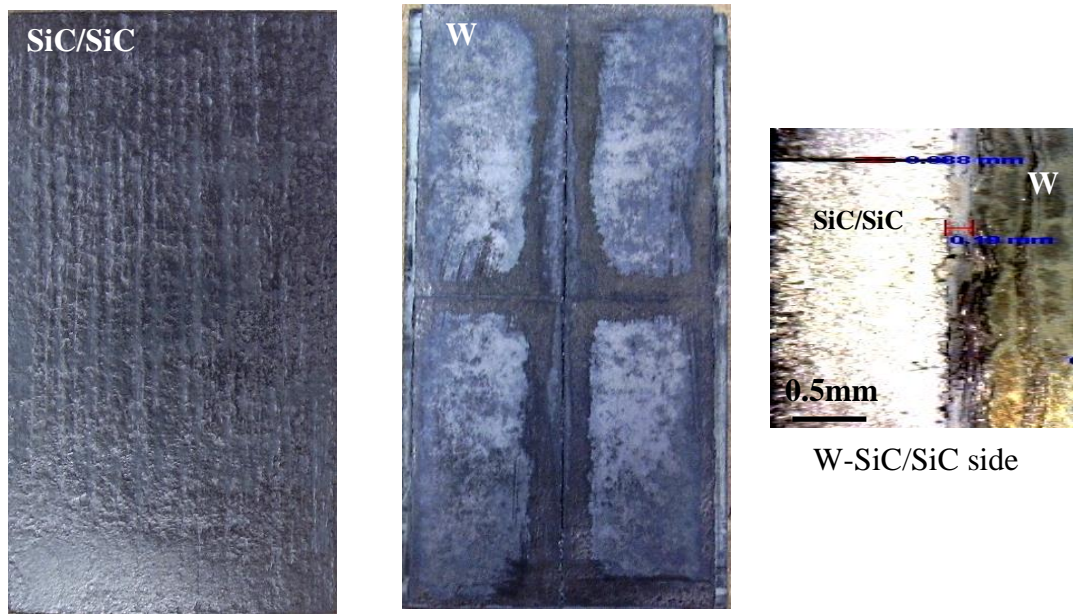


Fig.3.18.The hot pressed tile (NITE-W/SiC-Dv1)

One sample of the tile (NITE-W/SiC-Dv1) was cut and polished for the subsequent divertor plasma exposure test with the same dimensions of the other two tiles (30mm x10mm x1.5mm). The polished and cut sample is illustrating in **Fig.3.19**. The side view images of the side view W-SiC/SiC around the circumference is showing on the Fig.3.20.

3-8-Microstructure investigation of the tile (NITE-W/SiC-Dv1)

The micro structure investigation of the tile (NITE-W/SiC-Dv1) (**Fig.3.21**) showed that the profile of the interface looks a straight form, due to the starting materials of solid plate of SiC/SiC composite and vertical-rolled tungsten plate. The thickness of the interphase layer was up to 6 micrometer, due to the applied temperature up to 1600 °C, and applied pressure up to 20Mpa.

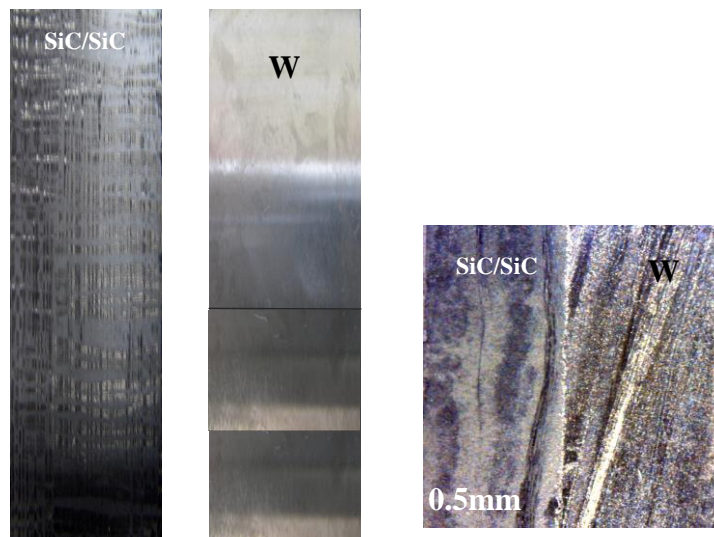


Fig.3.19.The tile (NITE-W/SiC-Dv1) after cutting

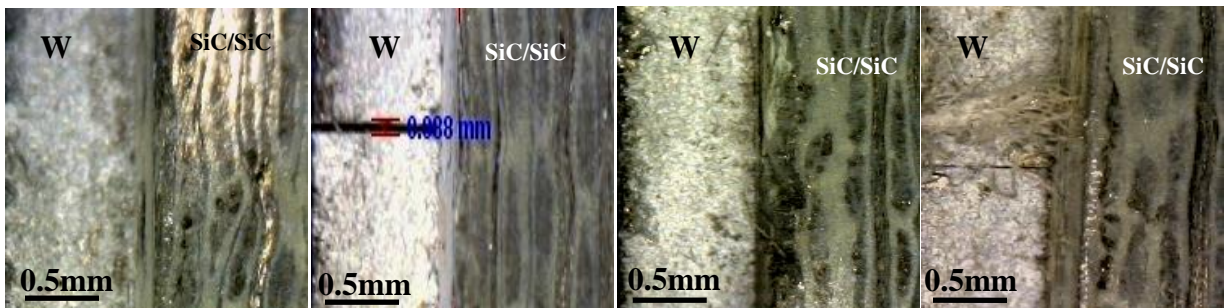


Fig.3.20.The side views of the tile (NITE-W/SiC-Dv1); around the circumference.

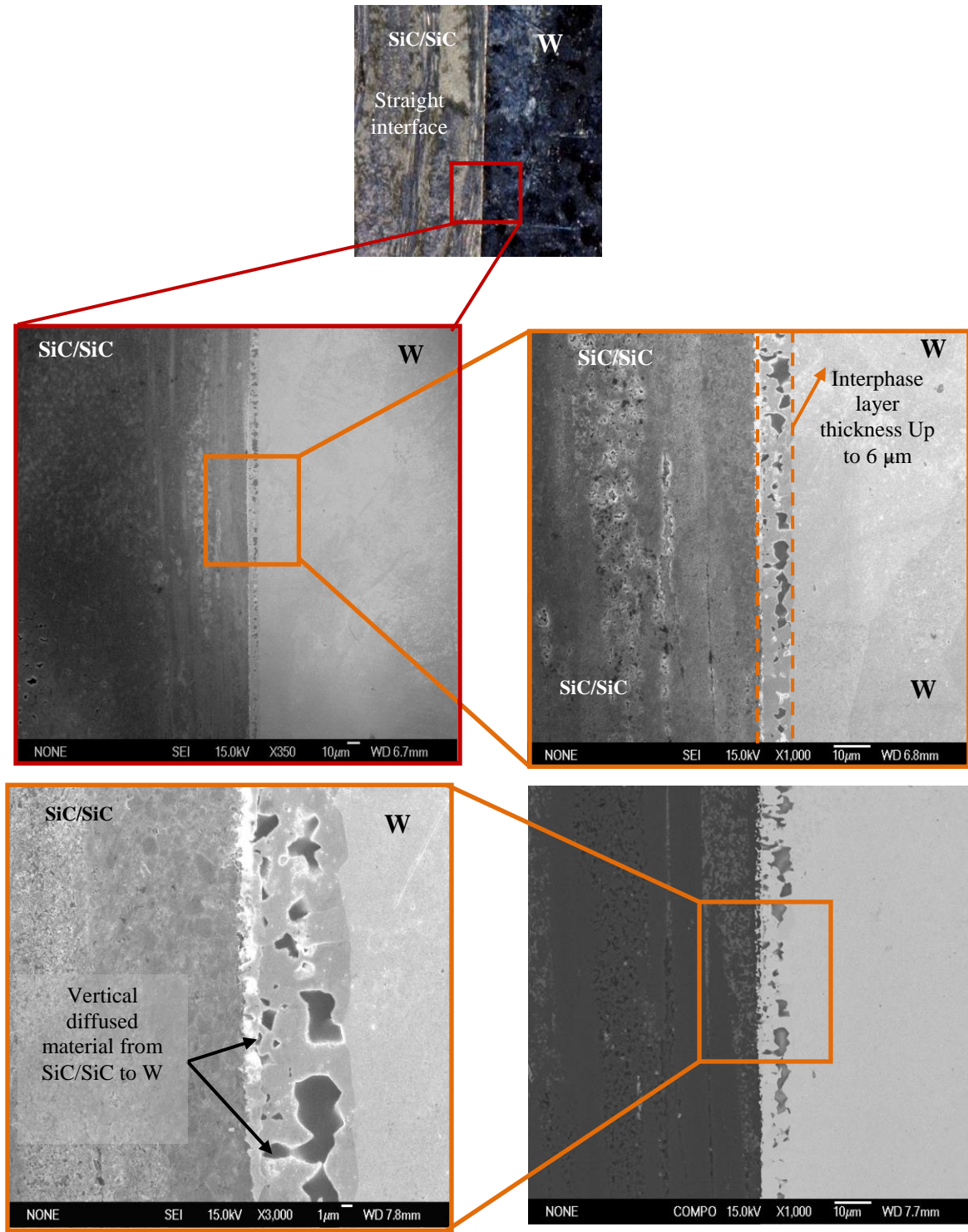


Fig.3.21. SEM images of W-SiC/SiC side of the tile (NITE-W/SiC-Dv1)

3-9-Results and Discussion

The fabrication of hybrid component of W-SiC/SiC, utilizing NITE process was accomplished successfully, where NITE process provided the advantage of simultaneous bonding between W and SiC/SiC and the solidification of the two different materials at one step, where this simultaneous process was accomplished in the case of fabrication of the tile (NITE-W/SiC-S2), and the fabrication of the other two tiles: (NITE-W/SiC-Dh1), (NITE-W/SiC-Dv1) was accomplished by two steps process of fabrication, where solid state diffusion bonding was used.

The micro structure investigation of the fabricated tiles; showed that the conditions of fabrication and starting materials affected on the profile and geometry of the interface layer as well as the thickness of interphase layer of each fabricated tiles.

In the case of the tile (NITE-W/SiC-S2) the profile of the interface (**Fig.3.9**) showed a corrugated form, due to the starting materials of pliable preform of SiC/SiC green sheets and using tungsten powder. The thickness of the interphase layer was up to 42 micrometer, due to the applied temperature up to 1870°C, and applied pressure up to 20Mpa.

In the case of the tiles (NITE-W/SiC-Dh1), (NITE-W/SiC-Dv1) (**Fig.3.15, Fig.3.21**; respectively) the profile of the interface showed a Straight form, due to the starting materials of solid plate of SiC/SiC composite and using horizontal and vertical rolled tungsten plate. The thickness of the interphase layer was up to 7 micrometer, due to the applied temperature up to 1600 °C, and applied pressure up to 20Mpa.

The shape of the diffused materials into tungsten was affected by the grain direction of tungsten, where the diffused materials appeared rounded in the case of using tungsten powder in the tile (NITE-W/SiC-S2), and appears horizontal and vertical in the case of (NITE-W/SiC-Dh1), (NITE-W/SiC-Dv1) respectively.

3.10-Conclusion

Three hybrid components of W-SiC/SiC were fabricated successfully, utilizing NITE process. Hot press technology was used to fabricate the three hybrid components with different operating conditions and different starting materials.

In the case of the tile ID (NITE-W/SiC-S2) the starting materials were the tungsten powder and the preform of SiC/SiC; where one step process of consolidation between W and SiC/SiC was achieved, and the interphase layer was formed with sufficient and coherent bonding conditions, with a corrugated profile at the interface.

In the case of the tile ID (NITE-W/SiC-Dh1), (NITE-W/SiC-Dv1) the starting materials were; a horizontal and vertical rolled tungsten plates respectively, beside SiC/SiC composite; where two steps of consolidation between W and SiC/SiC composite were achieved, the resulted interphase layer was straight and thinner than the case of the tile (NITE-W/SiC-S2).

The reasons of using W powder and different rolled tungsten plates; not only due to the anisotropic thermal conductivity of tungsten materials, but also to study the effect of the grains orientation of each case of tungsten materials toward the interface and study the effect of that anisotropic in the heat flux durability of each tiles after plasma exposure.

The fabricated tiles were polished and cut to be tested inside the large helical device, to study the heat flux durability of each fabricated tile.

References.

- [1] Yi-Hyun Park, Joon-Soo Park, Tatsuya Hinoki, Akira Kohyama, Development of manufacturing method for NITE-porous SiC ceramics using decarburization process, *Journal of the European Ceramic Society*, Volume 28, Issue 3, 2008, Pages 657-661.
- [2] Kazuya.Shimoda, Akira Kohyama, Tatsuya Hinoki, High mechanical performance SiC/SiC composites by NITE process with tailoring of appropriate fabrication temperature to fiber volume fraction, *Composites Science and Technology*, Volume 69, Issue 10, August 2009, Pages 1623-1628.
- [3] Kazuya.Shimoda, Tatsuya Hinoki, Yutai.Katoh, Akira Kohyama, Development of the tailored SiC/SiC composites by the combined fabrication process of ICVI and NITE methods, *Journal of Nuclear Materials*, Volume 384, Issue 2, 15 February 2009, Pages 103-108.
- [4] K. Shimoda, J.S. Park, T. Hinoki, A. Kohyama, Microstructural optimization of high-temperature SiC/SiC composites by NITE process, *Journal of Nuclear Materials*, Volumes 386–388, 30 April 2009, Pages 634-638.
- [5] Kazuya Shimoda, Joon-Soo Park, Tatsuya Hinoki, Akira Kohyama, Influence of pyrolytic carbon interface thickness on microstructure and mechanical properties of SiC/SiC composites by NITE process, *Composites Science and Technology*, Volume 68, Issue 1, January 2008, Pages 98-105.
- [6] Joon-Soo Park, Akira Kohyama, Tatsuya Hinoki, Kazuya Shimoda, Yi-Hyun Park, Efforts on large scale production of NITE-SiC/SiC composites, *Journal of Nuclear Materials*, Volumes 367–370, Part A, 1 August 2007, Pages 719-724.
- [7] Yi-Hyun Park, Tatsuya Hinoki, Akira Kohyama, Development of multi-functional NITE-porous SiC for ceramic insulators, *Journal of Nuclear Materials*, Volumes 386–388, 30 April 2009, Pages 1014-1017.
- [8] Kazuya Shimoda, Tatsuya Hinoki, Akira Kohyama, Effect of additive content on transient liquid phase sintering in SiC nanopowder infiltrated SiCf/SiC composites, *Composites Science and Technology*, Volume 71, Issue 5, 22 March 2011, Pages 609-615.

- [9] Y Katoh, S.M Dong, A Kohyama, Thermo-mechanical properties and microstructure of silicon carbide composites fabricated by nano-infiltrated transient eutectoid process, *Fusion Engineering and Design*, Volumes 61–62, November 2002, Pages 723-731.
- [10] Y Katoh, A.Kohyama, T.Nozawa, M Sato, SiC/SiC composites through transient eutectic-phase route for fusion applications, *Journal of Nuclear Materials*, Volumes 329–333, Part A, 1 August 2004, Pages 587-591.
- [11] M.-S.Suh, A.Kohyama. *Int.J.Mod.Phys.B* 24 (15-16)(2010) 2934-2939.
- [12] M.-S.Suh.T.Hinoki,A.Kohayam,*Tribol.lett.*,doi;10.1007/s11249-010\9658-5.
- [13] M.-S.Suh, et al., *Ceram.Eng.Sci.Proc.*31(2)(2010)275-284.
- [14] M.Reith, A.Hoffmann, B.Dafferner, S.Heger, U.Jäntschi, M.Klimenkov, et al., Tungsten as structure DEMO divertor material, in: *Proceedings of Annual Meeting on Nuclear Technology*, Dresden, Germany, 2009.

Chapter-4
Divertor Plasma Exposure Test Inside
LHD.

4-Divertor Plasma Exposure Test of W-SiC/SiC dual layer tiles Inside the Large Helical Device (LHD)

4-1-Overview of the Large Helical Device (LHD)

The Large Helical Device (LHD) project involves construction of the world's largest superconducting helical device, which employs a heliotron magnetic field originally developed in Japan. The objectives are to conduct fusion-plasma confinement research in a steady-state machine and to elucidate important research issues in physics and engineering for helical plasma reactors. The LHD comprises a Plasma confinement device that employs superconducting coils, plasma heating systems and devices to measure and record plasma properties and phenomena [1-7]. The schematic view as shown in **Fig.4.1.[8]** is layout of the main component of the LHD .The specifications of the LHD related to dimension and

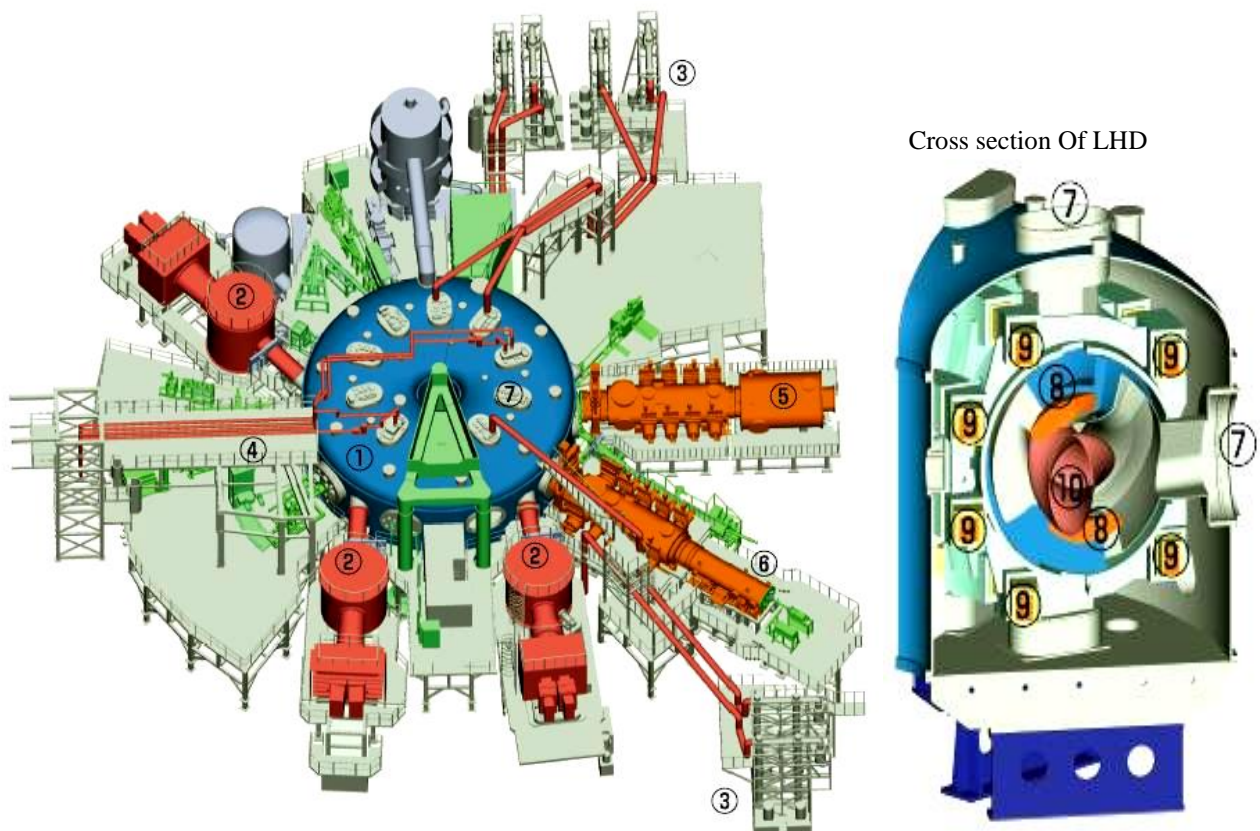


Fig.4.1.Schematic view of the main components of LHD, where
1-LHD ; 2-Neutral beam injection heating device ;3-Ion cyclotron range-of-frequency heating device (coaxial conduit for power transmission and stub tuner) ; 4-Electron cyclotron heating device (waveguide for power transmission);5-Local Island Divertor (LID) ;6-Vacuum pumps; 7-Diagnostic ports; 8-Superconducting helical coils; 9-Superconducting poloidal coils; 10-Plasma

Outer diameter of the machine	13.5m
Toroidal plasma diameter	Approx. 8m
Poloidal plasma diameter	1.0 to 1.2m
Magnetic field B_0/B_{max}	3/6.6T (4/9.2T)
Helical pitch number l/m	2/10
Net weight of the machine	1500t

Table4.1.The specification of the LHD

The general goal of the LHD plasma experiments is Fusion research which is an integrated-system project, was developed step by step with larger devices that were created and installed based on research and development long term plan, improved plasma performance and advances in theory and engineering technique. One objective of the LHD project is to identify physics and engineering issues in helical type fusion reactors. Research on Steady state operation, which is required for a commercial fusion reactor, is another important challenge for the LHD device. In the next step, it is planned to increase the strength of confinement magnetic field, to boost heating power and to extend operation time. These efforts will lead to elucidation of the physics of steady-state currentless plasma. National Institute of Fusion Science (NIFS) is conducting annual plasma exposure test as campaign and invite researchers to conduct their research activities during such campaign, and we used LHD as a facility to test our materials during divertor plasma exposure test, where the development of LHD is promising and providing considerable plasma loads, these plasma load is reliable to test the thermal durability of our test samples against heat flux value close to the condition of divertor plasma exposure of the commercial reactors or future DEMO. The schematic **Fig.4.2 [8]** is showing the status of LHD among the future commercial reactors and other current fusion reactors like JET-60 and Tore Supra and present Tokamak_s. Plasma control inside LHD is a key parameter to achieving high-performance fusion plasma, the plasma control involving the control of confinement field configuration, optimization of fueling, control of impurities in peripheral plasmas, keeping of steady-state plasmas and plasma-wall interaction.

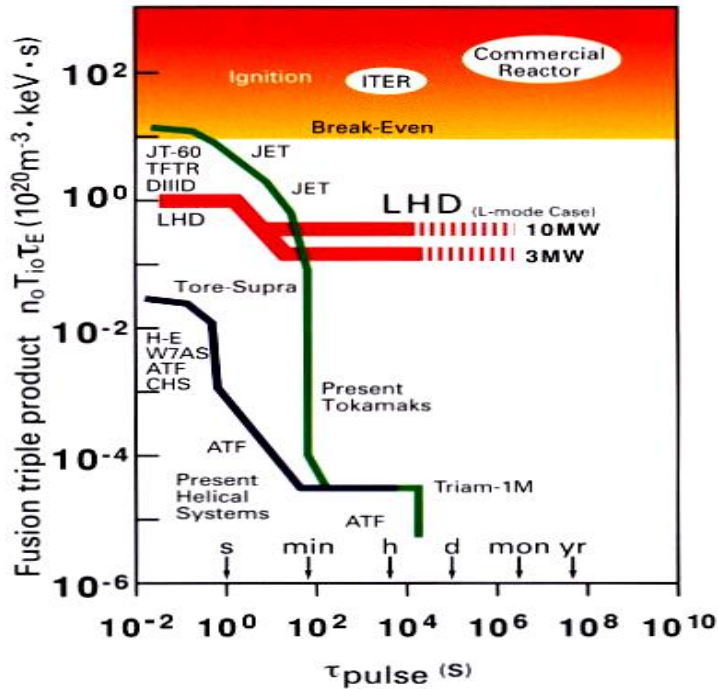


Fig.4.2. The status of LHD among the current and future commercial reactors

A wide range of research and development in plasma control is conducted in parallel with experimental research at the Large Helical Device. To increase plasma density, frozen hydrogen pellets are injected into plasma at high speed, creating high-density confined plasma. There is a facility fixed on the ports of LHD to inject frozen hydrogen pellet inside LHD to control the plasma density as shown in the following schematic **Fig.4.3** [7,8]

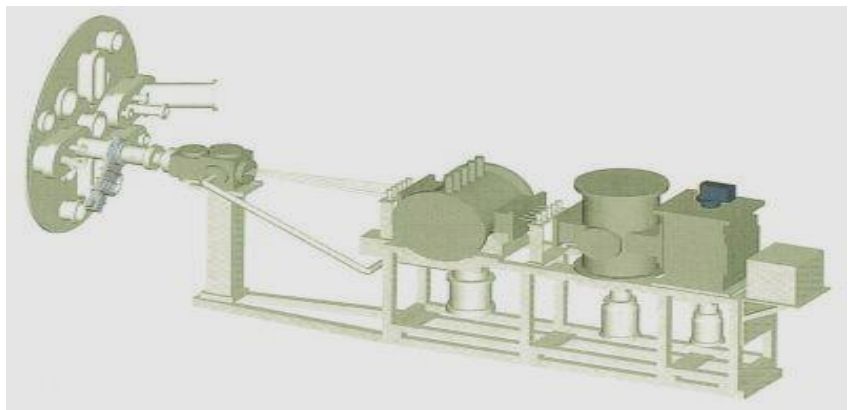
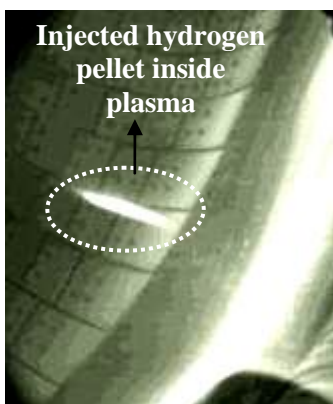


Fig.4.3. Schematic view of the facility to conduct plasma control

Superconducting helical coil of LHD is an important facility to control the confinement of plasma, the superconducting helical coils of LHD are presently cooled with liquid helium at 4.4K (-268.8°C). Sub-cooled liquid helium of 3K and/or pressurized superfluid helium of 1.8K will be used in the future to increase the achievable magnetic field so that the better plasma performance will be obtained. For this purpose, research is being conducted to examine the cryostability of superconductors cooled by sub-cooled liquid helium and to investigate the heat transfer characteristics of superfluid helium. An advanced current lead system using high temperature super conductors is also being developed for the future higher current applications. Plasma heating is other method of plasma control; where there is three heating methods are being applied to attain higher temperature plasmas required for nuclear fusion reactions (100 million degrees, $1 \times 10^{20} / \text{m}^3$) [7]. These methods are: neutral beam injection (NBI), which injects electrically neutral high-energy particles; ion cyclotron range-of-frequency (ICRF) heating and electron cyclotron resonance heating (ECH) [9]. which resonantly heat ions and electrons in a plasma by radio frequency waves or millimeter waves. Research for higher power injection technique and optimization of absorption in plasma is being progressed. **Fig.4.4** is showing schematic photo of ICRF for plasma heating. [7]

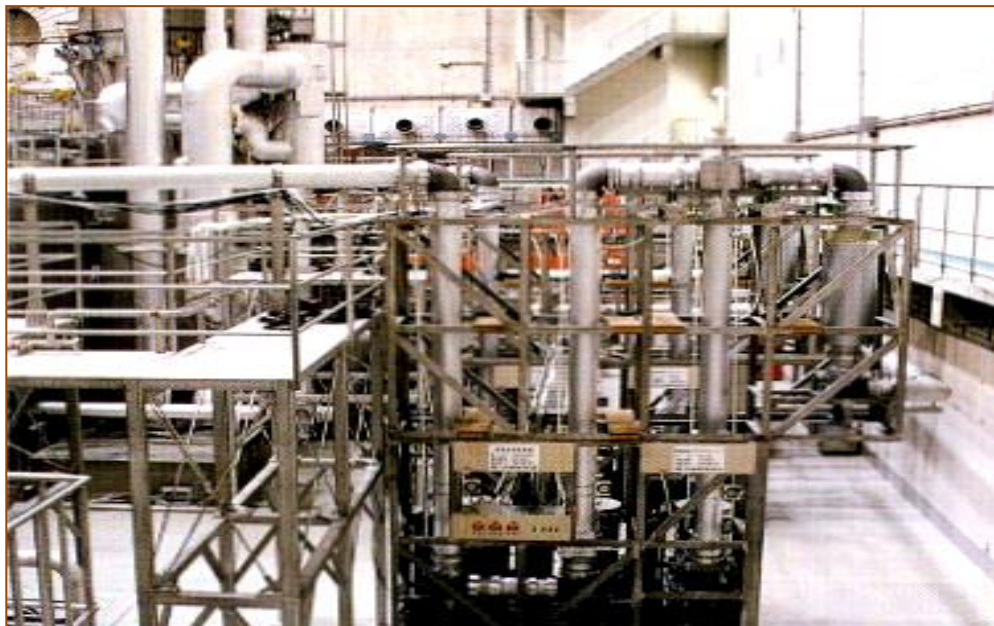


Fig.4.4. Schematic photo of ICRF for plasma heating.

Outside LHD there is many facilities are used to make in situ diagnostic of the plasma, to measure high temperature plasmas in the LHD. These are used to investigate a wide variety of plasma characteristics. Measurement by multiple devices improves reliability of information about the space and time variation of plasma parameters. Schematic overview of plasma diagnostic facilities is shown in **Fig.4.5. [7]**.

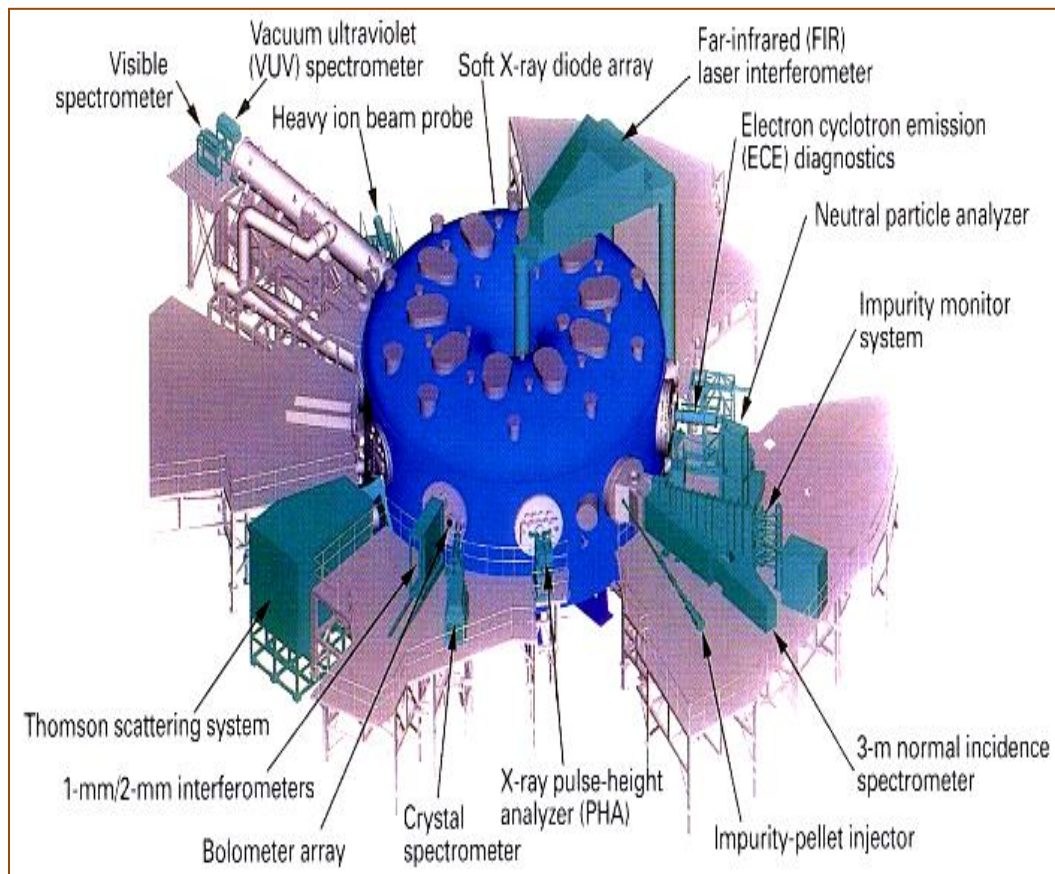


Fig.4.5.Schematic overview of plasma diagnostic facilities in LHD

4-2-Experimental work

The experimental work included; the preparation of the tiles for divertor plasma exposure test, and the mounting of the prepared tiles inside LHD.

4-2-1-Preparation of W-SiC/SiC dual layer tiles for plasma exposure in LHD

After fabrication; the hot pressed tiles: (NITE-W-SiC-S2), (NITE-W-SiC- Dh1), (NITE-W-SiC- Dv1) were prepared by cutting and polishing. Both sides of W and SiC/SiC were polished and cut to a sample dimension of 30x10x1.5mm as aforementioned in the chapter of fabrication of tiles .W layer thickness was 0.8mm and SiC/SiC layer thickness was 0.7mm, as shown in **Fig.4.6**. SiC/SiC side showed a high dense structure with neither pores nor cracks under digital macroscopic investigation up to 100 magnification. W surface showed an integral smooth surface without any observed cracks. Side view of the samples showed sufficient bonding between W and SiC/SiC beside good SiC fiber reinforcing structure observed in SiC/SiC layer.

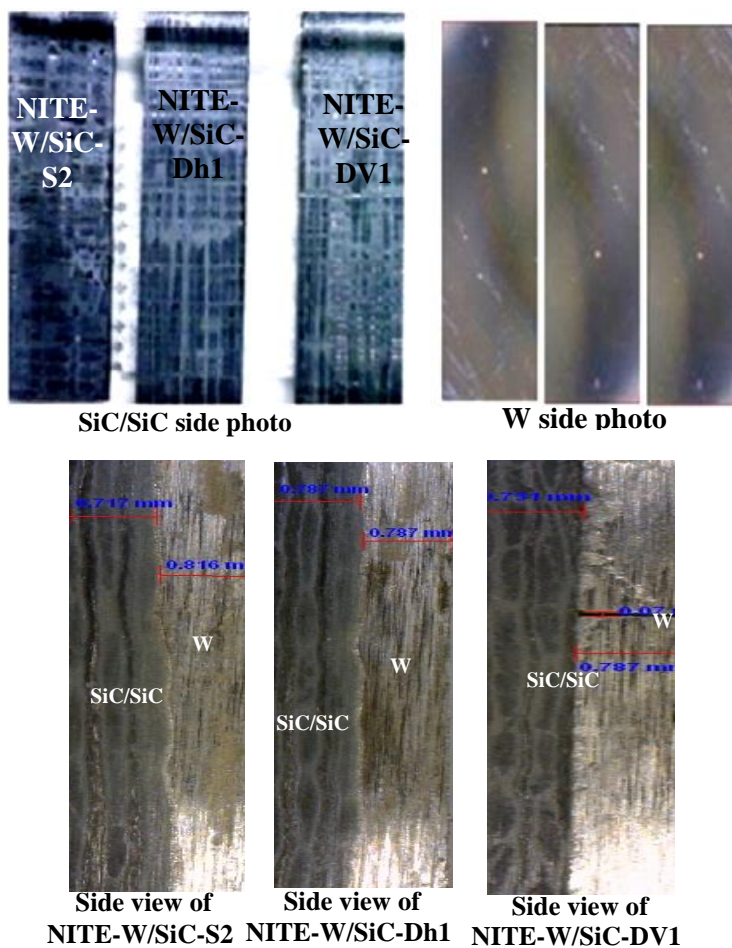


Fig.4.6.The fabricated tiles before LHD

It is noticed from the side view of the tiles the different interface profile, where the tile (NITE-W/SiC-S2) the interface showed corrugated profiles, whereas the tiles (NITE-W/SiCDh1), (NITE-W/SiC-DV1) showed straight interface profile and the gap opening of 0.7 mm in tungsten side at the tile (NITE-W/SiC-DV1) it was due to the fabrication conditions of the tile as aforementioned before where two adjacent plate were used in fabrication, the white nuggets on the tungsten surface were due to the polishing process and some peeled flakes of tungsten appeared on the cross section of the tile (NITE-W/SiC-DV1).

4-2-2-Tiles mounting inside LHD

The prepared tiles were mounted on a stainless steel holder with a molybdenum mask as shown in **Fig.4.7**, the tiles were fixed, where W surface will face the plasma exposure and SiC/SiC works as substrate layer. The mounted samples were placed in the upper port number 4.5 (4.5U) of LHD. Where the LHD has various levels of ports to insert and change ancillaries, also to make diagnosing of the plasma conditions, these ports are the upper and lower ports, beside the zero level and toroidal ports, the upper ports arrangements are shown in the **Fig.4.8**. The test tiles were inserted inside LHD by special device facility of local Island Divertor (LID) (**Fig.4.9.**)[10], where the (LID) is proposed to improve LHD plasma performance. A head of the LID is a 3D-shaped target covered with carbon tiles, which is made by special perturbation coils, and the plasma hits a back side of the head zone. For this reason, heat flux controllability and pumping efficiency are better than the case of a pump limiter [7,10,11]. The samples holder was mounted, where the vertical distance of samples holder was 3.9m from the bottom of the port.

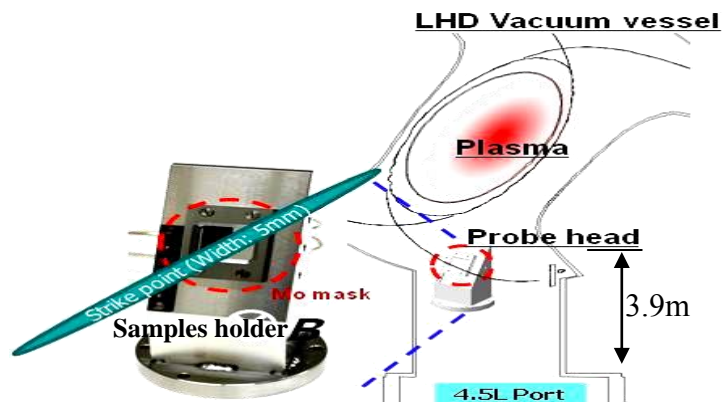


Fig.4.7. Schematic view of the samples holder and the position inside LHD

4-3- Results

4-3-1-Conditions of the Plasma Exposure

After mounting the sample holder inside the LHD in the helical divertor zone as shown in **Fig.4.10**, the tiles were exposed to the divertor plasma exposure test, which was performed followed to the LHD plasma experiment trying to maximize the plasma power with full neutral beam injection (NBI) heating on September 1, 2011. The shot number was #107703, the maximum NBI port through power was 27MW (**Fig.4.11.**), shot length was 5.3 second. The peak plasma stored energy was about 1200KJ (**Fig.4.12.**), and the maximum ion temperature was 2.7 KeV (**Fig.4.13.**). Based on these data, the heat load applied by divertor plasma exposure test of shot Number #107703 was tentatively estimated to be about $10\text{MW}/\text{m}^2$. the LID provided us the possibility to control on the plasma strike width in the location of the mounted sample holder, where it was planned to be 5 mm as shown in the **Fig.4.7**.

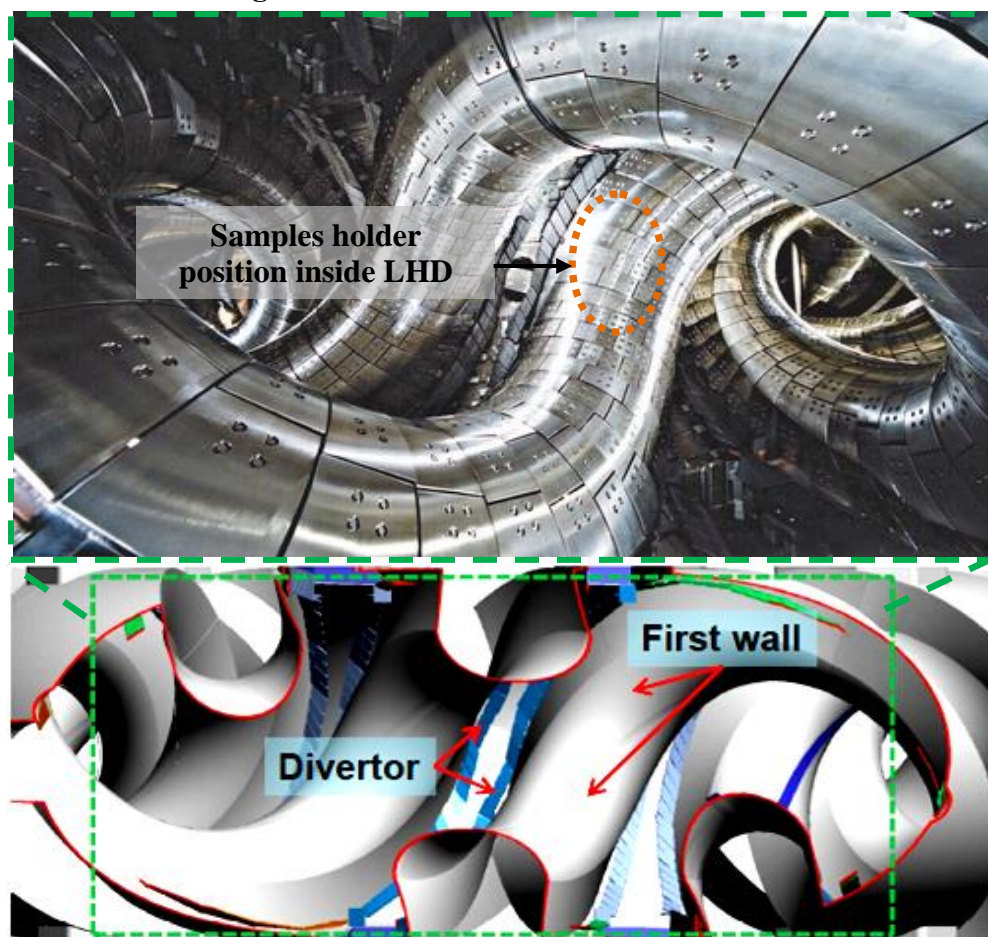


Fig.4.10.Schematic View of the helical divertor and the position of the sample holder

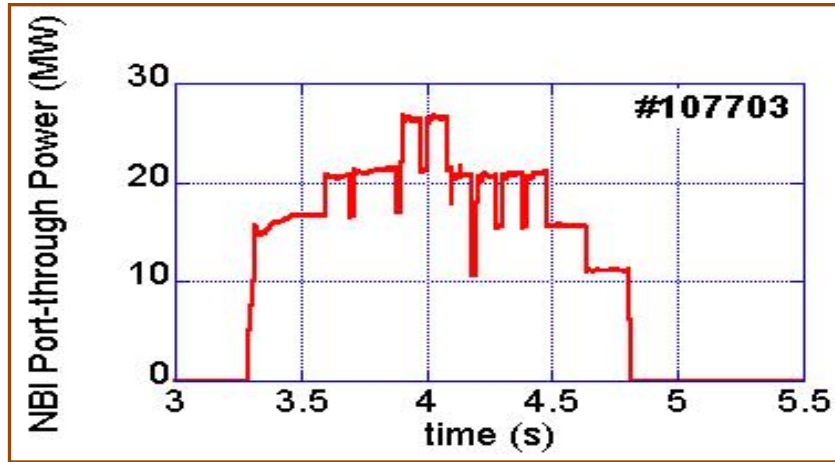


Fig.4.11. Neutral beam injection profile during plasma exposure

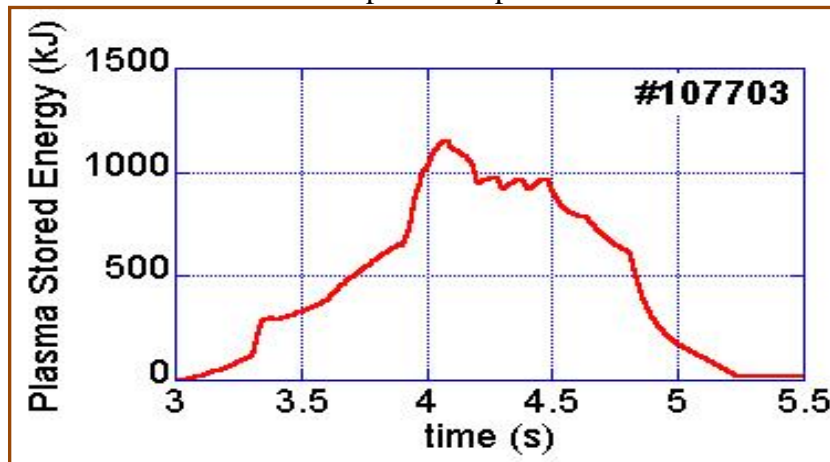


Fig.4.12. plasma stored energy profile during plasma exposure

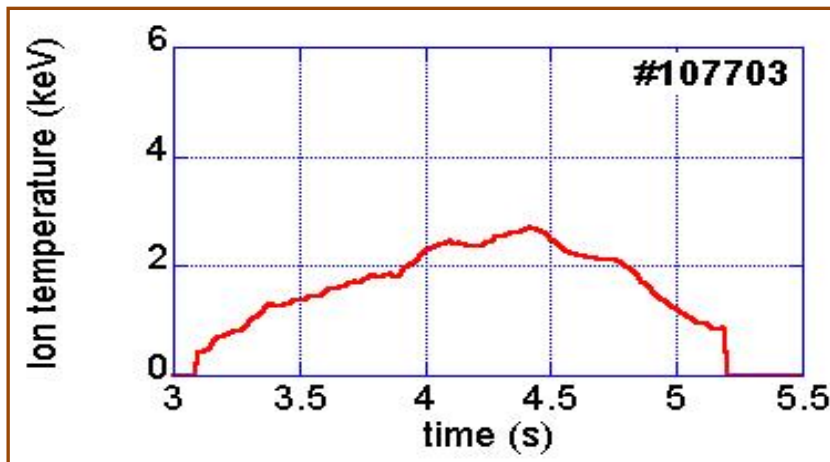


Fig.4.13. Ion temperature profile during plasma exposure

During plasma exposure it was recorded that the peak radiation power was tentatively calculated to be 3000 KW at the second 3.9 as shown in the **Fig.4.14**. As aforementioned that there was a facility to control and diagnosing the plasma condition during the reaction and one of the main plasma parameter it is the plasma density, where the peak of the plasma density was recorded to be 3.5×10^{19} ions/m³, after 5.2 second as shown in **Fig.4.15**. During plasma exposure there was glow discharge process this process caused glowing of 3D-graphite tiles of the Local Island Divertor, therefore it was recorded that the maximum carbon line intensity up to 45 a.u, after 4 seconds and it was recorded that the maximum oxygen line intensity was up to 33 a.u after 5.2 seconds as shown in **Fig.4.16**.

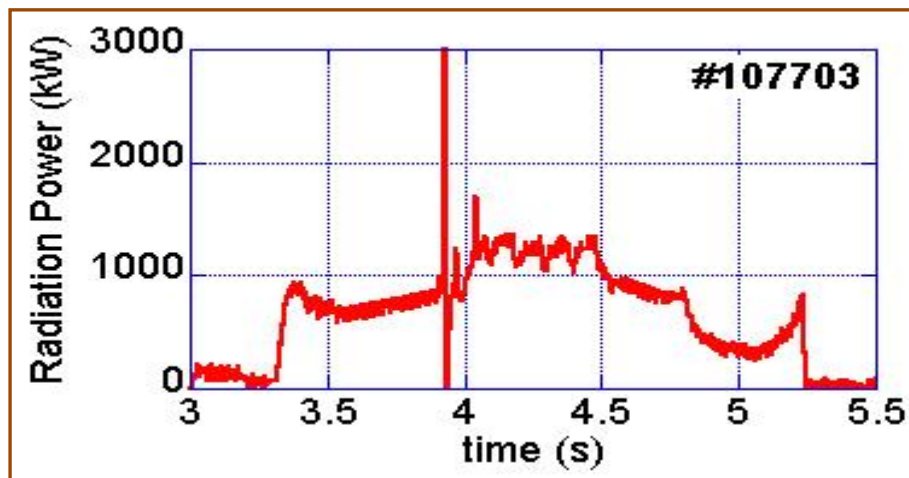


Fig.4.14. Radiation power profile during the plasma exposure

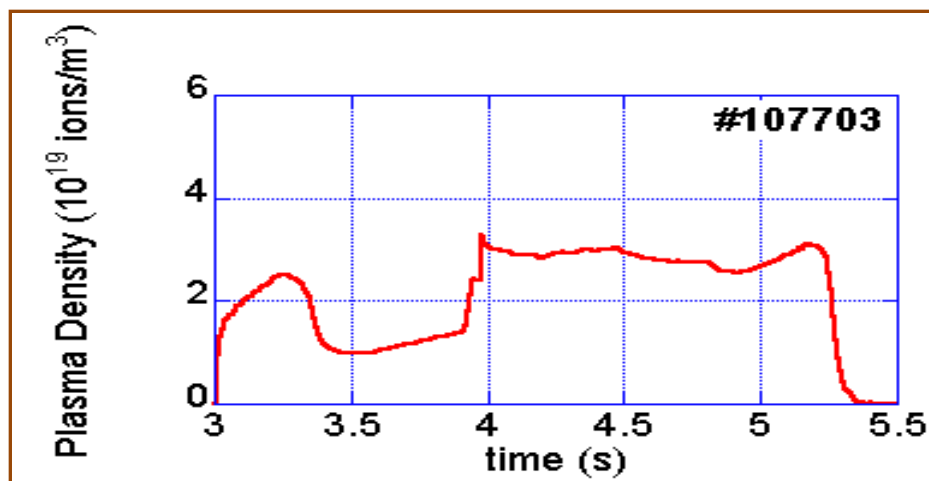


Fig.4.15. Plasma density profile during plasma exposure

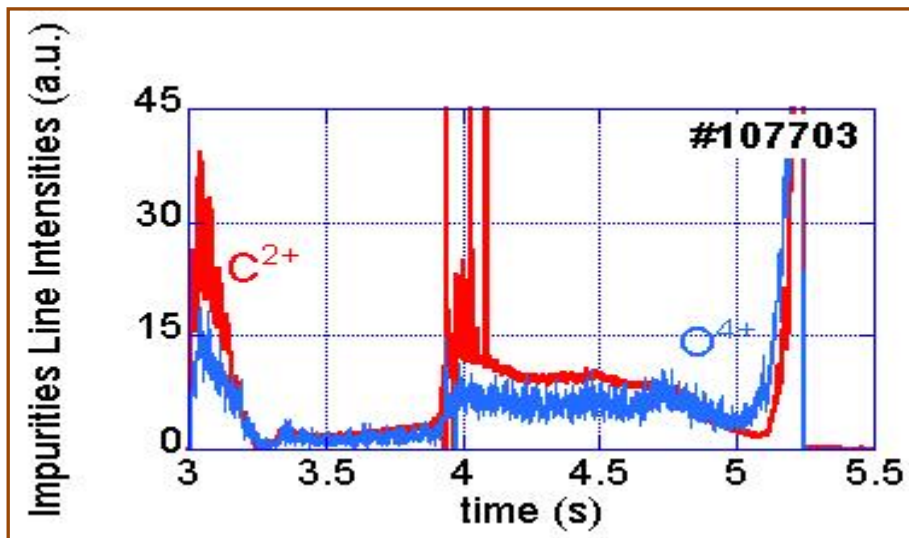


Fig.4.16. Plasma impurities profile during plasma exposure

Although the samples were electrically isolated from the samples holder placed at the top of the manipulator at the port 4.5U, during the plasma exposure very strong movement of the samples with several large sparks were clearly observed through the monitoring camera as illustrating in Fig.4.17.

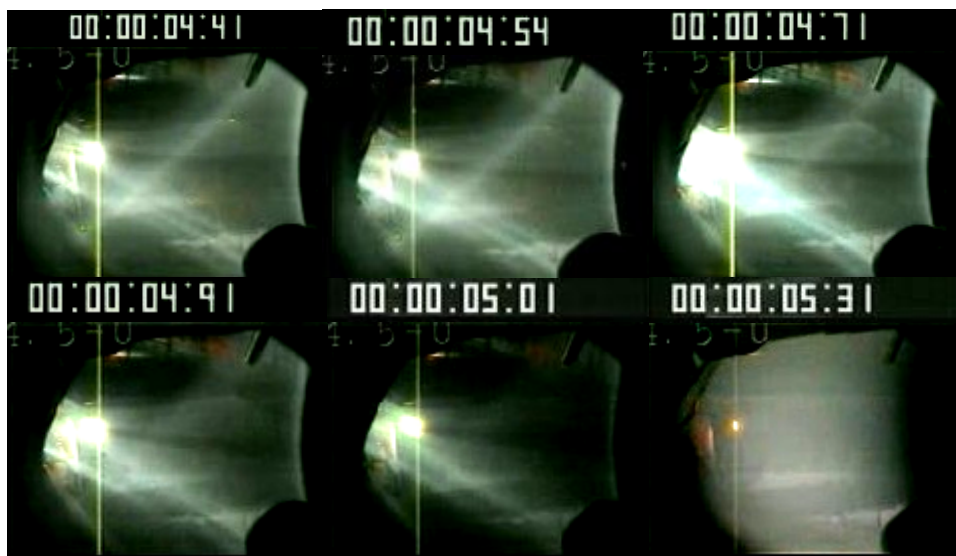


Fig.4.17. Monitoring camera image of samples inside LHD in 4.5U port, illustrating samples movement and strong sparks at different time

4-3-2-Cooling conditions during plasma exposure

After plasma exposure; the irradiated tiles were left to be cooled passively, where there were not any actively cooled tubes inside the samples holder, but there was a water cooling system to cool down the wall of the divertor during plasma exposure, due to the low thermal conductivity of stainless steel; the conduction cooling between the wall of sample holder and actively cooled divertor wall was not expected to be effectively enough to cool down the samples during plasma exposure.

4-3-3-Pick up the irradiated tiles outside the LHD

After the tiles were passively cooled down, the sample holder was picked up outside the LHD, by the same facility of Local Island Divertor (LID), and then the sample holder was investigated visually, and the irradiated tiles were prepared for subsequent investigation. The sample holder after divertor plasma exposure test is illustrating in the **Fig.4.18**. From the preliminary visual investigation it showed that the plasma hit the irradiated tiles almost as planned, and controlled by LID, where the plasma hit the diagonal of the molybdenum mask and there was a clear fused zones on both the three irradiated tiles and the edge of the sample holder, also there was a clear plasma impurities appeared on stainless steel holder, molybdenum mask and the irradiated tiles.

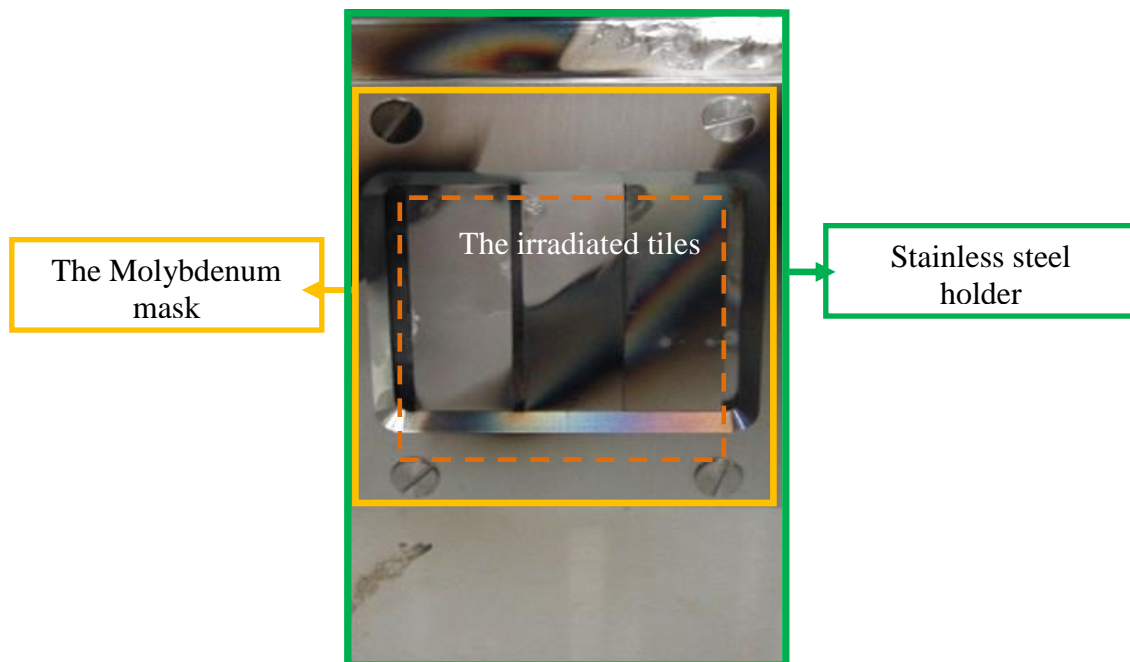


Fig.4.18. The sample holder after divertor plasma exposure test

4-4-Discussion

the irradiated tiles were exposed to a tentatively estimated heat flux up to 10 Mw/m² and the strike conditions of plasma was accomplished as designed and prepared before mounting the samples inside LHD. The plasma strike width was almost 5 mm, but the orientation of the strike direction was shifted upwards, where the effected zones was high on the region of the tile (NITE-W/SiC-S2), (NITE-W/SiC-Dh1), but the tile (NITE-W/SiC-Dv1) was affected in a slightly way. The facility of plasma control succeeded in the control of plasma strike intensity and plasma strike width, beside the facility of neutral beam injection to get the combined effect neutron heat and heat flux produced of plasma itself. The fused zones on the edges of the exposed tiles (NITE-W/SiC-S2), (NITE-W/SiC-Dh1) referred to that the surface temperature at the fused zones reached to the melting point of tungsten which is 3400 °c.

4-5-Conclusion.

The first divertor plasma exposure test inside LHD was successfully accomplished, where the plasma control facilities and the plasma heating ancillaries succeeded to expose the test tiles to the required heat flux where the tentatively estimation of the plasma exposure was 10 Mw/m² as average heat flux. The mounting of the test sample at the location inside LHD was key parameter to expose to such estimated heat flux. Although there was not actively cooled conditions of the exposed tiles during the divertor plasma exposure test; the preliminary investigation of the picked up tiles of hybrid component of W/SiC/SiC showed that the tiles survived from the catastrophic damage i.e. there was not complete melting of the tungsten surface, and there was not a complete debonding along the circumference of the exposed tiles at the interface. The precise macro and micro structure evolution due to the plasma exposure will be shown at Chapter#6.

References

- [1] O.Motojima, Overview of confinement and MHD stability in the Large Helical Device, Nucl. Fusion 45 (2005) 255–S265.
- [2] S.Sudo, Y.Nagayama, Control, data acquisition and remote participation for steady-state operation in LHD, FusionEng.Des.81 (2006)1713–1721.
- [3] H.Chikaraishi, S.Takami, T.Inoue, S.Sakakibara, K. Matsuoka, T.Ise, D.Eto, T.Haga, Current control system of the power supplies for LHD. superconducting coils, IEEE Trans. Appl. Superconductivity 14 (2004) 1431–1434.
- [4] H.Chikaraishi, S.Takami, T.Inoue, K.Nishimura, T.Ise, H.Niwa et al., Control system of dc power supplies for LHD superconducting coils, Fusion Eng. Design 83 (2008) 260–264.
- [5] S.Kubo, Long pulse ECH plasma in LHD, AIP Conf. Proc. 787 (2005) 411–414.
- [6] S.Kubo, T.Shimozuma, Y.Yoshimura, H.Igami, T.Notake, Y.Takitaetal. , Control system for electron cyclotron resonance heating in LHD, Fusion Eng. Design 83 (2008) 256–259.
- [7] http://www.lhd.nifs.ac.jp/en/lhd/LHD_info/home_lhd.html.
- [8] R.Sakamoto, Repetitive pellet fuelling for high-density/steady-state operation on LHD, Nucl. Fusion 46 (2006) 884–889.
- [9] T.Mutoh, Thirty-minute plasma sustainment by ICRF, EC and NBI heating in the Large Helical Device, J. Plasma Fusion Res. 81 (2005) 229–230.
- [10] A.Komori, T.Morisaki, R.Sakamoto, N.Ohyabu, S.Morita, B.J.Perterson, S.Masuzaki, H.Suzuki, M. Shoji, Y.Nakamura, S.Sakakibara, K.Narihara, N. Noda, O.Motojima, The LHD Experimental Group, Edge plasma control with a local island divertor, Journal of Nuclear Materials 313–316 (2003) 1267–1271.
- [11] T.Morisaki, S.Masuzaki, H.Suzuki, A.Komori, N.Ohyabu, O.Motojima, S.Okamura, K.Matsuoka, LHD Experimental Group and CHS Group, Progress of local island divertor experiment, Fusion Engineering and Design 65 (2003) 475–481.

Chapter-5

**[Damage Analysis of Plasma Exposed W
SiC/SiC Tiles By Means of Ultra Sonic
Testing Method.]**

5-Damage Analysis of Plasma Exposed W-SiC/SiC tiles By Means of Ultra Sonic Testing Method

5-1-Overview and background of ultra sonic testing

Ultrasonic Testing (UT) uses high frequency sound energy to conduct examinations and make measurements. Ultrasonic inspection can be used for flaw detection/evaluation, dimensional measurements, material characterization, and more. To illustrate the general inspection principle, a typical pulse/echo inspection configuration as illustrating in **Fig.5.1** A typical UT inspection system consists of several functional units, such as the pulser/receiver, transducer, and display devices. A pulser/receiver is an electronic device that can produce high voltage electrical pulses. Driven by the pulser, the transducer generates high frequency ultrasonic energy. The sound energy is introduced and propagates through the materials in the form of waves. When there is a discontinuity (such as a crack) in the wave path, part of the energy will be reflected back from the flaw surface. The reflected wave signal is transformed into an electrical signal by the transducer and is displayed on a screen. In the applet below, the reflected signal strength is displayed versus the time from signal generation to when a echo was received. Signal travel time can be directly related to the distance that the signal traveled. From the signal, information about the reflector location, size, orientation and other features can sometimes be gained. [1-4].

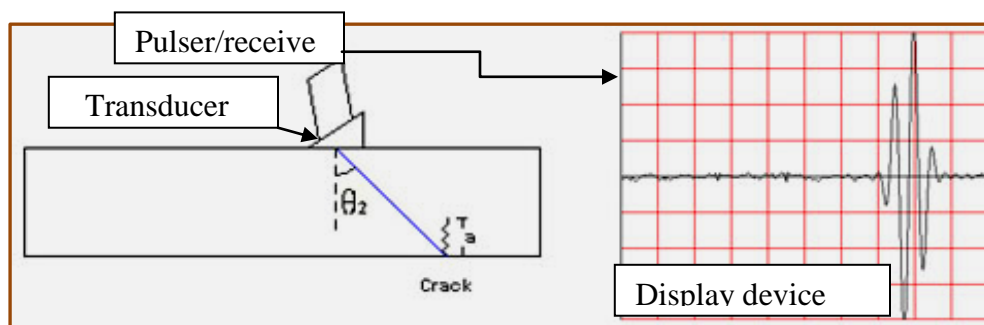


Fig.5.1. Typical pulse/echo inspection configuration

Ultrasonic Inspection is a very useful and versatile NDT method. Some of the advantages of ultrasonic inspection that are often cited include: [1-3]

- 1-It is sensitive to both surface and subsurface discontinuities.
- 2-The depth of penetration for flaw detection or measurement is superior to other NDT methods.
- 3-Only single-sided access is needed when the pulse-echo technique is used.
- 4-It is highly accurate in determining reflector position and estimating size and shape.
- 5-Minimal part preparation is required.
- 6-Electronic equipment provides instantaneous results.
- 7-Detailed images can be produced with automated systems.
- 8-It has other uses, such as thickness measurement, in addition to flaw detection.

As with all NDT methods, ultrasonic inspection also has its limitations, which include

- 1-Surface must be accessible to transmit ultrasound.
- 2-Skill and training is more extensive than with some other methods.
- 3-It normally requires a coupling medium to promote the transfer of sound energy into the test specimen.
- 4-Materials that are rough, irregular in shape, very small, exceptionally thin or not homogeneous are difficult to inspect.
- 5-Cast iron and other coarse grained materials are difficult to inspect due to low sound transmission and high signal noise.
- 6-Linear defects oriented parallel to the sound beam may go undetected.

Reference standards are required for both equipment calibration and the characterization of flaws.

5-2-Sound wave propagation in materials

Ultrasonic testing is based on time-varying deformations or vibrations in materials, which is generally referred to as acoustics. All material substances are comprised of atoms, which may be forced into vibrational motion about their equilibrium positions. Many different patterns of vibrational motion exist at the atomic level; however, most are irrelevant to acoustics and ultrasonic testing. Acoustics is focused on particles that contain many atoms that move in unison to produce a mechanical wave. When a material is not stressed in tension or compression beyond its elastic limit, its individual particles perform elastic oscillations. When the particles of a medium are displaced from their equilibrium positions, internal (electrostatic) restoration forces arise. These elastic restoring forces between particles, combined with inertia of the particles, which leads to the oscillatory motions of the medium. [3].

In solids, sound waves can propagate in four principle modes that are based on the way the particles oscillate. Sound can propagate as longitudinal waves, shear waves, surface waves, and in thin materials as plate waves. Longitudinal and shear waves are the two modes of propagation most widely used in ultrasonic testing. The particle movement responsible for the propagation of longitudinal and shear waves is illustrated in Fig.5.2. [3].

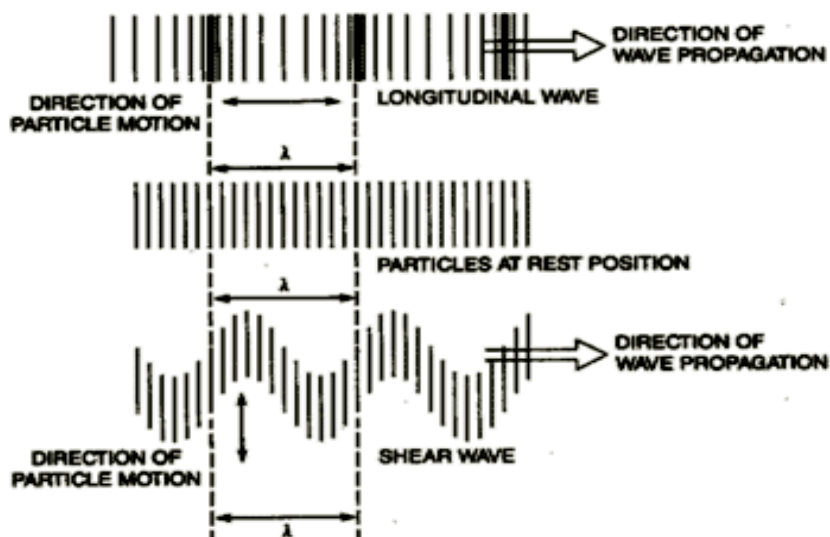


Fig.5.2. Modes of particles movements during sound wave propagation

In longitudinal waves, the oscillations occur in the longitudinal direction or the direction of wave propagation. Since compressional and dilational forces are active in these waves, they are also called pressure or compressional waves. They are also sometimes called density waves because their particle density fluctuates as they move. Compression waves can be generated in liquids, as well as solids because the energy travels through the atomic structure by a series of compressions and expansion (rarefaction) movements. In the transverse or shear wave, the particles oscillate at a right angle or transverse to the direction of propagation. Shear waves require an acoustically solid material for effective propagation, and therefore, are not effectively propagated in materials such as liquids or gasses. Shear waves are relatively weak when compared to longitudinal waves. In fact, shear waves are usually generated in materials using some of the energy from longitudinal waves. [3]

5-3-Wavelength and Defect Detection

In ultrasonic testing, the inspector must make a decision about the frequency of the transducer that will be used. Changing the frequency when the sound velocity is fixed will result in a change in the wavelength of the sound. The wavelength of the ultrasound used has a significant effect on the probability of detecting a discontinuity. A general rule of thumb is that a discontinuity must be larger than one-half the wavelength to stand a reasonable chance of being detected. Therefore, selecting the optimal inspection frequency often involves maintaining a balance between the favorable and unfavorable results of the selection. Before selecting an inspection frequency, the material's grain structure and thickness, and the discontinuity's type, size, and probable location should be considered. As frequency increases, sound tends to scatter from large or coarse grain structure and from small imperfections within a material. It should be mentioned, so as not to be misleading, that a number of other variables will also affect the ability of ultrasound to locate defects. These include the pulse length, type and voltage applied to the crystal, properties of the crystal, backing material, transducer diameter, and the receiver circuitry of the instrument. These are discussed in more detail in the material on signal-to-noise ratio. [1-5]

5-4-Introduction :in this study; ultrasonic method was applied to evaluate the structural integrity of Dual layer Tiles of W-SiC/SiC as HHFC for divertor, by detection surfacial and interfacial flaws resulted after divertor plasma exposure test inside LHD, where The quality control by nondestructive test method provided good indication before subsequent investigation, whereas ultrasonic data provided evidences to evaluate the bonding interface between tungsten and SiC/SiC by B-scanning imaging and provided an image of the features that reflect and scatter the sound within and on the surfaces of the test piece by C-Scanning imaging), the irradiated tiles were tested by Ultrasonic test image processing apparatus (SDS6500) (Flaw detector HIS3HF to evaluate the surface integrity and to evaluate the integrity of the diffusion bonding layer between W and SiC/SiC, thus we can speculate from the conditions of bonding layer the temperature distribution on the plasma exposed surface of the tiles inside LHD, where complete and partial debonding is function on the implanted heat during the plasma exposure test

5-5-Experimental work and achievements

The experimental work of this study included the scanning of the irradiated tiles after divertor plasma exposure test inside LHD by the means of Ultra sonic method, where the scanning was conducted on the tungsten surface of each irradiated tile .then the output data were analyzed and interpreted to evaluate the damage of each tile .the irradiated tiles ID and dimensions and it is conditions of fabrication are tabulated in **table.5.1**.Ultrasonic test image processing apparatus (SDS6500)-Flaw detector HIS3HF) by pulse-echo method with straight beam rout as shown in **Fig.5.3**.The inspection was accomplished by tank immersion technique with pre-calibrated Transducer. The surface of tungsten was scanned (**Fig.5.4.**); the SiC/SiC surface wasn't scanned because the difficulty of scanning reinforced composite material by acoustic methods where the roughness and natural changes of the texture of composite materials are natural impedance towards the sound waves, therefore resulting to misleading interpretation[2,3]

Table.5.1. Irradiated tiles ID and their dimensions

Tiles ID& Dimension(mm)	Raw Materials of Tungsten	Raw Materials of SiC/SiC	Hot press operating conditions (temperature °c, pressure in Mpa)
NITE-W/SiC-S2 (30x10x1.5)	W powder with purity 99.99% with rang size of 0.6 -0.99 μm	2D Preform	1800°c , 20 Mpa
NITE-W/SiC-Dh1 (30x10x1.5)	W plate (rolling direction: horizontal to plate axis)	2D SiC/SiC Composite	1600°c , 17.6 Mpa
NITE-W/SiC-v1 (30x10x1.5)	W plate (rolling direction: vertical to plate axis)	2D SiC/SiC Composite	1600°c, 16 Mpa



Fig.5.3. SDS6500)-Flaw detector HIS3HF

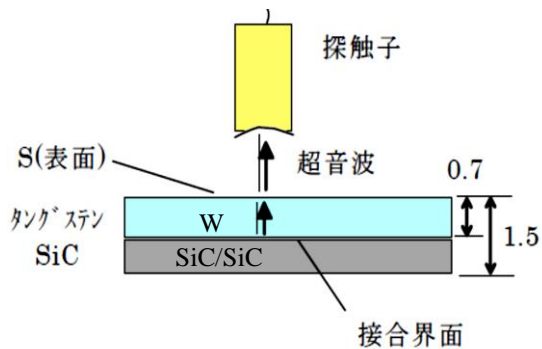
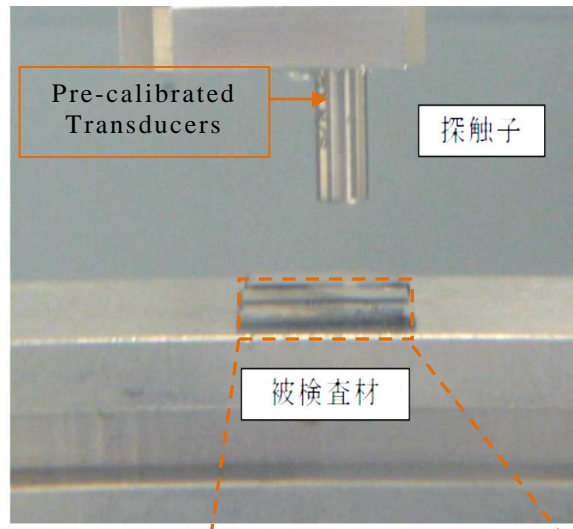
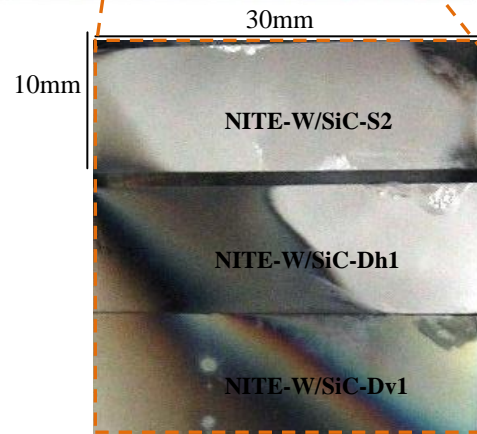


Fig.5.4. Schematic view of Scanning on W surface



The irradiated tiles after divertor plasma exposure test

5-6-Scanning conditions and sensitivity calibration:

The scanning was conducted by pre-calibrated transducer with host polymer media, the frequency 50 MHz, diameter $\phi 5$, PF 12.5 mm. The horizontal travelling distance =9.5 mm, scanning profile was in zigzag paths, (**Fig.5.5**). The transducer was calibrated by miniature resolution block of steel, where the sensitivity of the transducer was set up by the punched hole with diameter 0.39 mm and depth of 0.64 mm as illustrating in **Fig.5.6**. The reflection mode showed that the surface and interface reflection could be detected but the base reflection couldn't be detected (**Fig.5.7**.)

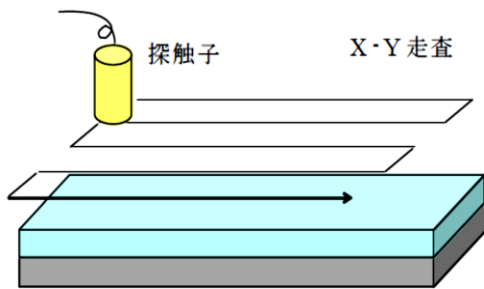


Fig.5.5. Horizontal scanning of tungsten

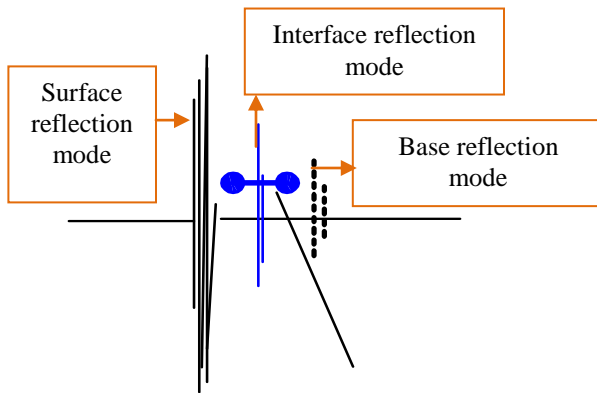


Fig.5.7. Reflection mode of scanning

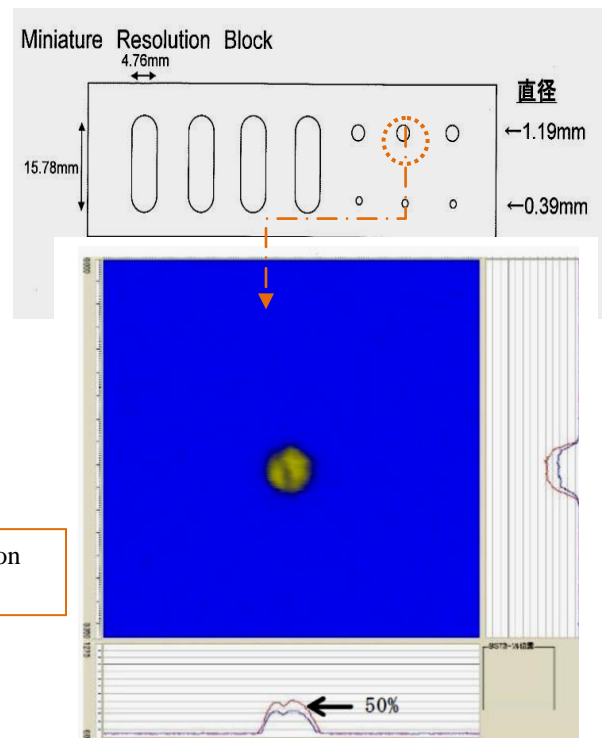


Fig.5.6. Calibration of sensitivity mode (50%)

5-7-Results and discussion

The results of the ultra sonic scanning of the three irradiated tiles were presented into three types of scanning; C-scanning, A, B-scanning images, where C-scanning presentation provides a plan-type view of the location and size of test specimen features. The plane of the image is parallel to the scan pattern of the transducer. The C-scan presentation provides an image of the features that reflect and scatter the sound within and on the surfaces of the test piece. C-scan presentations are produced with an automated data acquisition system, such as a computer controlled immersion scanning system [6-9] .C-scanning provided a data as color contrast images, the different colors are due to the different impedance of acoustic waves, which reflected and implanted in each tile. C-scanning images of the three irradiated tiles are showing if **Fig.5.8.**

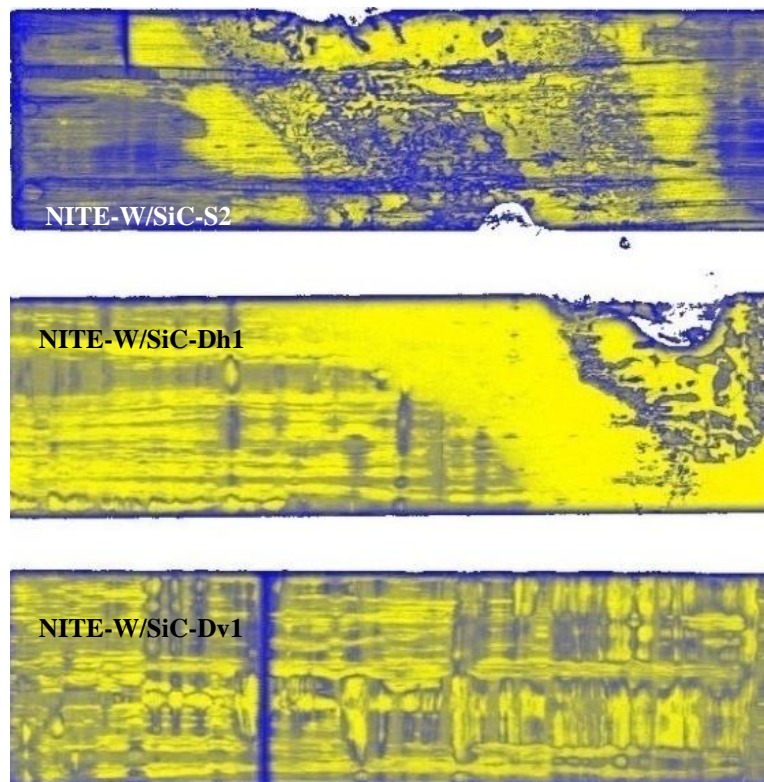


Fig.5.8.C-scanning images of the

C-Scanning images of ultra sonic test provided an evidence of discontinuities by color contrasts. These discontinuity contrasts are supposed to be caused by the interface. The color contrasts were interpreted by cutting samples at each different color zone; to investigate the interface layer between tungsten and SiC/SiC, and correlate it's discontinuity with its color contrast. The colors contrasts were classified into five different zones: (1) solid yellow, (2)yellow with blue nuggets, (3)scattered-blue/yellow,(4) blue with yellow nuggets and, (5)-intermittent–yellow/light-blue. Each tile was cut at its different color contrast zone to investigate the interpretation of each color contrast.

5-7-1-C-scanning of the tile (NITE-W/SiC-S2)

C-scanning image of the tile (NITE-W/SiC-S2) has a three different colors contrast zone (**Fig.5.9**): blue with yellow nuggets, solid yellow, scattered –blue/yellow zones. The first sample was cut at the solid yellow zone and the interface, where the interface layer was coherently and completely bonded the second sample was at scattered –blue/yellow zone, where some tiny pores up to ≈ 30 micron and complete debonding gap up to ≈ 100 micron at the interface layer were appeared. The third sample was cut at the blue with yellow nuggets zone, where interface showed at this sample intermittent bonded/debonded behavior, where debonding gap was up to ≈ 150 micron.

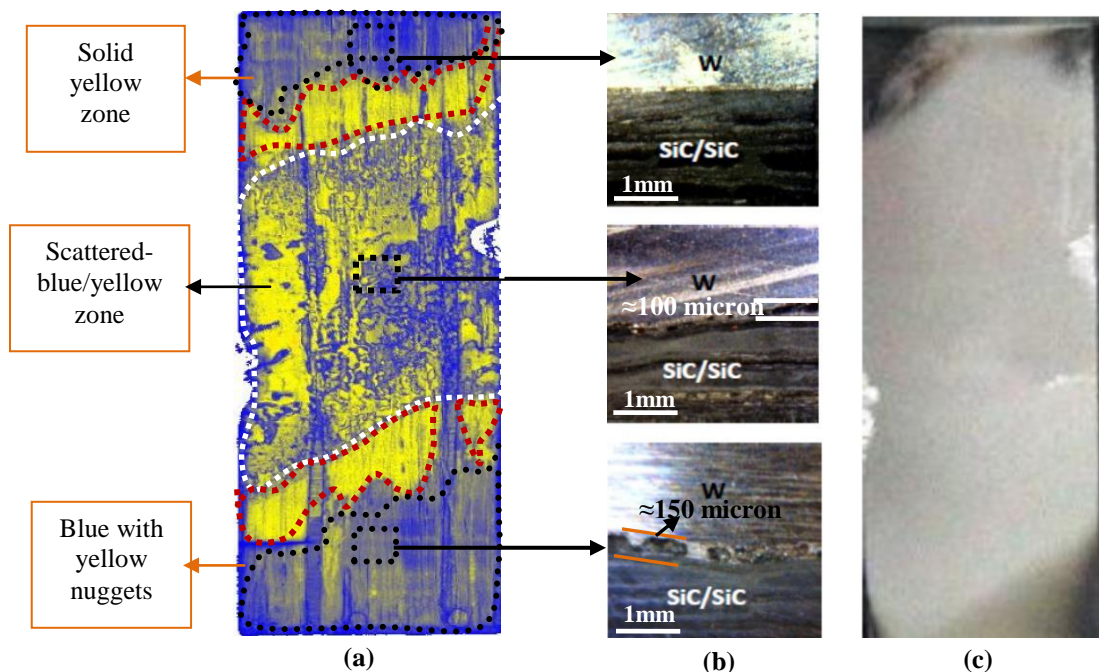


Fig.5.9. C-scanning images of the irradiated tile (NITE-W/SiC-S2) (a), cross section of cut sample at different color contrasts zone (b), tungsten surface of the irradiated tile

5-7-2-C-scanning of the tile (NITE-W/SiC-Dh1)

Regarding to the tile (NITE-W/SiC-Dh1) (**Fig.5.10.**); C-scanning image showed three different colors zones: intermittent-yellow/light-blue zone beside fused zone, solid yellow zone, yellow with blue nuggets zone. Three samples also were cut at the three different color contrasts zones ,where the first sample was cut at the intermittent-yellow/light-blue zone ,where interface layer showed at this zone debonding region with a gap opening up to ≈ 200 micron ,but the debonding appeared between tungsten and diffusion bonding layer, whereas SiC/SiC kept coherently with diffusion bonding layer, the second sample was cut at the solid yellow zone, where interface region showed complete bonded interface .The third sample was cut at the yellow with blue nuggets zone ,where interface showed partial debonding with tiny gap opening up to ≈ 50 micron

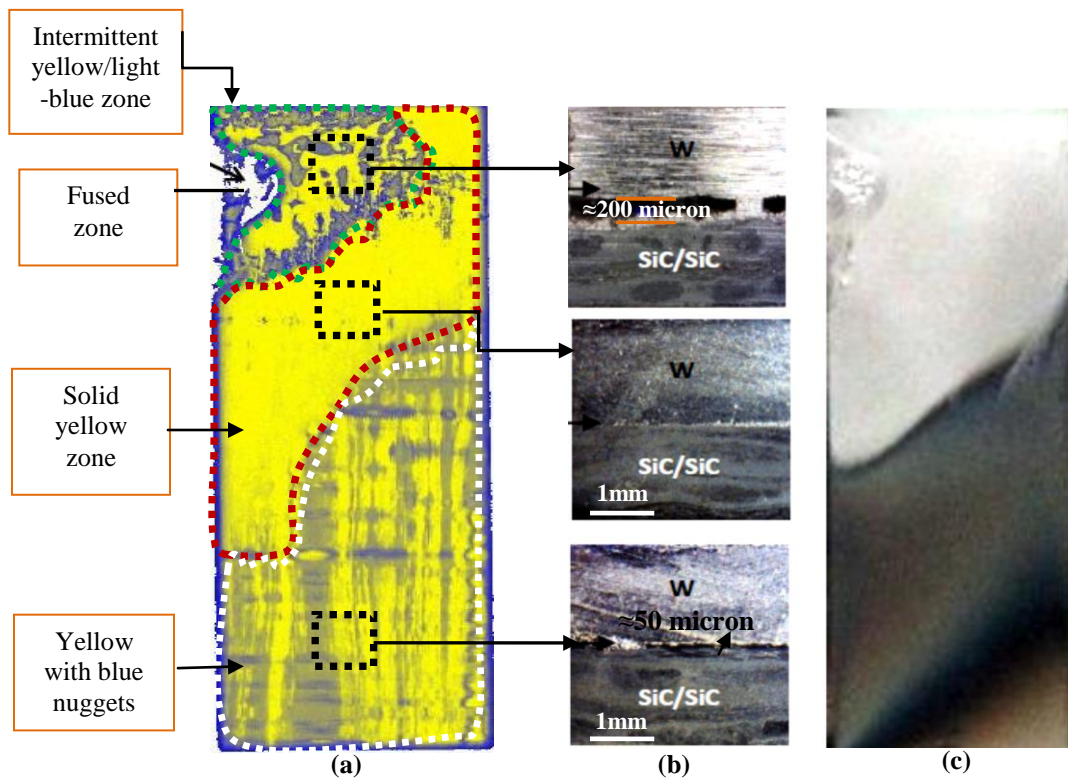


Fig.5.10.C-scanning images of the irradiated tile (NITE-W/SiC-Dh1) (a), cross section of cut samples at different colors contrasts zones (b), tungsten surface of the irradiated tile (b).

5-7-3-C-scanning of the tile (NITE-W/SiC-Dv1)

Regarding to the tile (NITE-W/SiC-Dv1) (Fig.5.11.); C-scanning image showed one phase of color contrast which it is the yellow with blue nuggets, where the samples which were cut showed almost the same behavior of partial debonding at interface. It is noticed that the one phase color zone reflecting the 0,90° cross ply structure of reinforcing fiber of SiC/SiC side, where the yellow points refers to integral coherent diffusion bonding layer, whereas the attenuated blue zone reflecting to partial debonding, the horizontal solid blue line refers to gap opening between the two adjacent tungsten plates, which were used to fabricate the tungsten layer, therefore it is a reliable evidence that the blue color reflecting discontinuity.

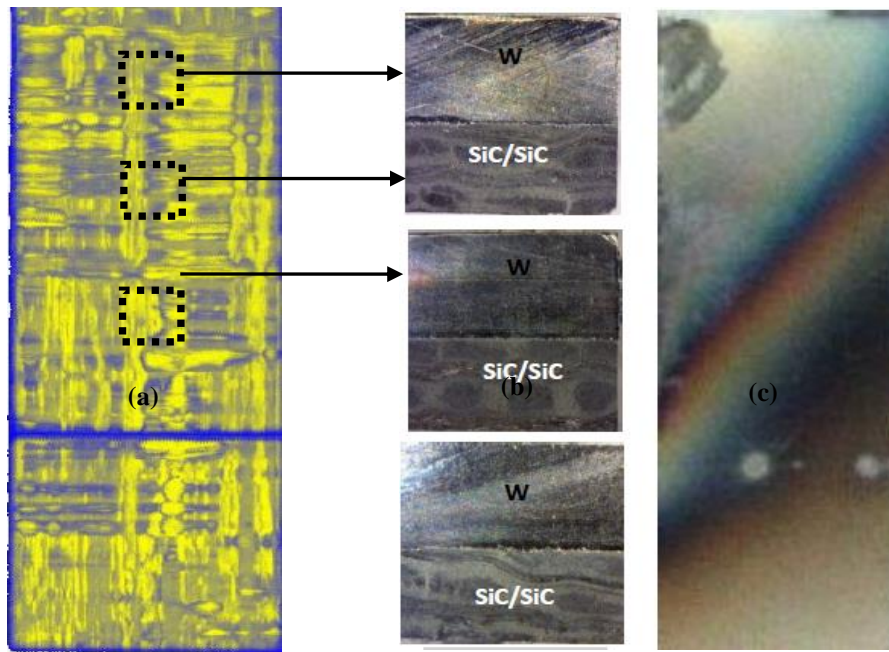


Fig.5.11.C-scanning images of the irradiated tile (NITE-W/SiC-Dv1) (a), cross section of cut samples at different colors contrasts zones (b), tungsten surface of the irradiated tile (b).

5-7-4-The temperature distribution on the tiles surface

Temperature distribution on each tile surface could be speculated; based on the correlation between the fabrication temperature, and the condition of the diffusion bonding layer at the interface, where the interface condition is a function in the color contrast zone of C-scanning images of each tile. Based on this hypothesis, the colors contrast on the tile (NITE-W/SiC-S2): solid yellow zone represents surface temperature less than 1800°C; the scattered blue –yellow zone represents surface temperature equal or greater that 1800°C; the blue with yellow nuggets zone represents surface temperature greater than 1800°C. Regarding to the tile (NITE-W/SiC-Dh1) the three colors contrast: intermittent yellow/light-blue zone represents surface temperature greater than 1600°C; the solid yellow zone represents surface temperature less than 1600°C; the yellow with blue nuggets zone represents surface temperature equal or greater than 1600°C. Regarding to the tile (NITE-W/SiC-Dv1) C-scanning showed one phase color contrast: (yellow with blue nuggets) which represents surface temperature greater than 1600°C. Regarding to the fused zone at the tiles: (NITE-W/SiC-S2), (NITE-W/SiC-Dh1) the surface temperature reached to the melting point of the tungsten which it is 3400°C. **Fig.5.12.** showed the temperature distribution on the surface of each irradiated tiles at each different color contrast zone of C-scanning images.

5-7-5-A&B-Scan of the irradiated tiles.

The A-scan presentation displays the amount of received ultrasonic energy as a function of time. The relative amount of received energy is plotted along the vertical axis and the elapsed time (which may be related to the sound energy travel time within the material) is displayed along the horizontal axis. Most instruments with an A-scan display allow the signal to be displayed in its natural radio frequency form (RF), as a fully rectified RF signal, or as either the positive or negative half of the RF signal. In the A-scan presentation, relative discontinuity size can be estimated by comparing the signal amplitude obtained from an unknown reflector to that from a known reflector. Reflector depth can be determined by the position of the signal on the horizontal sweep [4].

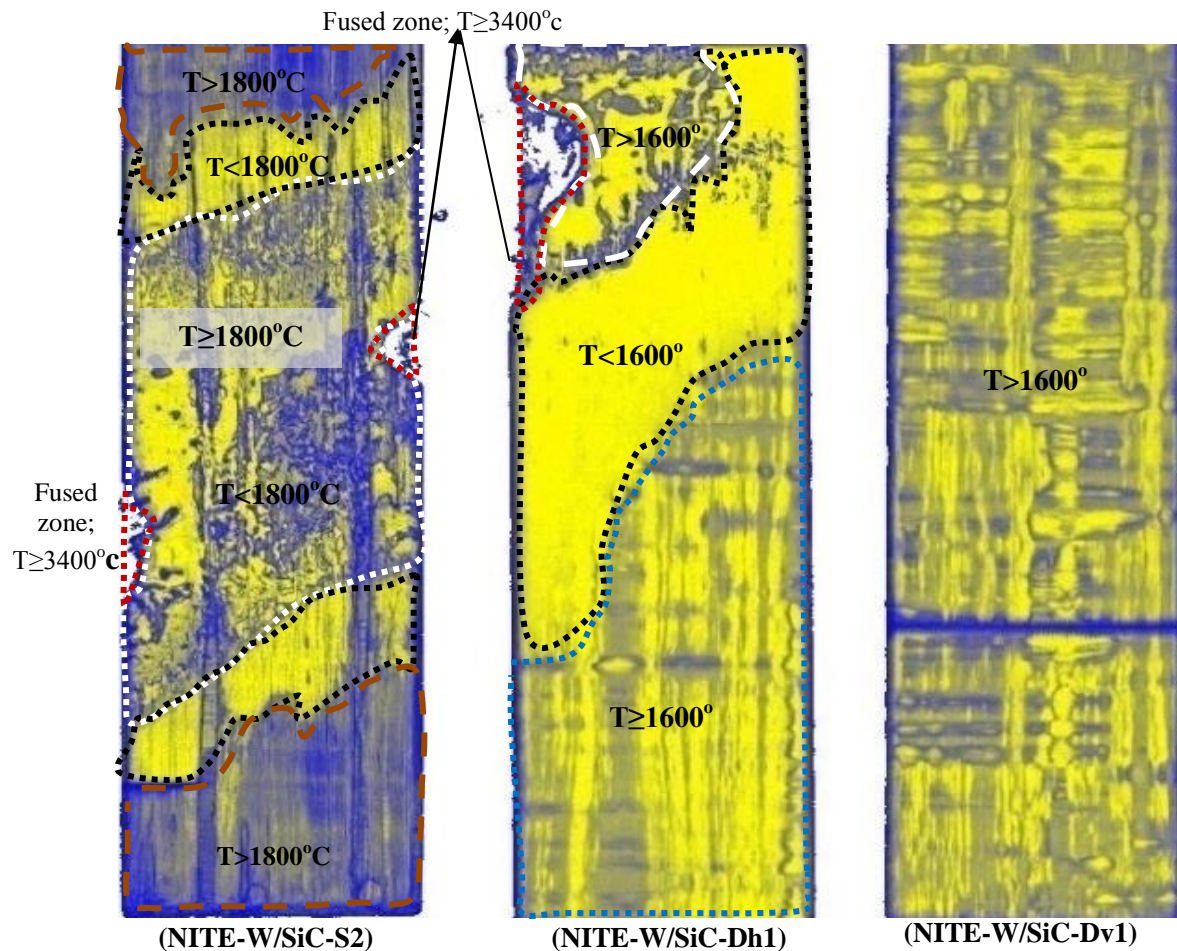


Fig.5.12. Temperature distribution on tungsten surface of the irradiated tiles at different color contrast zone of C-scanning images

The reflection mode of A-scan as aforementioned (see Fig.5.7.) was used to interpret the interface reflected wave, where A-scan of the tiles (NITE-W/SiC-S2), (NITE-W/SiC-Dh1), (NITE-W/SiC-Dv1) showed only one considerable flaw on the subsurface of tungsten, where there was one reflected-attenuated wave of the interface was strong enough to exceed the gate of 50% sensitivity, whereas the other attenuated reflected interface waves was not strong enough to exceed the calibrated 50% sensitivity. Regarding to B-scan it was used only to show the profile (cross-sectional) view of the test specimen [4]. Where the profile of the tile (NITE-W/SiC-S2) appeared as corrugated profile, where the tile was fabricated by sintering of tungsten powder and preform of SiC/SiC, thus the interface

produced was corrugated, due to the loose form of the two phases before solidification, B-scan also showed that the defects due to the plasma exposure on the diffusion bonding layer agreed with the interpretation of these defects at C-scanning image. Regarding to the cross section profile of both the tile (NITE-W/SiC-Dh1), (NITE-W/SiC-Dv1) appeared by B-scan as straight line, where the interface and interphase line are agreed along the tile length except at the defected region; especial the area near the fused zone. **Fig.5.13**; (a), (b), (c) Showed A&B –scan of the irradiated tiles: (NITE-W/SiC-S2), (NITE-W/SiC-Dh1), (NITE-W/SiC-Dv1) respectively .

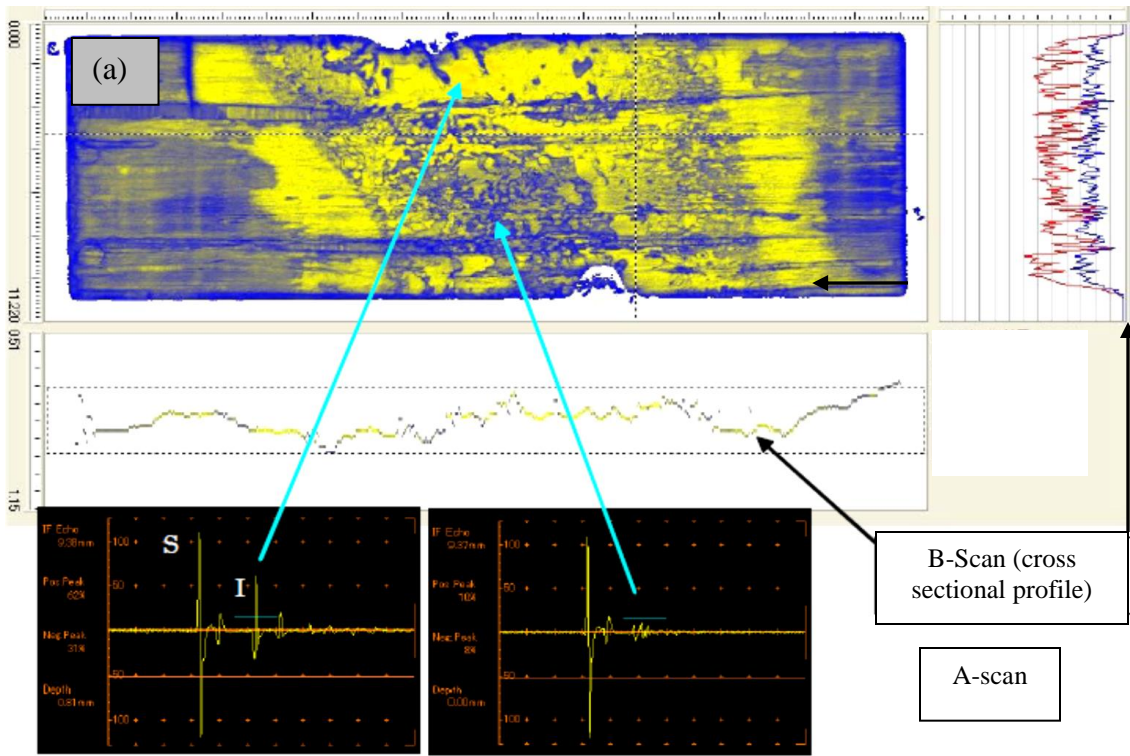


Fig.5.13. (a) A&B-scan of the irradiated tile (NITE-W/SiC-S2)

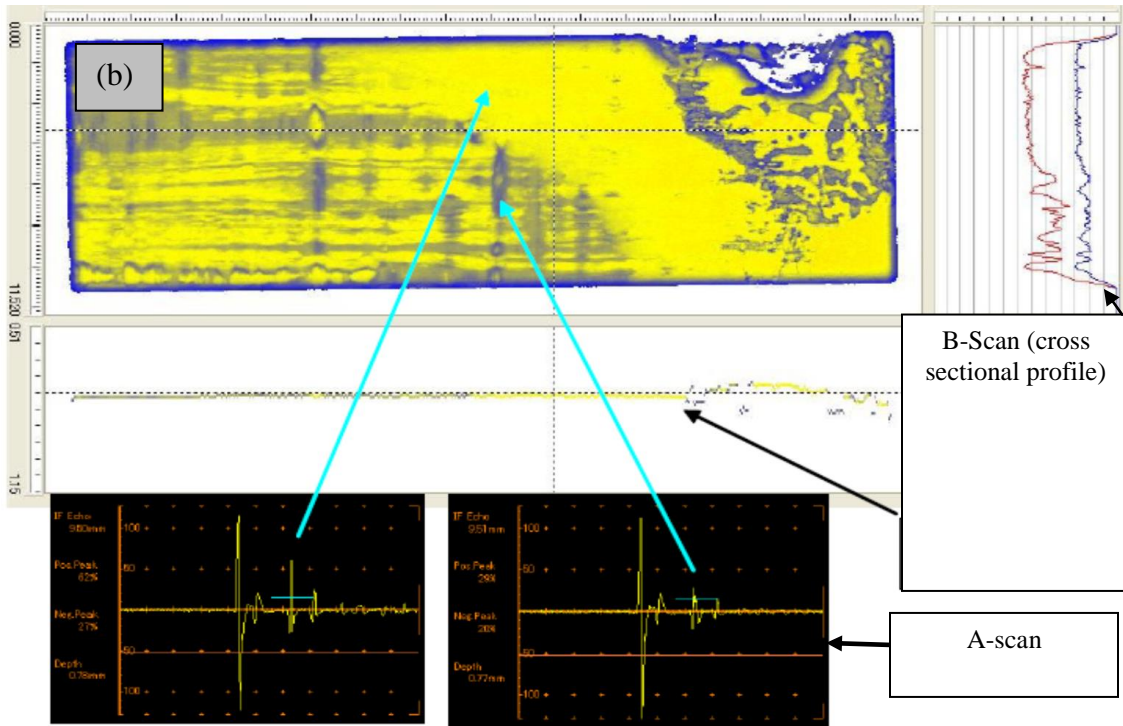


Fig.5.13. (b) A&B-scan of the irradiated tile (NITE-W/SiC-Dh1)

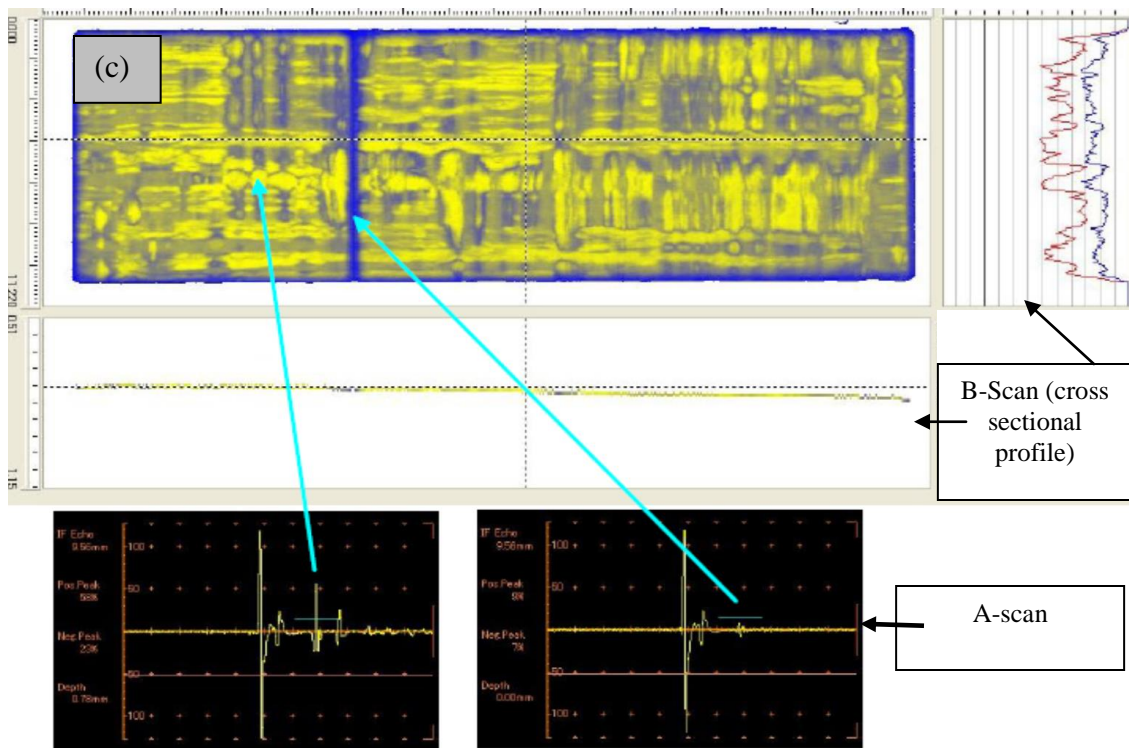


Fig.5.13. (c) A&B-scan of the irradiated tile (NITE-W/SiC-Dv1)

5-8-Conclusion

Damage analysis of dual layers tiles of Tungsten and SiC/SiC after plasma exposure inside LHD by means of Ultra sonic methods showed reliable and clear evaluation of bonding layer at the interface between tungsten and SiC/SiC, where two types of presentation data showed and evaluated the diffusion bonding layer, by C-scanning images, B-scanning images, where C-scanning showed partial and complete bonding interface beside the thick and integral bonding interface, such variant in the diffusion bonding interface is due to the variable temperature distribution inside the reactor ,thus we could speculate the temperature distribution on the surface of each tile by referring to the temperature of diffusion bonding of fabrication, B-Scanning images gave a reliable view about the profile of each interface of each tile. Ultra sonic method can be used as quality control method to evaluate the tiles inside the reactor in the future during the operation with sufficient degree of reliability.

References

- [1] L. Cartz, *Nondestructive Testing* (Materials Park, OH: ASM, 1995).
- [2] P.E. Mix, *Introduction to Nondestructive Testing* (New York: John Wiley & Sons, 1987).
- [3] A. Kelly: *Concise Encyclopedia of Composite Materials* (New York: Pergamon, 1989), p. 199.
- [4] Diederichs, Rolf and Ginzler, Ed, *Nondestructive Testing Encyclopedia, UT Formulae, NDT net Ultrasonic Characterization of Materials*, NIST, Materials Reliability Division.
- [5] Krautkramer, Josef and Krautkramer, Herbert, *Ultrasonic Testing of Materials*, 4th/revised edition, Springer Verlag, November 1990, ISBN: 03875123.
- [6] Auld, B.A., *Acoustic Fields and Waves in Solids, Vol I & II*, 2nd edition Krieger Publishing Company, February 1990; ISBN: 089874783X.
- [7] Gordon GA, Canumallas, Titman BR. Ultrasonic C-scan imaging for materials characterization. *Ultrasonics* 1993; 31 (5): 373-380.
- [8] Moghisi M, Almond DP. An inexpensive computer-controlled ultrasonic C scan system. *NDT Intl.* 1983; 16 (1) 9-12.
- [9] Anish Kumar et al. Development and applications of C-scan Ultrasonic Facility BARC News Letter Founder's day Special. 2007; 49-57.

Chapter-6
Macro and Microstructure Evolution of
W-SiC/SiC Tiles after Divertor Plasma
Exposure Test.

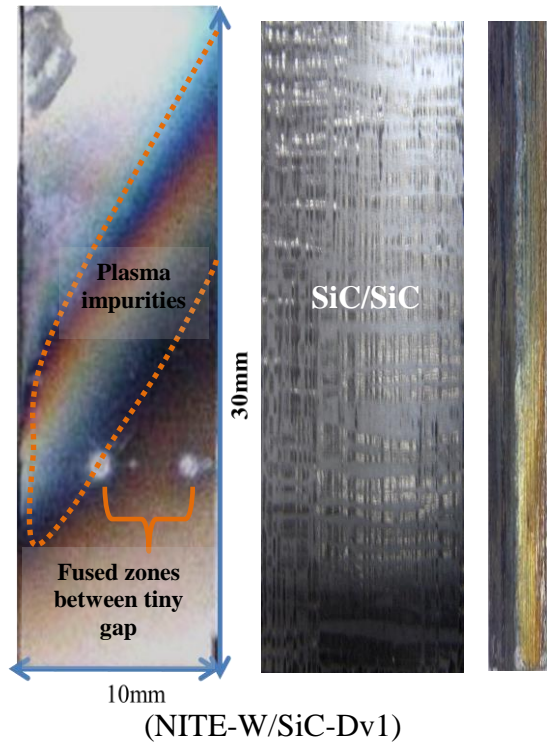
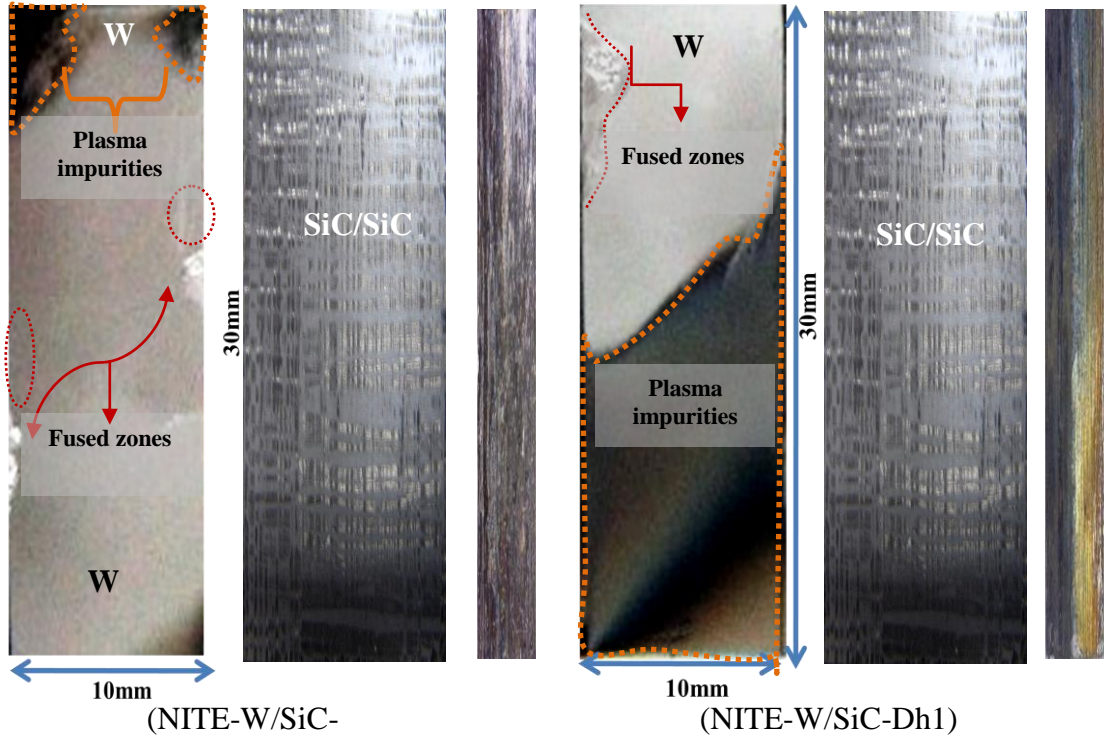
6-Macro and Microstructure evolution of W-SiC/SiC tiles after Divertor Plasma Exposure

6-1-Introduction

After the irradiated tiles were picked out from the LHD, the tiles were cut at different positions to investigate the macro and micro structure at these positions; to study the effect of heat flux loaded on tungsten armor, SiC/SiC side and to evaluate the bonding durability between tungsten and SiC/SiC. Macroscopic and SEM were used to investigate the results. Electron probe Micro-analyzer (EPMA) was used to investigate the diffusion behavior on W-SiC/SiC side and to compare between the diffusion behaviors before and after the loading of high heat flux on the tiles.

6-2- Results

The irradiated tiles were inspected visually after the divertor plasma exposure test. Visual test of the three irradiated tiles after divertor plasma exposure test is shown in **Fig.6.1** where it is showed that there was not severe damage occurred due to the divertor plasma exposure test; i.e. there was not complete debonding between tungsten and SiC/SiC along the whole length of the exposed tiles, and there weren't complete transverse cracks were observed along the thickness of the tiles, but there were clear fused zones on the edge of W surface of (NITE-W/SiC-S2) and (NITE-W/SiC-Dh1). Such fused zones weren't observed on W edge of (NITE-W/SiC-Dv1) but were observed in the tiny gap between two adjacent W plates and there was some plasma contamination appeared on W surface of the three exposed tiles. Regarding to the back side of the tiles (SiC/SiC); neither delamination nor cracks were observed, and the original densified and integral Fiber/Matrix structure were coherently kept. Visual test provided roughly guidance to determine the positions of cut lines on the irradiated tiles, for subsequent investigation, where small samples will be cut to conduct more specific investigation.



After the visual test, the irradiated tiles were cut at different positions; as shown in **Fig.6.2**, macroscopic analysis of both tungsten and SiC/SiC side showed the morphology of the two surfaces by Macro and microstructure analysis of the exposed tiles which was conducted by a digital microscope and SEM respectively. The surface of tungsten and SiC/SiC images are shown in **Fig.6.3**. Images of (NITE-W/SiC-S2) (position#2) and (NITE-W/SiC-Dh1) (position#1) are shown in **Fig.6.4**, **Fig.6.5**, respectively showed that: on tungsten surface of an irradiated tiles there were some arc traces looked like tiny scratches, and fused zones on edges were observed. The arc traces were not observed on the tungsten surface of (NITE-W/SiC-Dv1) (position#1) as shown in **Fig.6.5**, but there were accumulated contamination were observed as peeled tungsten flakes and blisters of re-solidified tungsten. SiC/SiC side of the three irradiated tiles showed integral and densified structure except tiny uniaxial cracks appeared on the tiles (NITE-W/SiC-S2) and (NITE-W/SiC-Dh1). These cracks could be caused due to thermal effect of plasma exposure, but there was possibility that these cracks were originally existed due to samples preparation (cutting and polishing) as delayed cracks.

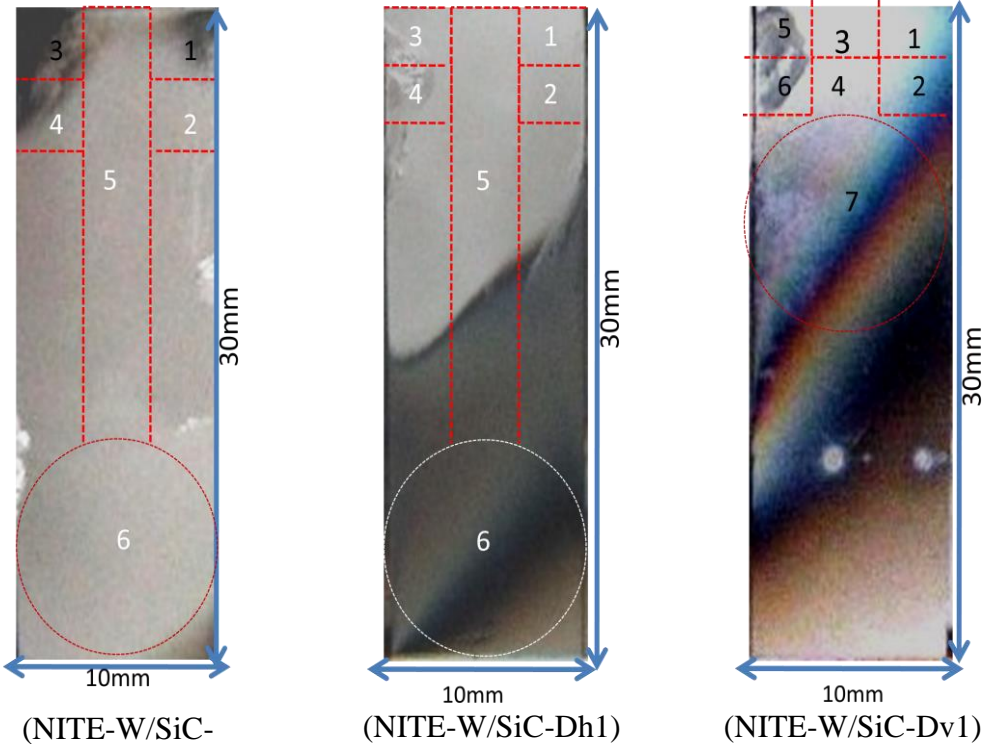


Fig.6.2 The draw cut of irradiated tiles.

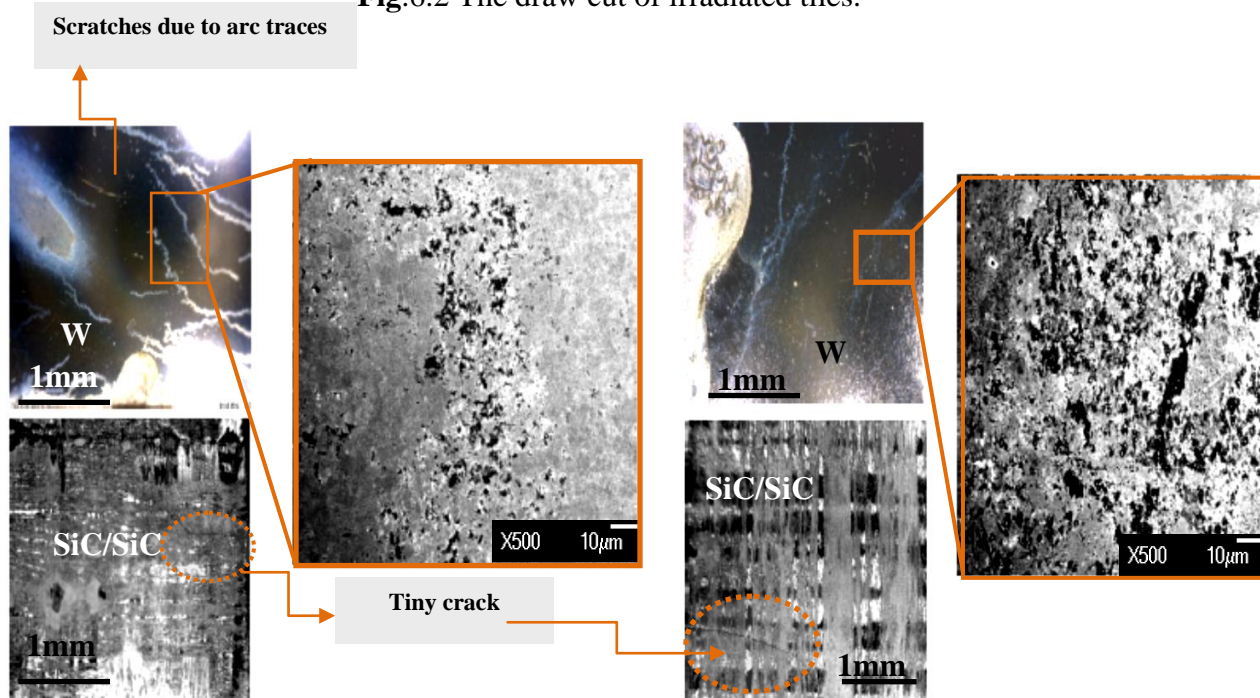


Fig.6.3. Surface of Tungsten and SiC/SiC (NITE-W/SiC-S2) position#2

Fig.6.4.Surface of Tungsten and SiC/SiC (NITE-W/SiC-Dh1) position#1

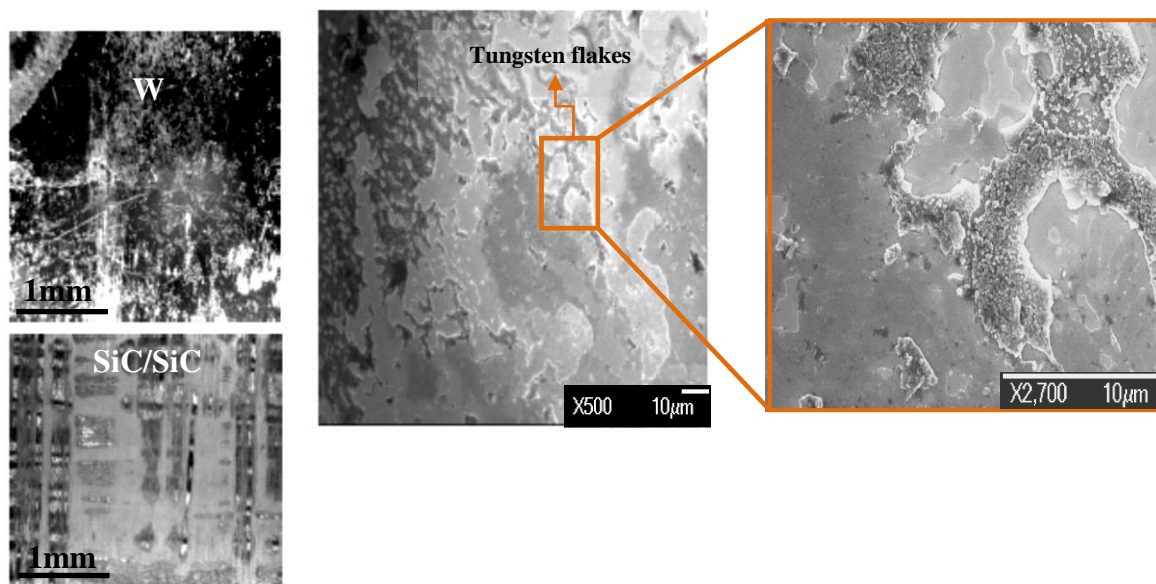


Fig.6.5. Surface of Tungsten and SiC/SiC (NITE-W/SiC-Dv1) position#1

Macro and micro structure analyses was conducted to evaluate the W-SiC/SiC bonding by selecting positions of each irradiated tile, where the macro structure images of tile (NITE-W-SiC-S2),position#1 ;the side X+,X-,Y+,Y- showed complete bonding between W and SiC/SiC, around the circumference of the sample(**Fig.6.6**),whereas position#2 (**Fig6.7**); sides X+,X-; showed partial debonding between W and SiC/SiC, whereas at the sides Y+,Y- ,there was tiny pores at the interphase layer, but the rest of the interphase layer was coherently kept and completely bonded between W and SiC/SiC, SEM image of the side Y+ at position#2 showed there was fused tungsten layer; covered the interphase region and extended to the side of SiC/SiC (**Fig6.8**), regarding to position#3(**Fig6.9**) at side Y-, there was tiny pores appeared at the interphase, at the side Y+ there was complete bonding between W, SiC/SiC, the sides X+,X- showed complete bonding, regarding to position #4(**Fig.6.10**); the sides X+X-,Y+ showed partial debonding, whereas the Y- showed complete bonding.

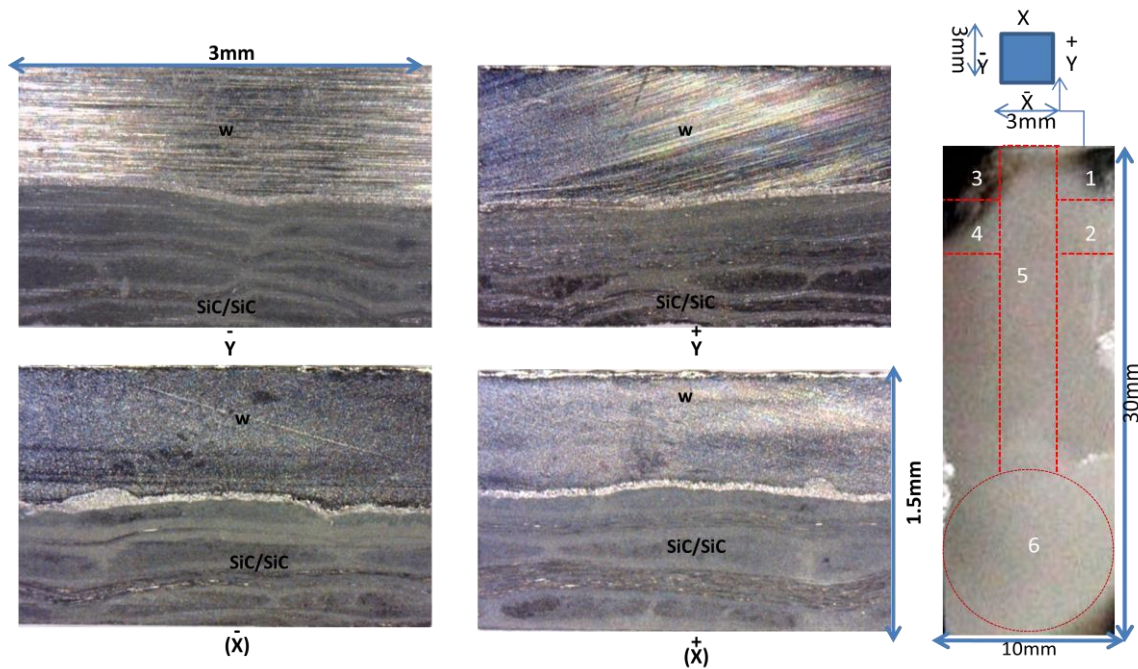


Fig.6.6.Macrostructure of W- SiC/SiC side (NITE-W/SiC-S2)

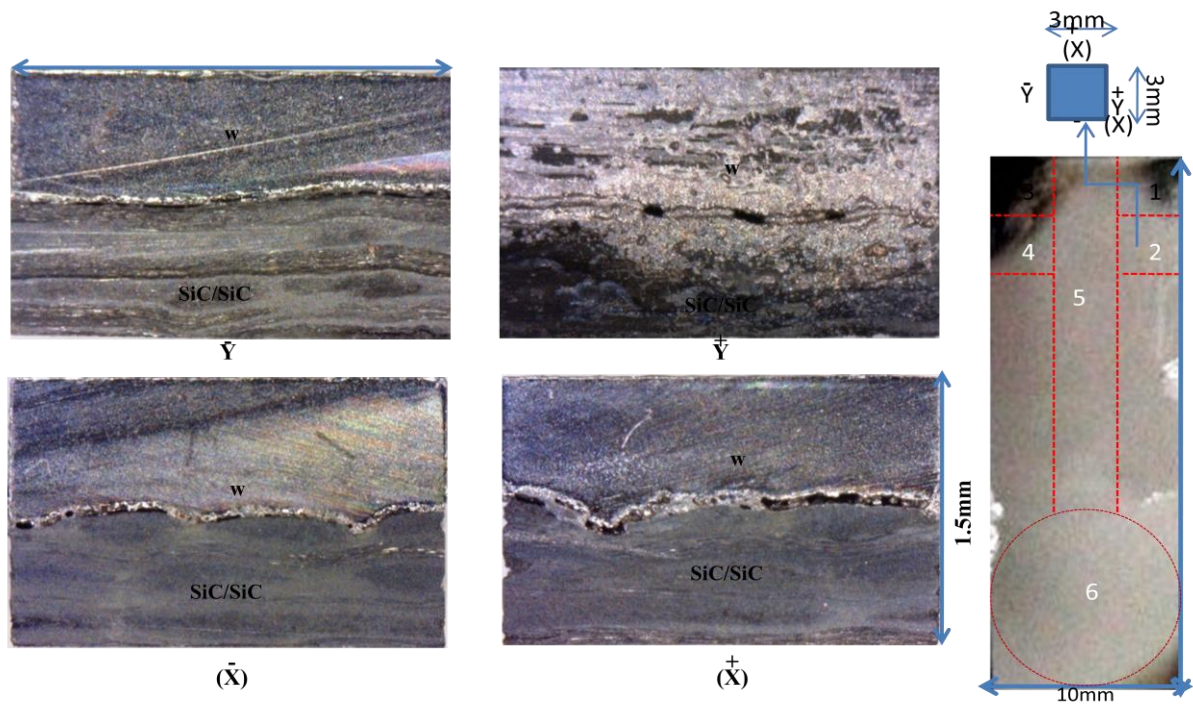


Fig.6.7.Macrostructure of W- SiC/SiC side (NITE-W/SiC-S2) position#2

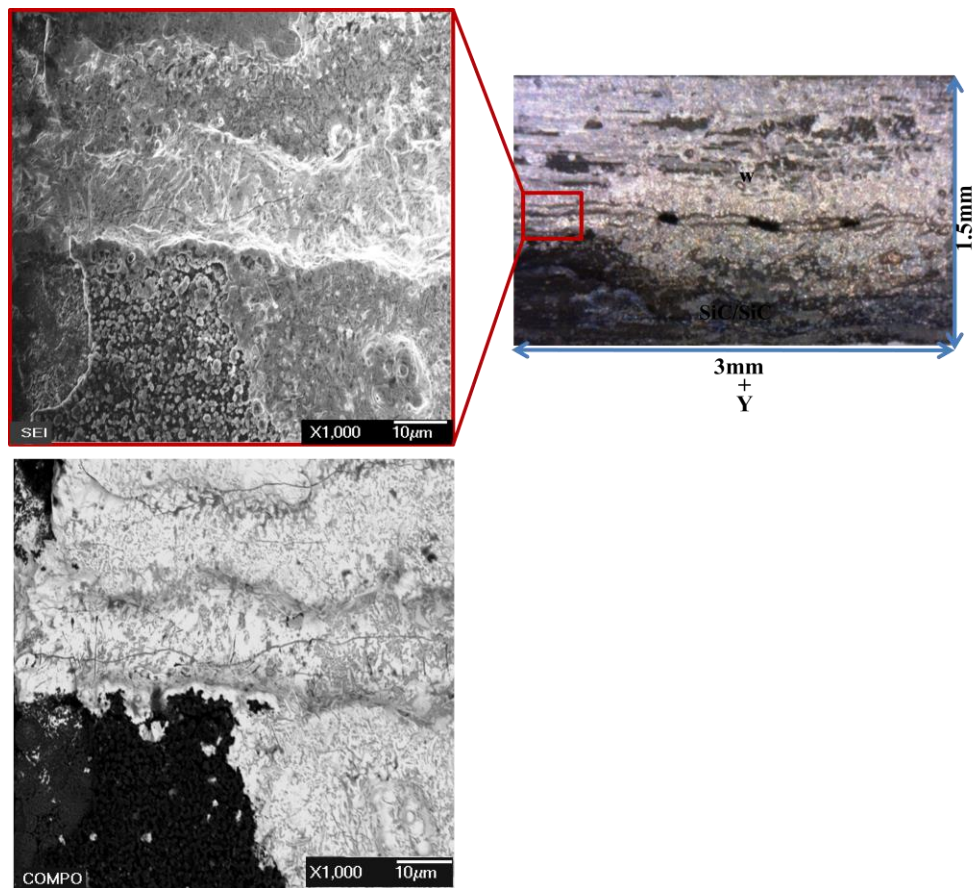


Fig.6.8. SEM image of W- SiC/SiC side (NITE-W/SiC-S2) position#2, Side Y+

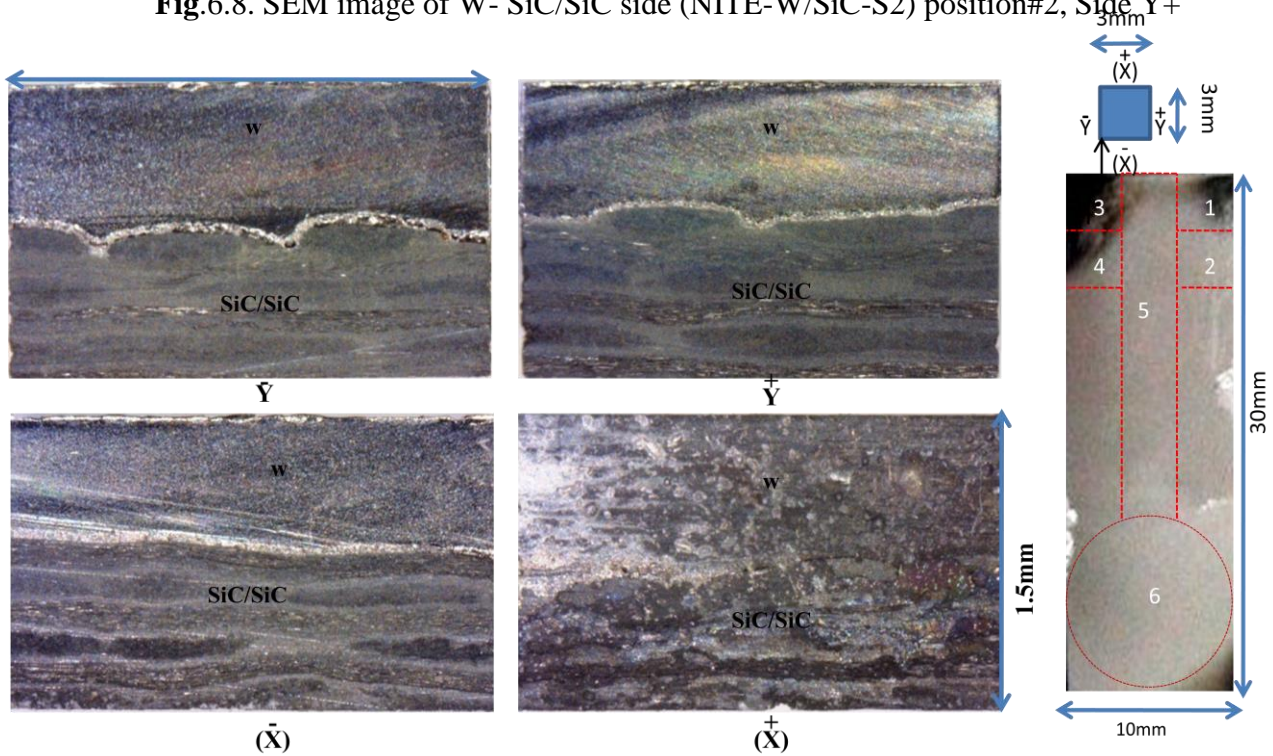


Fig.6.9. Macrostructure of W- SiC/SiC side (NITE-W/SiC-S2) position#3

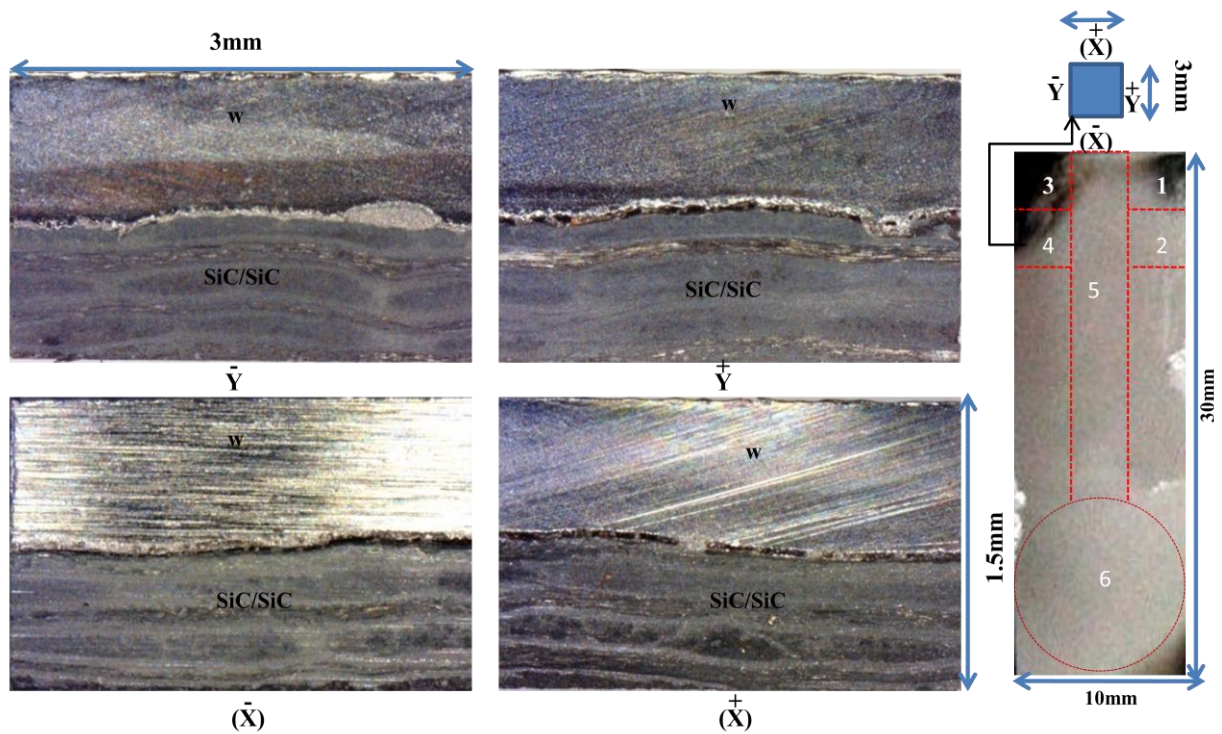


Fig.6.10. Macrostructure of W- SiC/SiC side (NITE-W/SiC-S2)

Sample position#5(**Fig.6.11**) was investigated, where its dimension is long and provided more evaluation of the W-SiC/SiC bonding conditions, where the investigation was accomplished around its circumference, where at side X+ the interphase was coherently bonded ,whereas the side X- showed partial debonding, the long side Y+ showed one portion with debonding gab and there was pores were appeared at the interphase, whereas the rest of the side appeared coherently bonded and the interphase layer showed excellent integration, the side Y- showed partial debonding, whereas the rest of the side showed excellent bonding with coherent interphase layer. The position #6 (**Fig.6.12**) is rounded sample, where the direction (0,90°) showed intermittent profile of bonding/debonding phase. The directions (90°, 180°), (180°, 270°), showed complete bonding region and coherent interphase layer, the direction (270° 360°); showed intermittent profile of bonding/debonding phase.

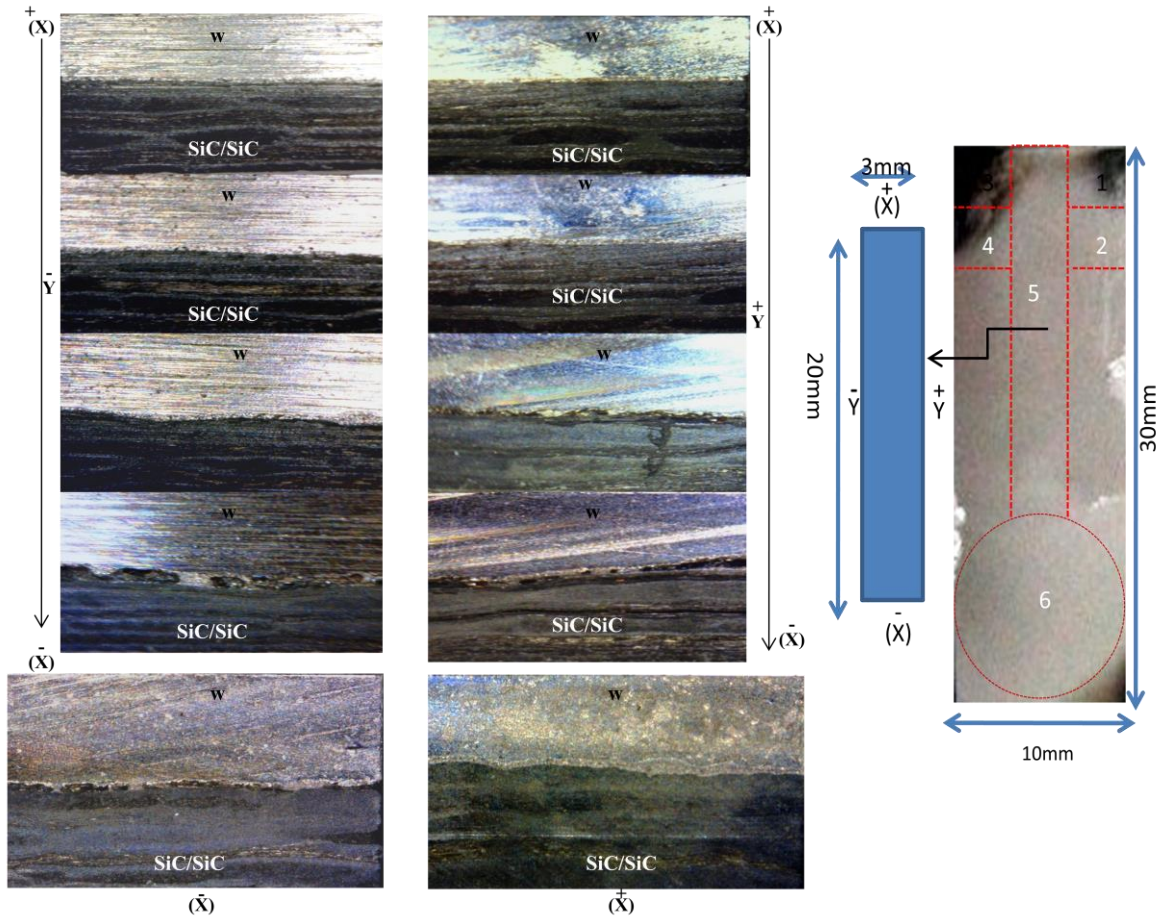


Fig.6.11.Macrostructure of W- SiC/SiC side (NITE-W/SiC-S2) position#5

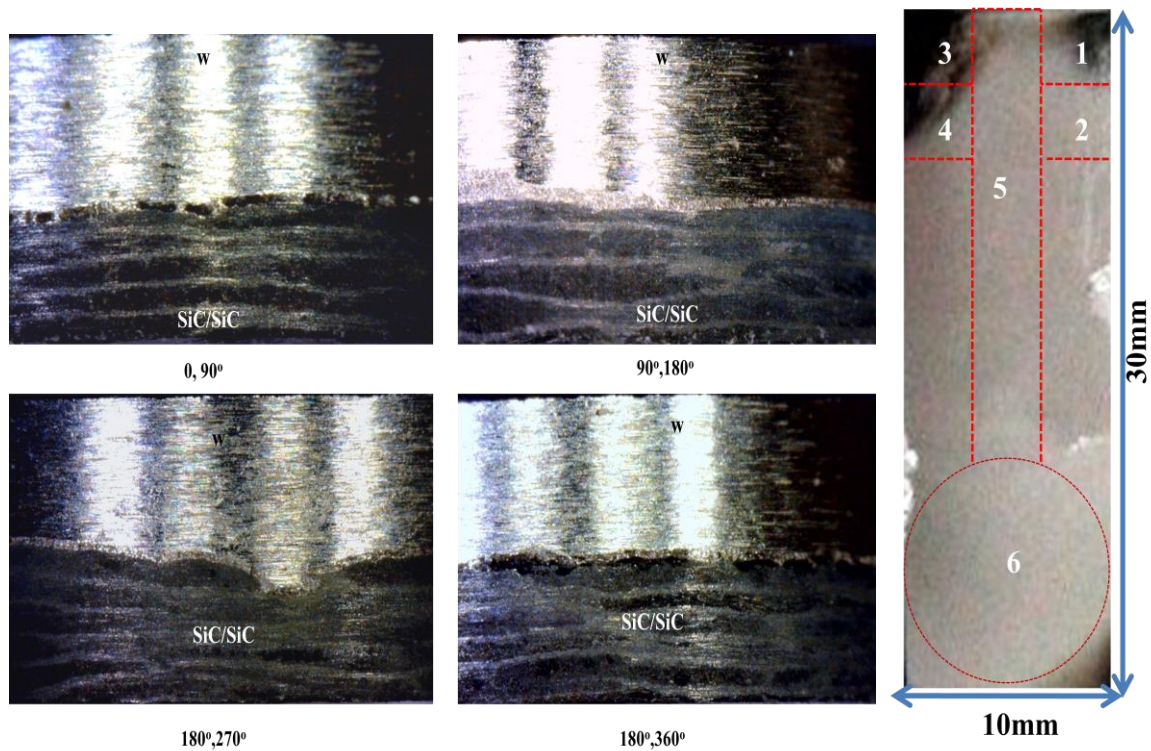


Fig.6.12.Macrostructure of W- SiC/SiC side (NITE-W/SiC-S2) position#5

The tile (NITE-W-SiC-Dh1) was investigated; with the same procedure as aforementioned in the tile (NITE-W-SiC-S2), where position#1(**Fig.6.13**), the side Y+ showed no clear interphase layer was appeared ,and there was partial debonding, the side Y- showed that the interphase layer was existed, but there was partial debonding was appeared, both sides of X-, X+ showed sufficient bonding, SEM images(**Fig.6.14**) of the side Y+ showed that the gap opening occurred due to the complete debonding between interphase layer with tungsten and SiC/SiC side , there was a transverse crack appeared on the side of SiC/SiC. The position #2(**Fig.6.15.**) was investigated, where both sides Y+,Y- showed disappearing of the interphase layer, whereas the side of X+,X- showed clear interphase layer and sufficient bonding.

Regarding to position#3(**Fig.6.16.**) the side Y+ showed sufficient bonding, whereas the side Y- showed complete debonding, both sides X-,X+, showed intermittent bonding/debonding phase, and there was also transverse crack was appeared on SiC/SiC side.

Position #4(**Fig.6.17**)both side Y+,Y- showed partial debonding, the side X- showed complete debonding, except tiny portion with coherent interphase layer, the side X+ showed complete bonding, except tiny pores on the interphase layer.

Position #5(**Fig.6.18**) is long sample, where the both sides Y+, Y- showed intermittent bonding, debonding phase, whereas the side X- showed complete debonding, beside plasma impurities and fused tungsten flakes.

Position #6 (**Fig.6.19**) is the circular sample, showed complete bonding from 0° to 360°.

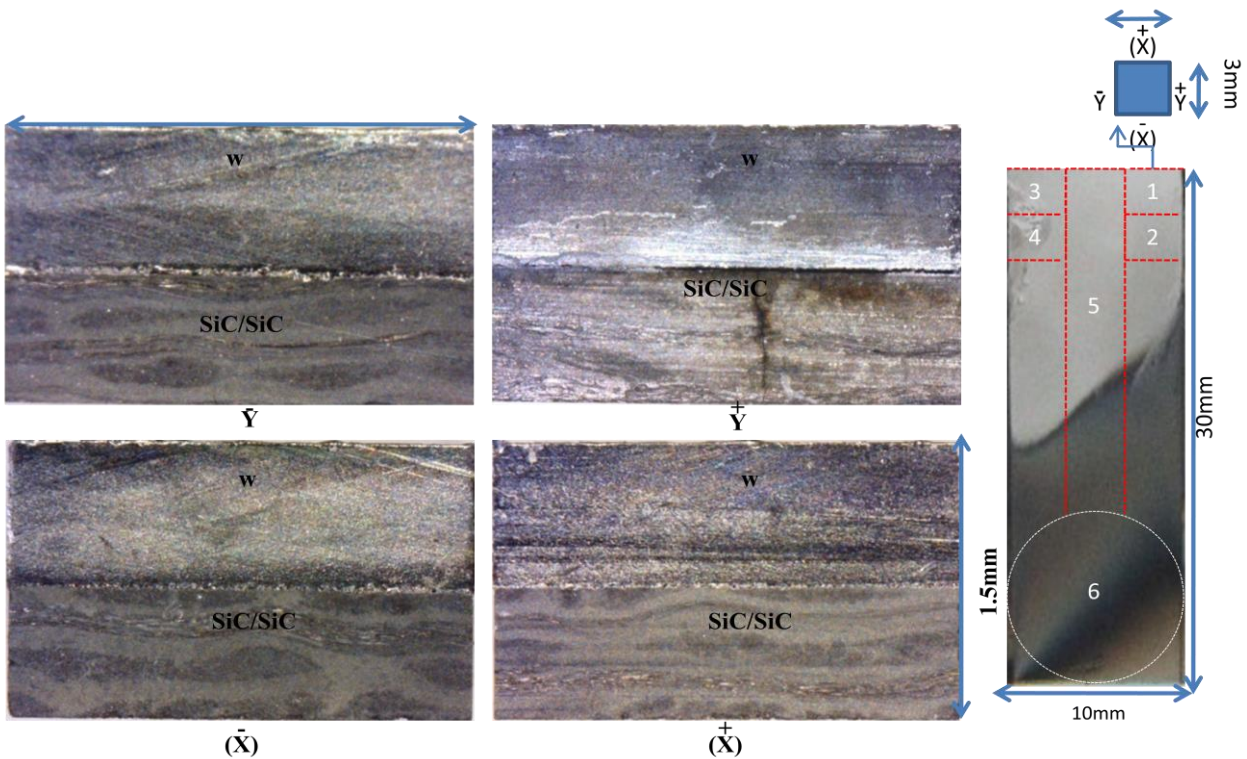


Fig.6.13. Macrostructure of W- SiC/SiC side (NITE-W/SiC-Dh1) position#1

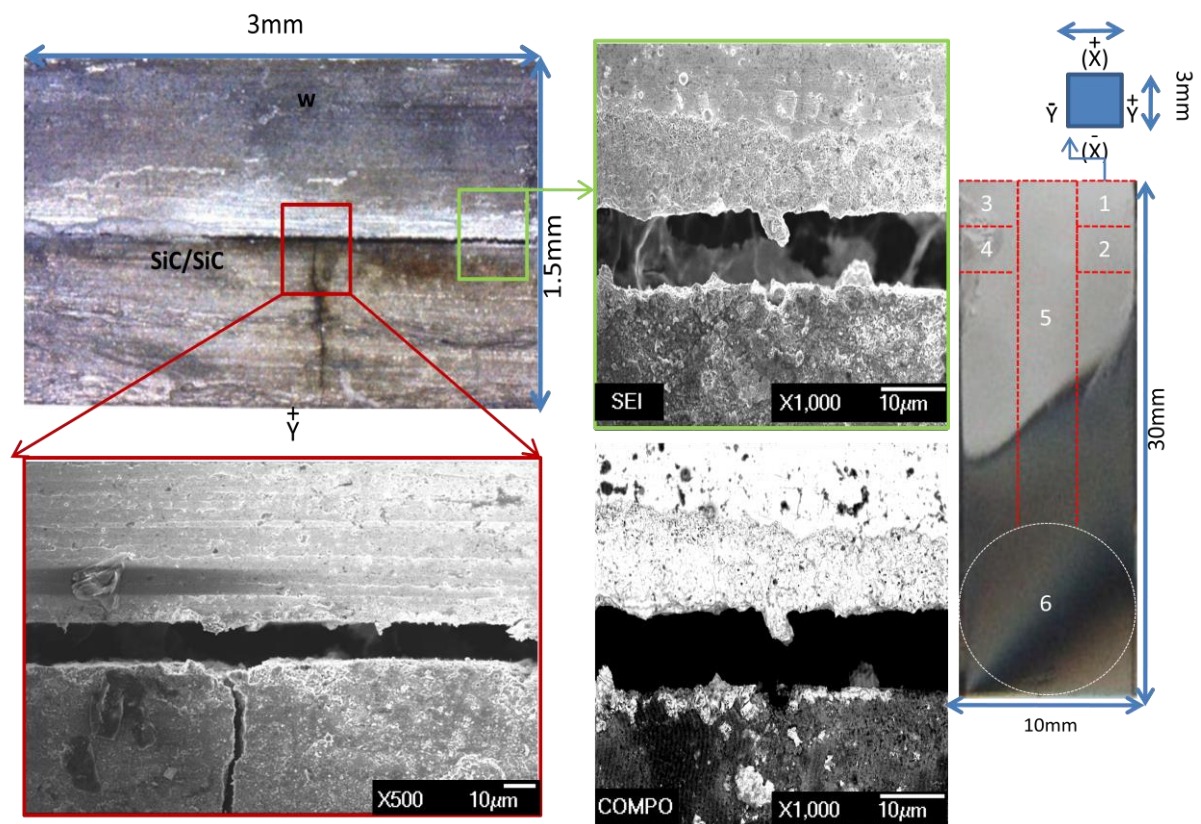


Fig.6.14. Macrostructure and SEM of W- SiC/SiC side (NITE-W/SiC-Dh1) position#1, side Y+

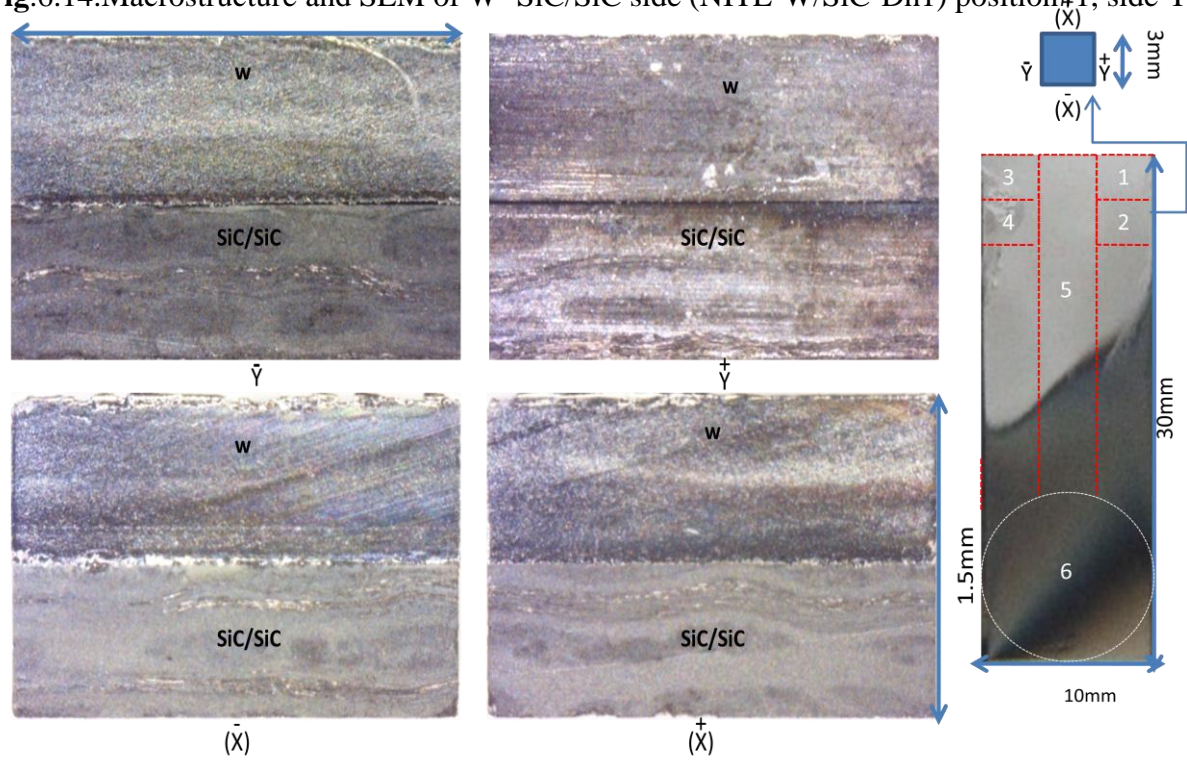


Fig.6.15. Macrostructure and SEM of W- SiC/SiC side (NITE-W/SiC-Dh1) position#2

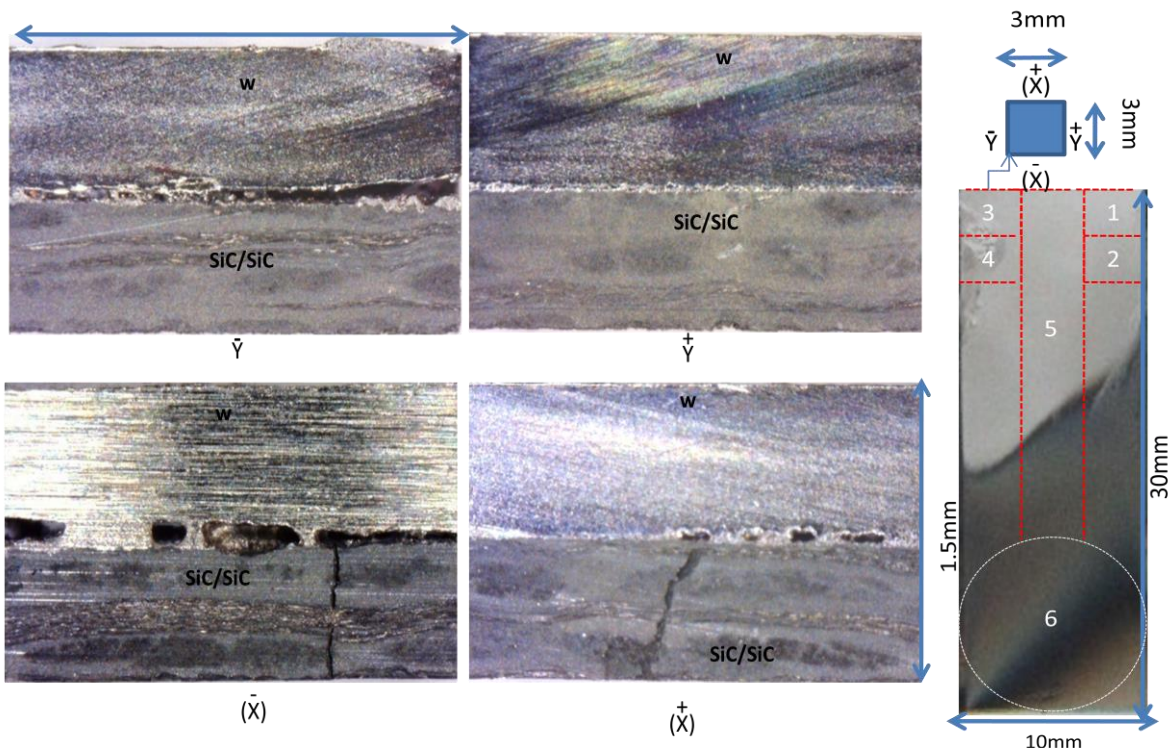


Fig.6.16. Macrostructure and SEM of W- SiC/SiC side (NITE-W/SiC-Dh1) position#3

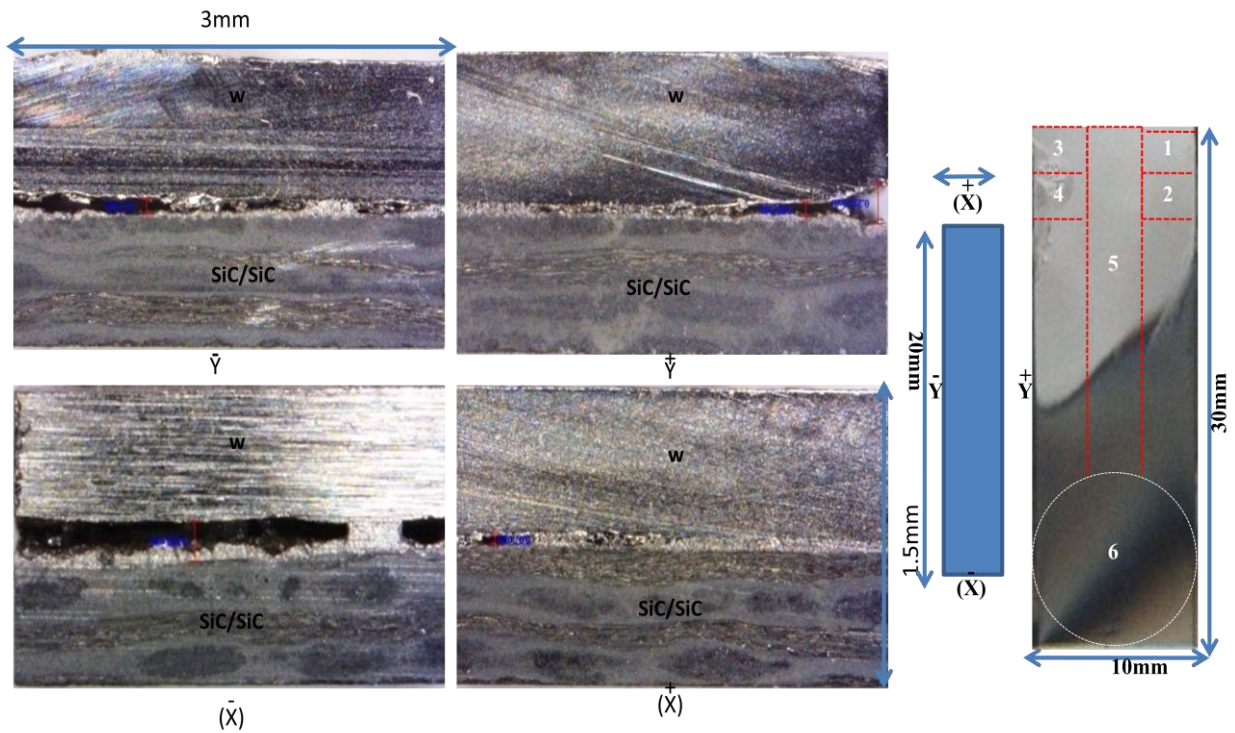


Fig.6.17. Macrostructure and SEM of W- SiC/SiC side (NITE-W/SiC-Dh1) position#4

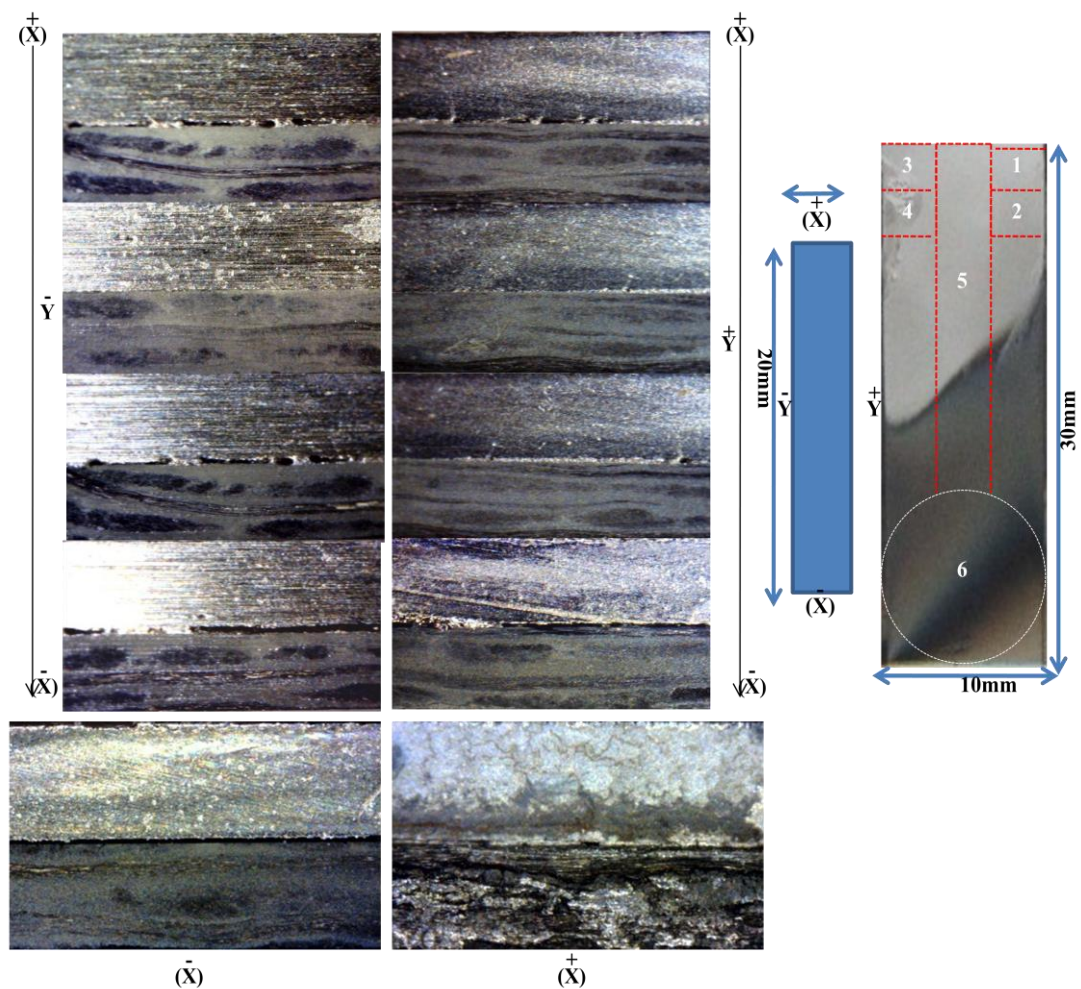


Fig.6.18. Macrostructure and SEM of W- SiC/SiC side (NITE-W/SiC-Dh1) position#5

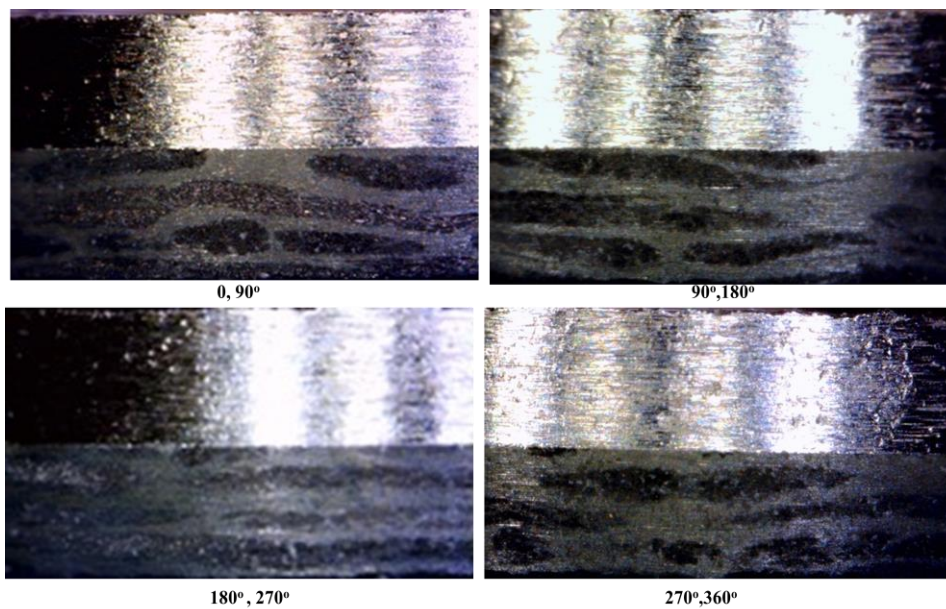


Fig.6.19. Macrostructure of W- SiC/SiC side (NITE-W/SiC-Dh1) position#6

The tile (NITE-W/SiC-Dv1) was investigated, where position #1(**Fig.6.20**) showed that the sides Y+, Y-, X+, X- appeared with sufficient bonding, but some plasma impurities and tungsten blisters were appeared.

Position#2 (**Fig.6.21**),the side Y-,X- showed sufficient bonding, whereas the sides Y+,X+ showed insufficient bonding, beside some plasma traces and tungsten blisters were appeared, SEM image of Y+ (**Fig.6.22**), showed segregation between tungsten and interphase layer.

Position#3(**Fig.6.23**); the side Y-, X-, X+ showed sufficient bonding, but the side Y+ showed the same phase of tiny segregation.

Position#4(**Fig.6.24**); the sides Y-,X- showed sufficient bonding, whereas the side Y+ showed partial debonding and the side X+ showed the phase of segregation between W, interphase layer and SiC/SiC.

Position#5(**Fig.6.25**); the sides Y+, X- showed sufficient bonding, whereas the other two sides; Y-, X+ showed the phase of segregation between W, interphase layer and SiC/SiC, also there was clear flakes of re-solidified blisters of tungsten.

Position#6(**Fig.6.26**); the sides Y+,X+,X- showed sufficient bonding and clear interphase layer, whereas the side Y- showed tiny pores at the interphase layer, beside re-solidified blisters of tungsten.

Position#7(**Fig.6.27**); showed excellent and sufficient bonding around the circumference of the circular sample from 0° to 360° .

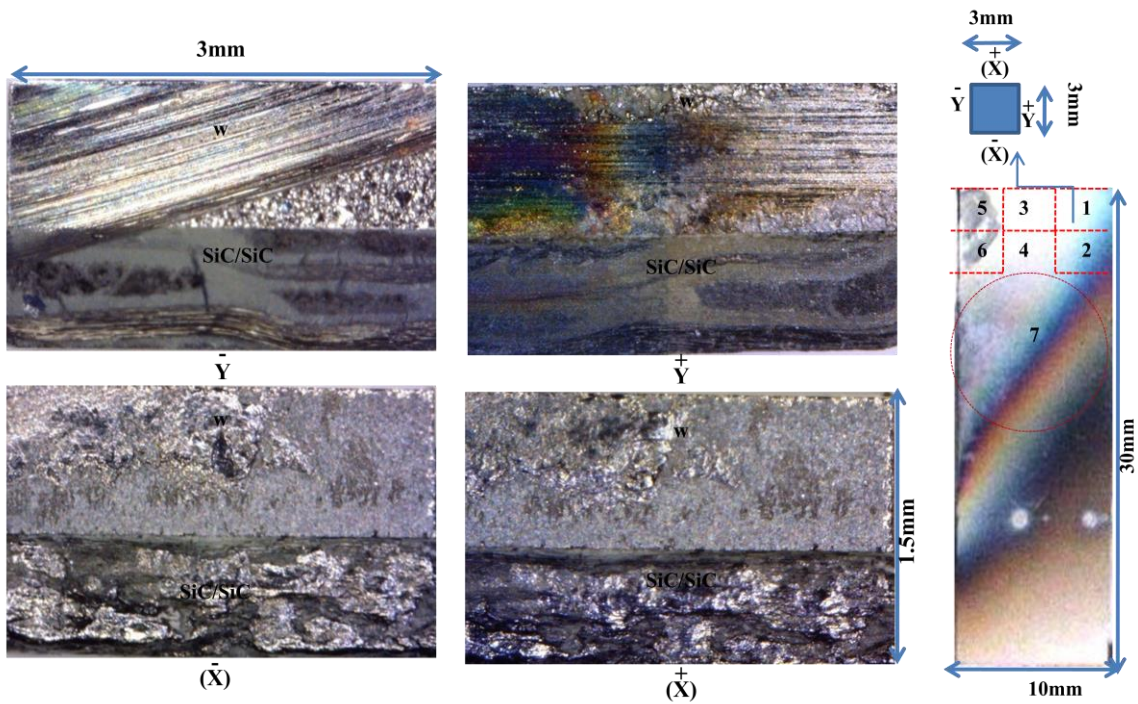


Fig.6.20. Macrostructure of W- SiC/SiC side (NITE-W/SiC-Dv1) position#1

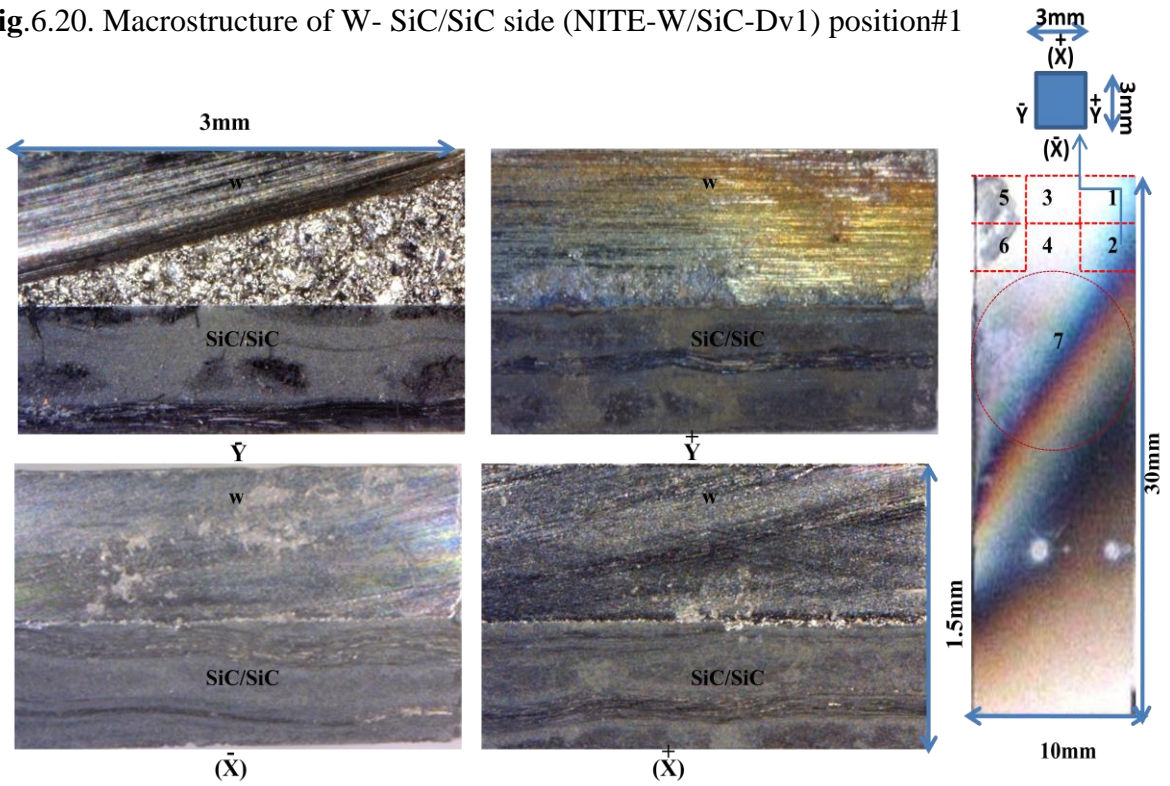


Fig.6.21. Macrostructure of W- SiC/SiC side (NITE-W/SiC-Dv1) position#2

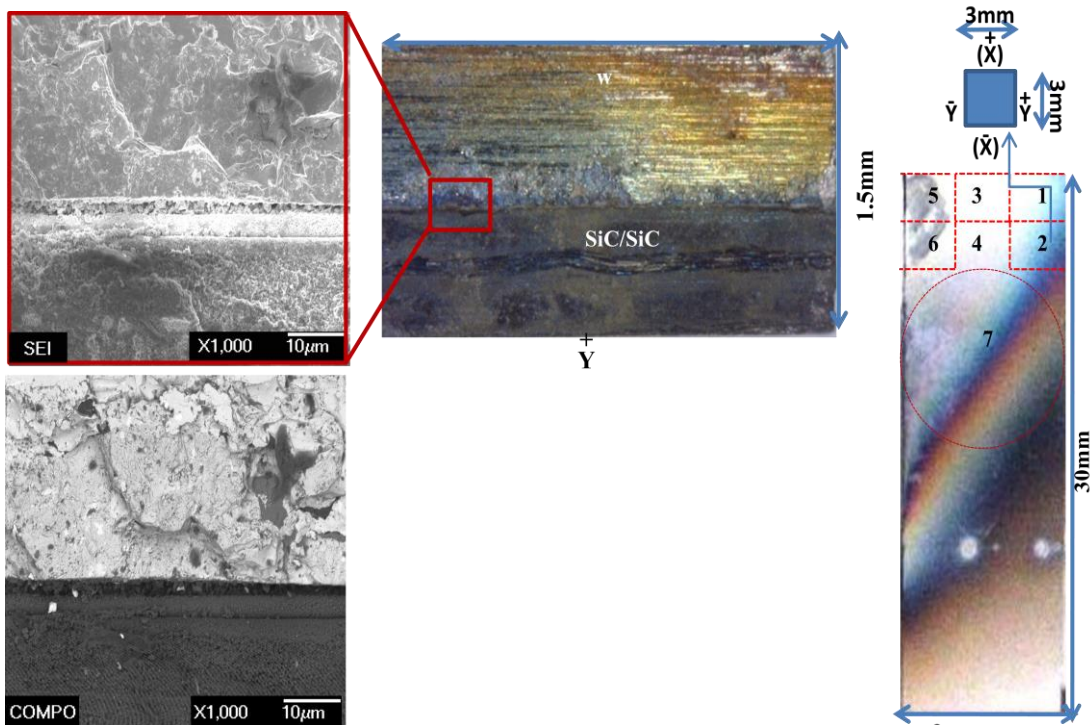


Fig.6.22. Macrostructure SEM of W- SiC/SiC side (NITE-W/SiC-Dv1) position#2 the side Y+

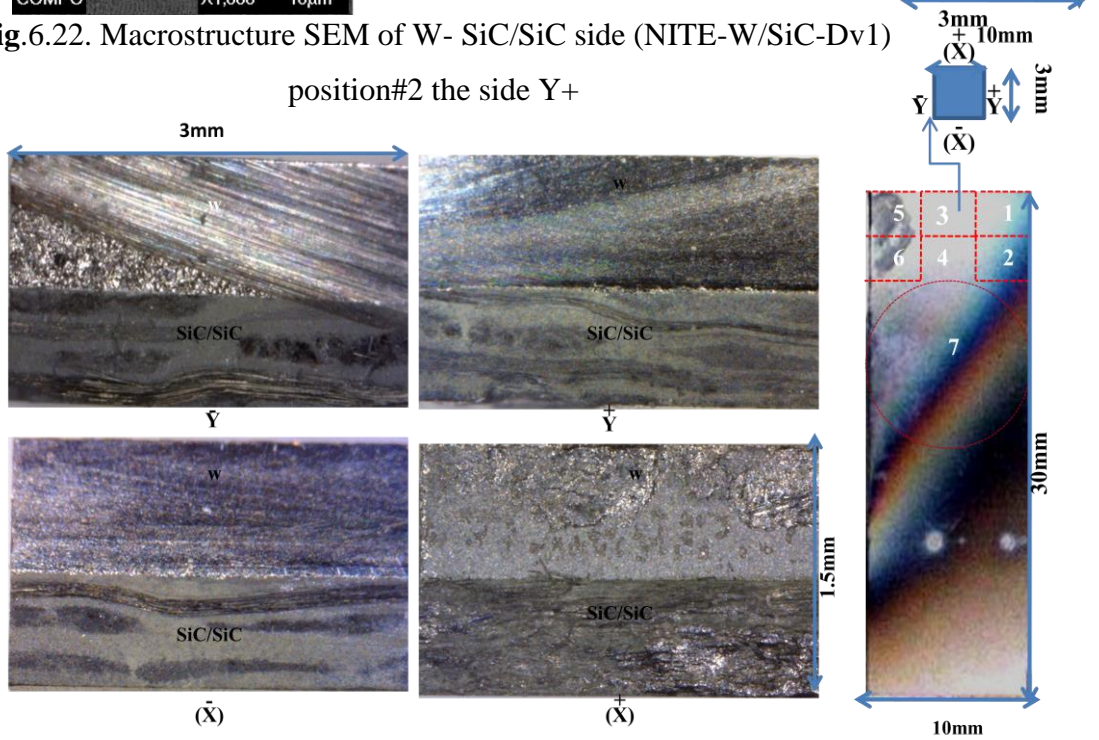


Fig.6.23. Macrostructure of W- SiC/SiC side (NITE-W/SiC-Dv1) position#3

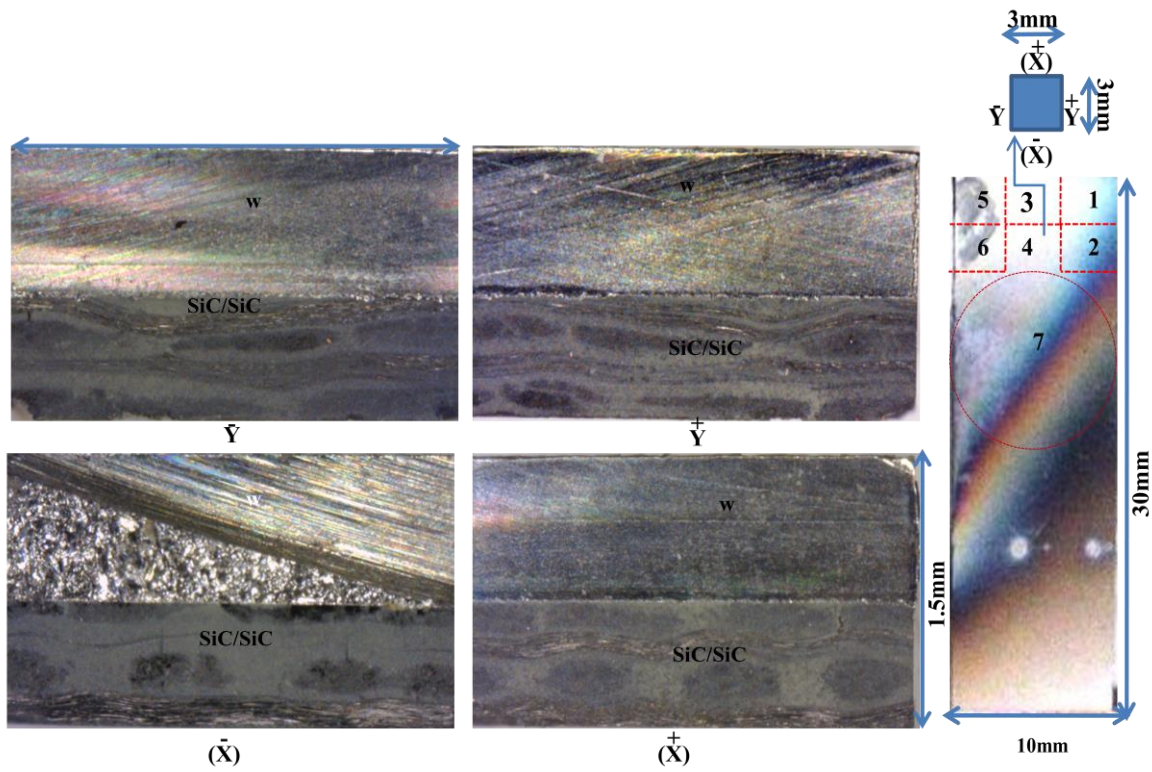


Fig.6.24. Macrostructure of W- SiC/SiC side (NITE-W/SiC-Dv1) position#4

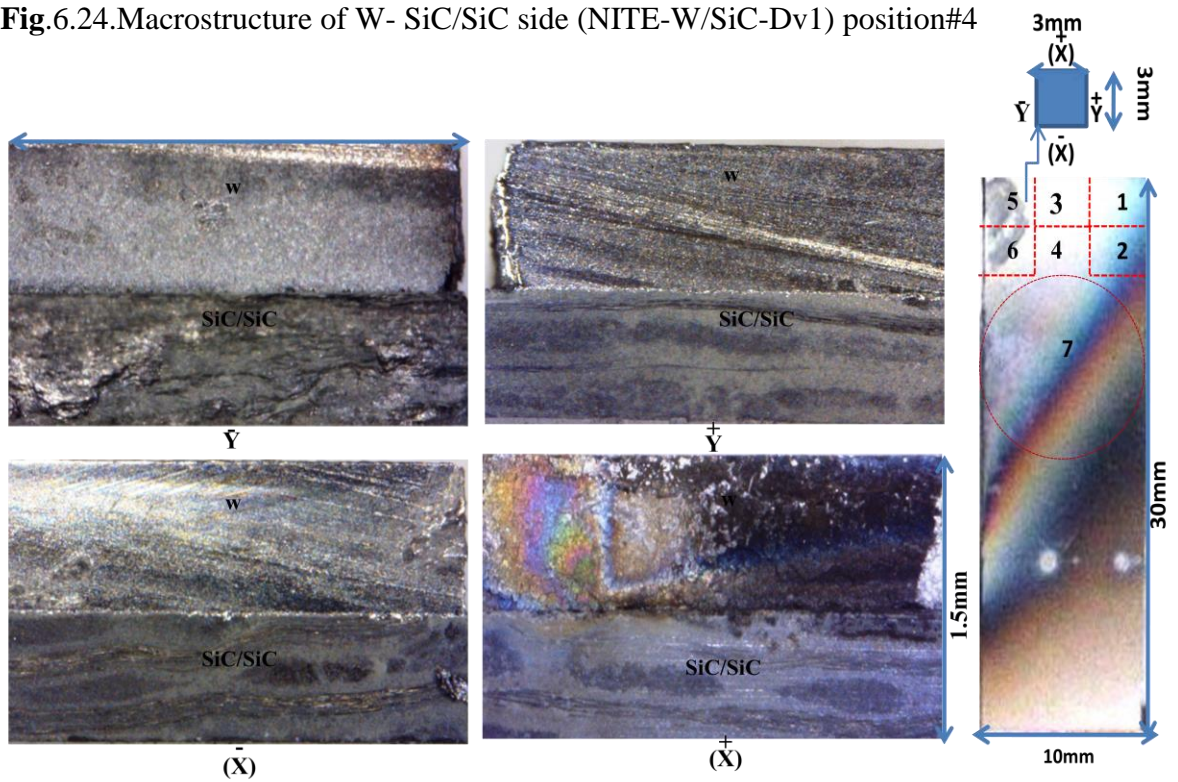


Fig.6.25. Macrostructure of W- SiC/SiC side (NITE-W/SiC-Dv1) position#5

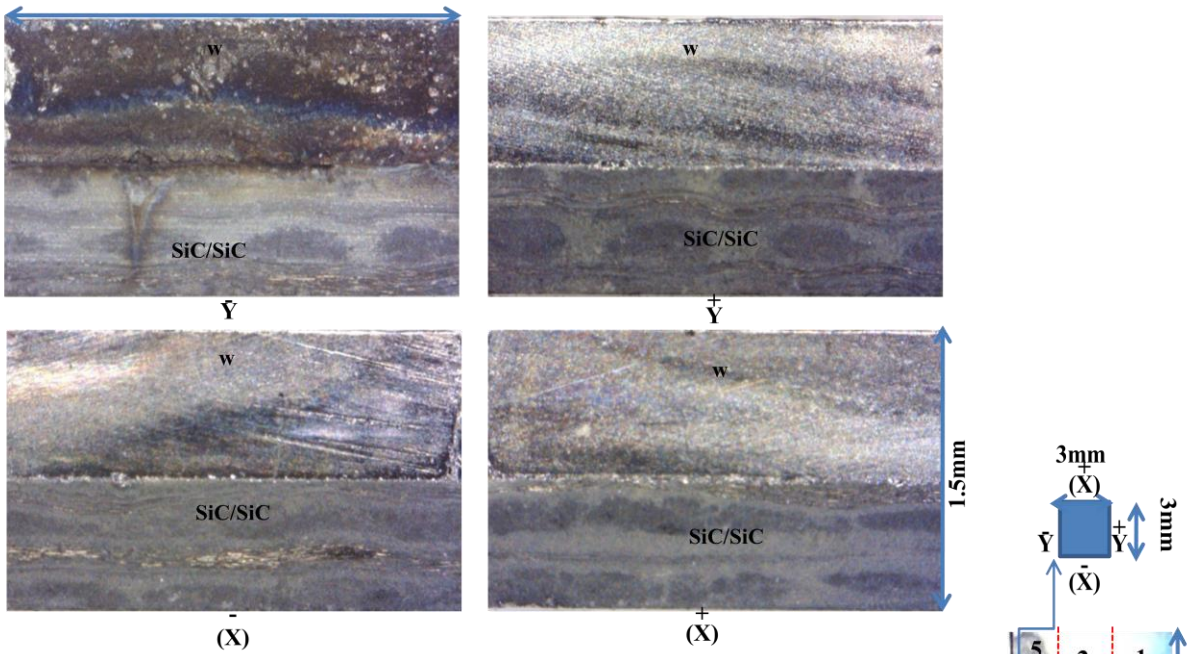


Fig.6.26. Macrostructure of W- SiC/SiC side (NITE-W/SiC-Dv1) position#6

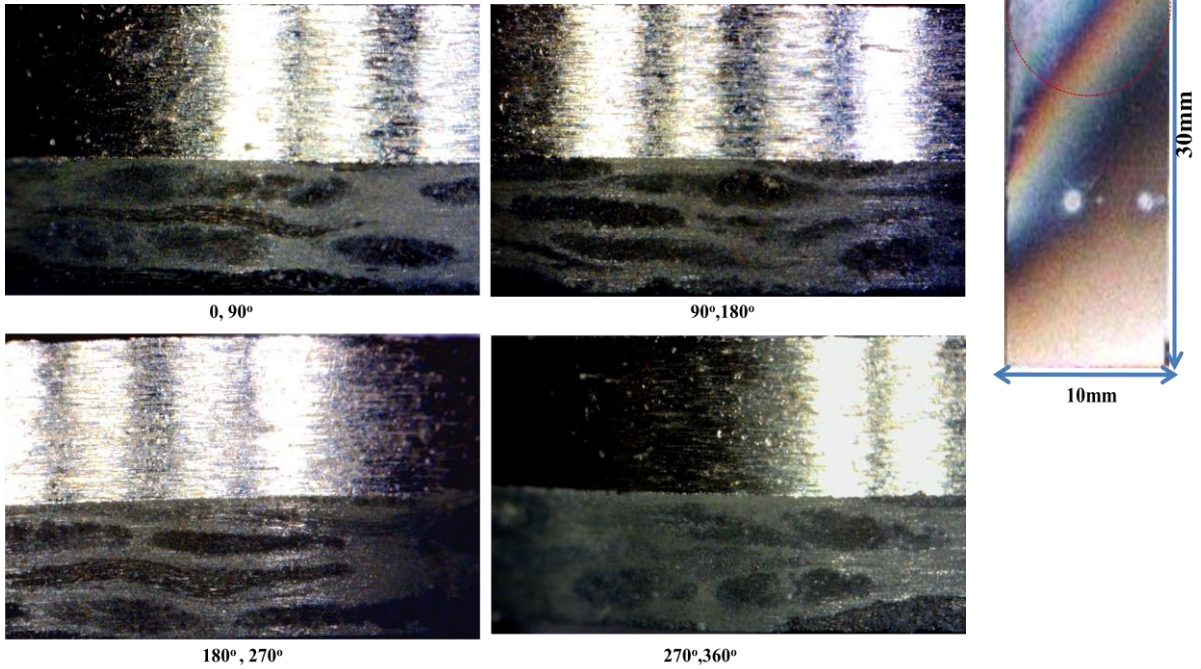


Fig.6.27. Macrostructure of W- SiC/SiC side (NITE-W/SiC-Dv1) position#7

6-3-Diffusion behavior analysis by Electron probe Micro-analyzer (EPMA).

Diffusion behavior analysis by electron probe micro-analyzer (EPMA) was conducted to the tiles before and after plasma exposure to study the diffusion behavior of elements (W, Si, C).

EPMA of the three tiles before and after plasma exposure showed that: no apparent diffusion of tungsten into SiC/SiC was detected, but there is a possibility that the interface transition caused by uniform volumetric diffusion of tungsten. Silicon and carbon diffusion behavior of the tile (NITE-W/SiC-S2) was changed before and after plasma exposure as shown in **Fig.6.28**, where shape of column-like silicon diffusion phases before the exposure were collapsed after the exposure. High concentrate uniform carbon diffusion phase before the exposure turned to be lower concentrate after exposure.

Fig.6.29, shows NITE-W/SiC-Dh1, where low concentrate uniform silicon diffusion could be detect before exposure and almost no apparent of silicon after the exposure. Uniform carbon diffusion phase also became invisible after the exposure.

Regarding to the tile (NITE-W/SiC-Dv1) as shown in **Fig.6.30**, silicon and carbon diffusion phases before the exposure are very similar to the phases on NITE-W/SiC-S2. Change by the exposure is also very close to the NITE-W/SiC-S2, column-like silicon phase became invisible and the contrast of uniform carbon diffusion phase became lower.

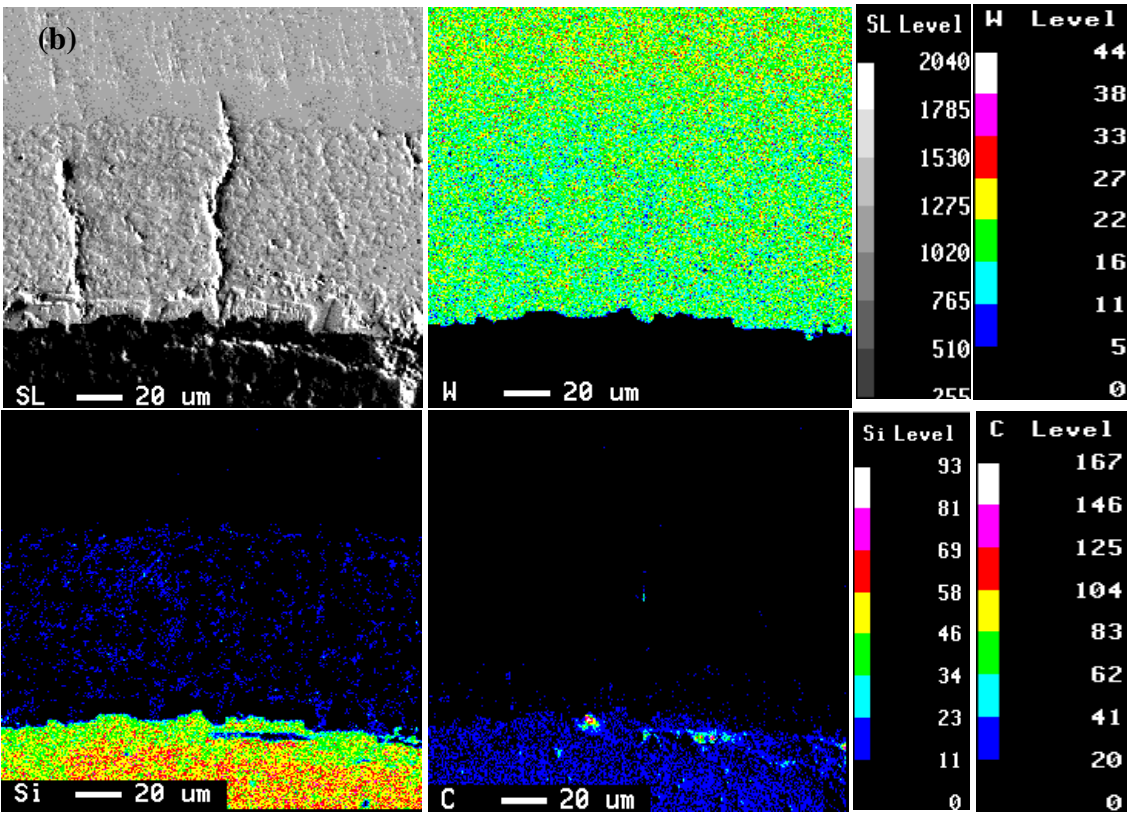
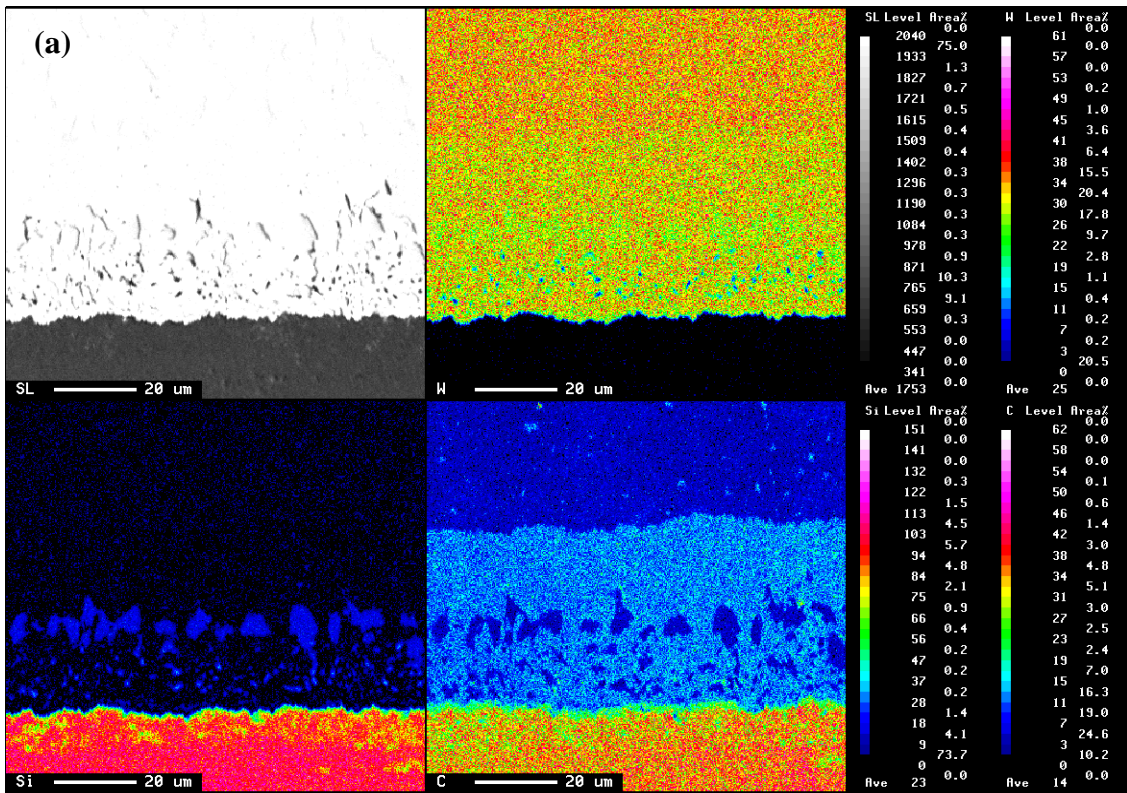


Fig.6.28. EPMA of the Tile (NITE-W/SiC-S2) before (a) and after Plasma Exposure (b)

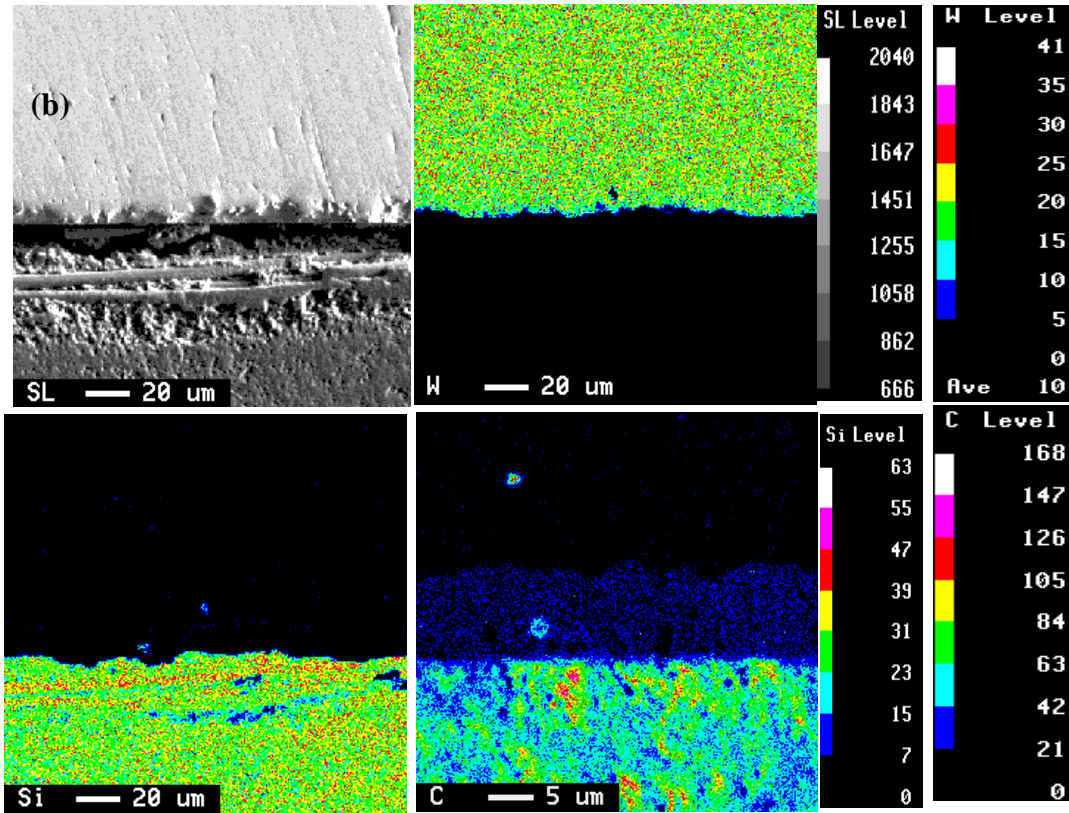
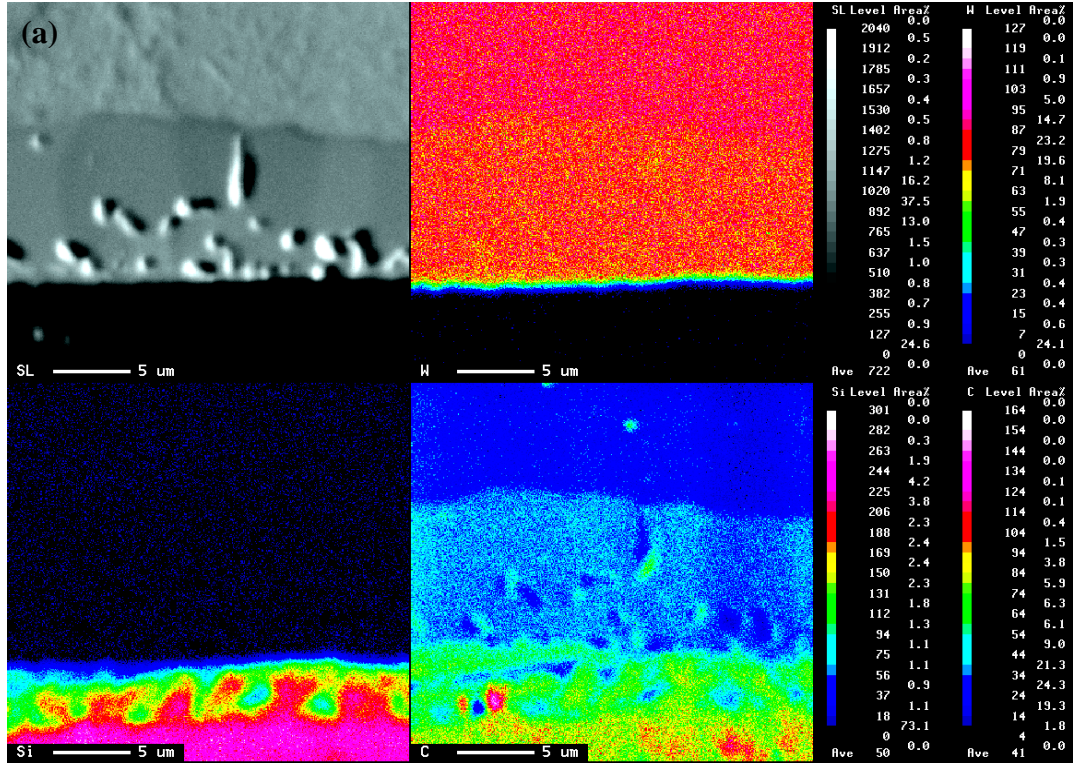


Fig.6.29. EPMA of the Tile (NITE-W/SiC-Dh1) before (a) and after Plasma Exposure (b)

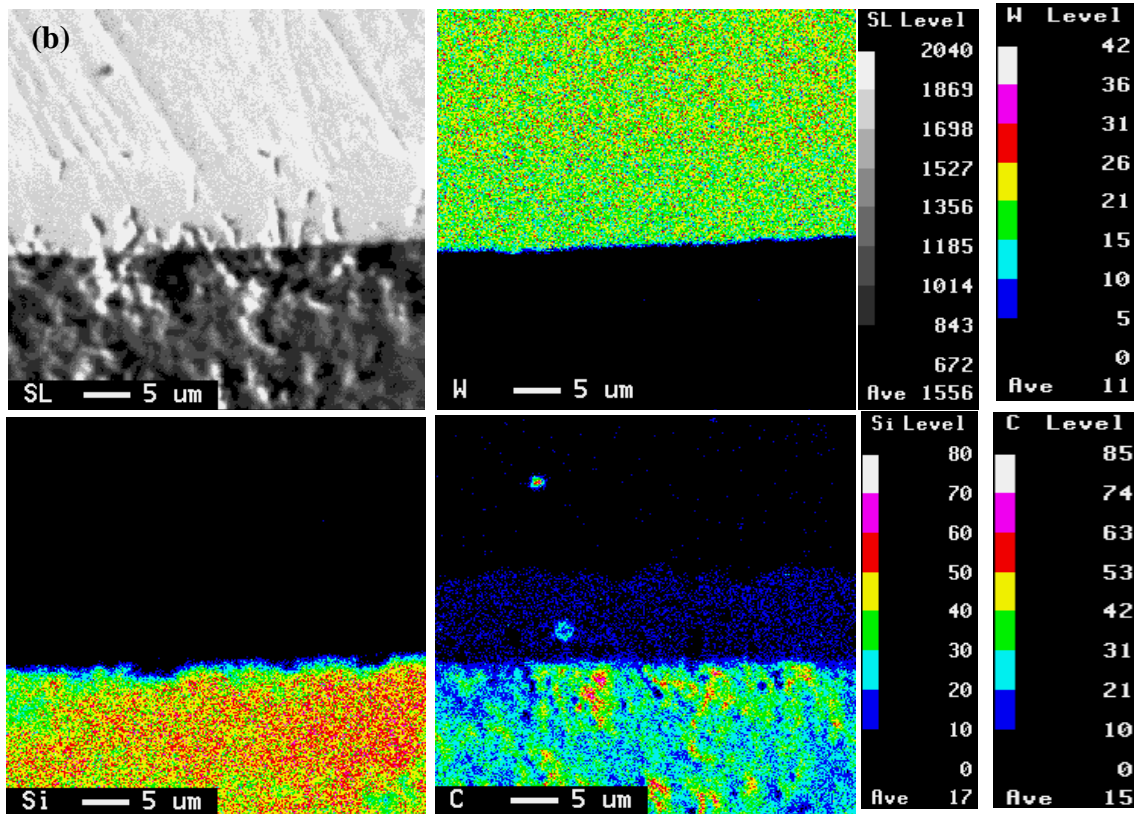
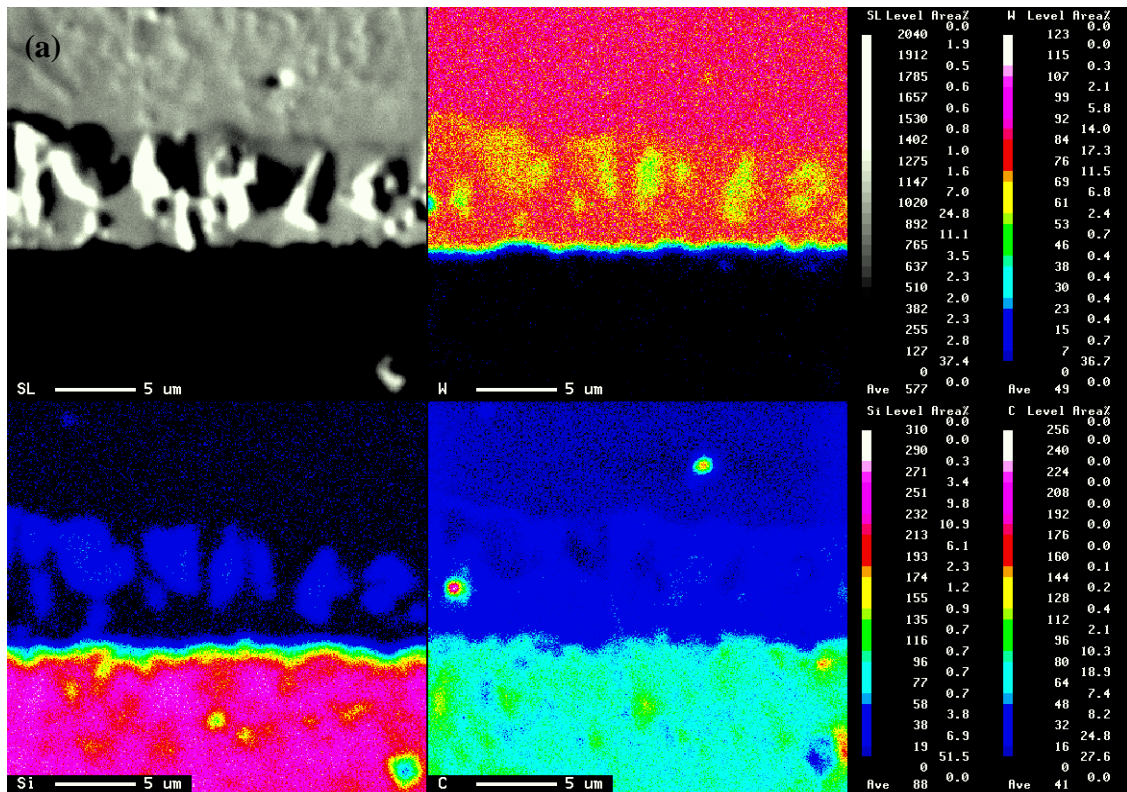


Fig.6.30. EPMA of the Tile (NITE-W/SiC-Dv1) before (a) and after Plasma Exposure (b)

6-4 -Deducing the surface and implanted temperature of the W-SiC/SiC irradiated tiles

To evaluate the heat flux durability of the hybrid component W-SiC/SiC, after the divertor plasma exposure test, due to 10 Mw/m^2 high heat flux load, it was indispensable to provide data about the temperature distribution through the thickness of the irradiated tiles, and investigate; if the applied temperature, due to the exposed heat flux was exceeded the limit of the degradation of tungsten armor; i.e. the DBTT and recrystallization limit of tungsten armor, for this purpose we used four techniques to deduce the temperature distribution from the surface to the interface region between Tungsten and SiC/SiC.

Three techniques were used; utilizing the micro structure evolution and one technique was conducted; utilizing finite element method. The techniques of deducing the temperature by using the micro structure evolution were reliable to deduce the implanted temperature into the interphase region, where one technique used; the comparison between the grain size distribution of the irradiated and the heat treated W-SiC/SiC tiles at the interphase region.

Second technique was used; utilizing the data of the damage analysis by ultrasonic method, which was studied in Chapter #5, where ultra sonic data provided reliable results about the debonding and changes occurred at the interface.

Third technique was used; utilizing EPMA analysis of the irradiated tiles, where the tracking of silicon diffusion behavior in the interphase layer, after the divertor plasma exposure test, enabled us to calculate the temperature required for achieving such diffusion of silicon, due to the plasma exposure test.

The fourth technique was used; utilizing the finite element method, where it was reliable calculation to deduce the surface temperature and distribution of the temperature through the thickness of the irradiated tiles, due to 10 Mw/m^2 heat flux of plasma exposure.

6-4-1-Deducing the implanted temperature by: the comparison between the grain size distributions.

By the comparison between microstructure evolutions at W-SiC/SiC interface, after heat treatment at 1600 °c for 10 hours, and the microstructure evolutions at the interface of irradiated tiles after divertor plasma exposure, we can make inference of the implanted temperature at the interface of the irradiated tile, by calculating the average grain size of both the heat treated microstructure and irradiated tile at the interphase region for a distance 40 micron from the interface, **Fig.6.31**, showed the granulation of tungsten at the interphase region, due to heat treatment, **Fig.6.32** showed the granulation of tungsten at the interphase region, due to the divertor plasma exposure to a heat flux up to 10Mw/m².

The average grain size of the heat treated microstructure and the irradiated tile due to divertor plasma exposure calculated to be 4.3µm, 4.5µm respectively. The correlation between grain size distribution of heat treated and irradiated tile is showing at **Fig.6.33**

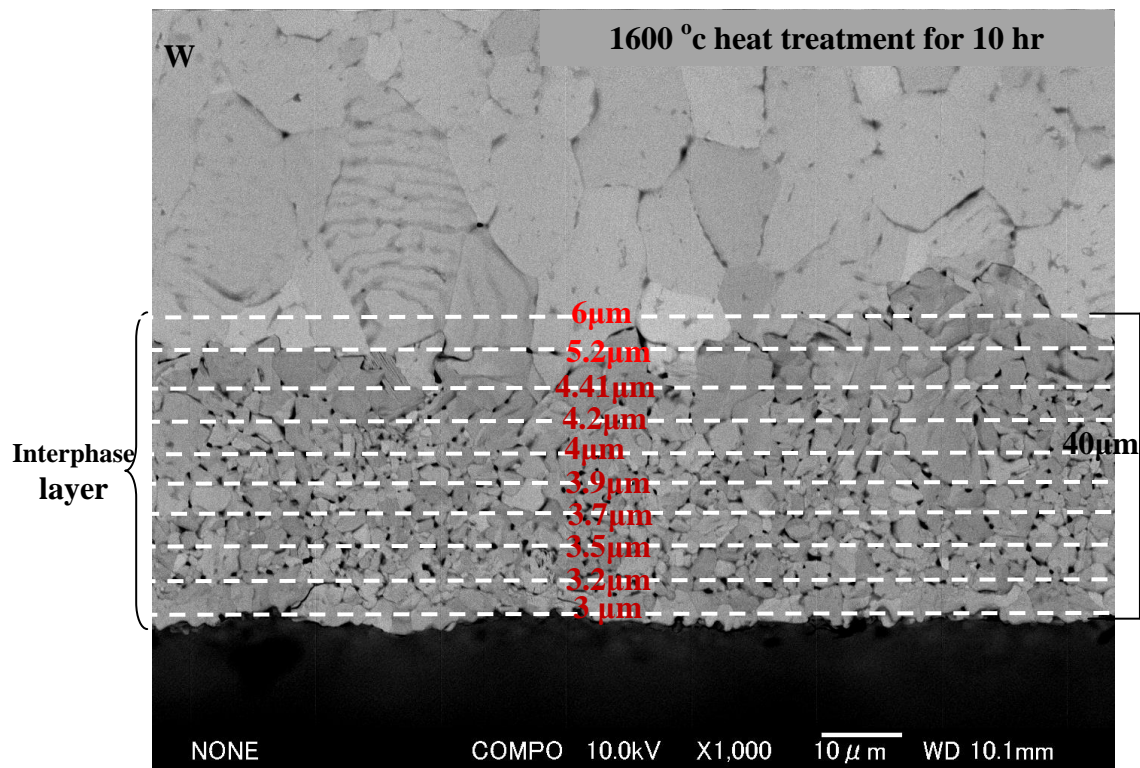


Fig.31. Granulation of tungsten at the interphase region, due to heat treatment of 1600 °c

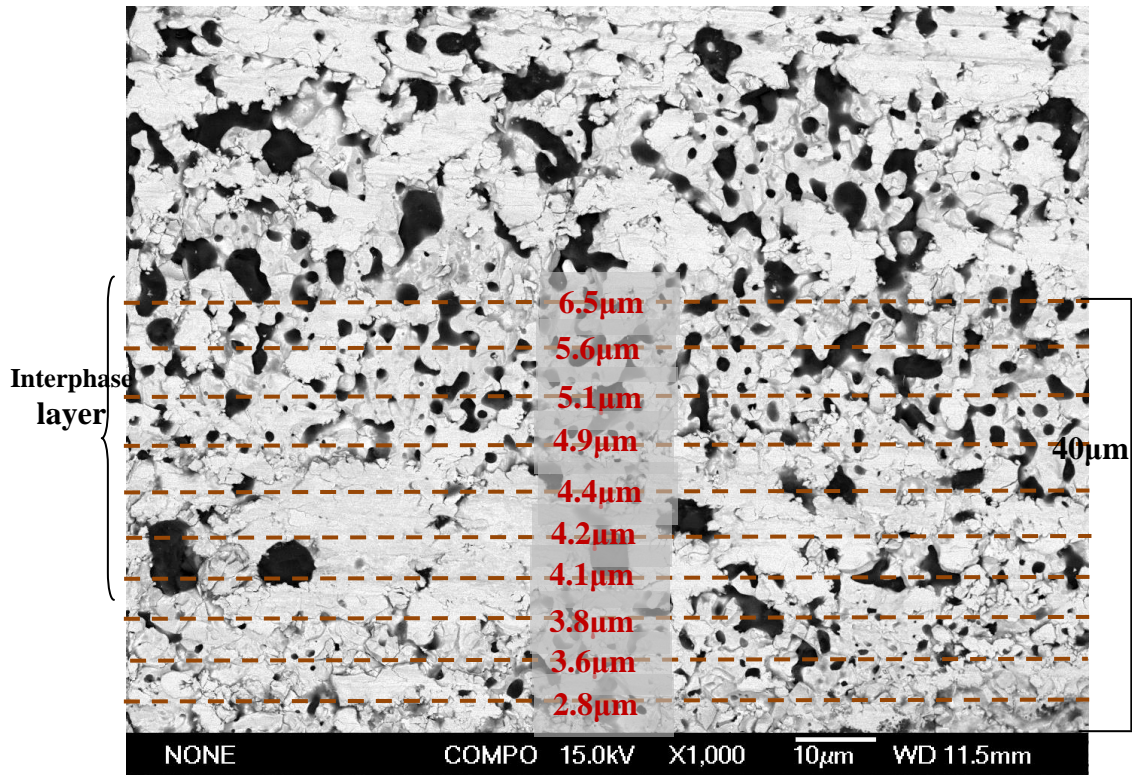


Fig.6.32. Granulation of tungsten at the interphase region, due to plasma exposure of heat flux up to 10 Mw/m²

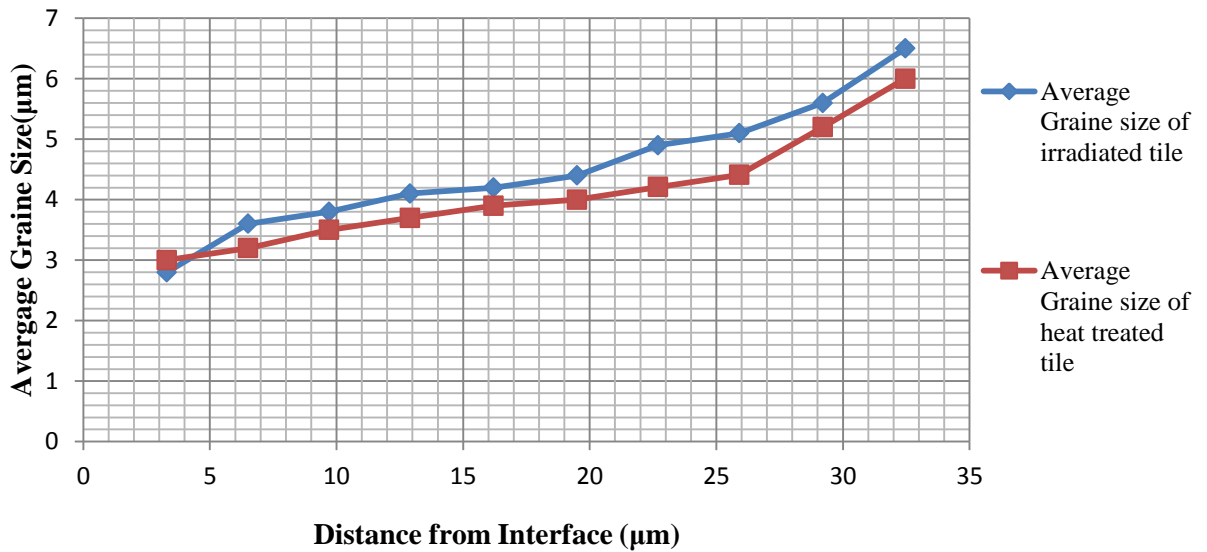


Fig.6.33. The correlation between grain size distributions of heat treated and irradiated tile

the agreement of the grain size distribution between heat-treated and irradiated microstructure as shown in **Fig.6.33** , provide an evidence; that the implanted temperature of the irradiated tile to the interface is conforming with the temperature of the heat treatment, which was 1600 °c . Although the time of exposure inside large helical device was 10 seconds, but the exposure was heat flux not only steady heat treatment.

6-4-2-Deducing the implanted temperature; utilizing the damage analysis by ultrasonic method.

Although this study were discussed at chapter #5, it provided qualitative damage analysis of the irradiated tiles, after the plasma exposure, and we tried by the color contrast appeared by C-scanning images to speculate the implanted temperature, but currently we will try to promote the speculated implanted temperature to be more reliable data depending on the C-scanning image and the debonding occurred at the interphase region, where the debonding is an evidence of the melting of the diffusion layer, where the EDS and XRD data showed that; the main composition of the diffusion bonding layer is tungsten silicides, which means that the implanted temperature could be reached to the eutectic temperature of the tungsten silicides.

For that purpose we investigated the eutectic temperature of tungsten silicides by using W-Silicon equilibrium phase diagram, and we used the percentage of dissolved silicon from EPMA data which was up to 20 % . The eutectic temperature of the tungsten silicides of silicon percentage up to 20% was ranging from 1700° C to 2000 °C.

Fig.6.34 and Fig.6.35 showed the damage analyses on the tile (**NITE-W/SiC-Dh1**) by C-Scanning image & W-Silicon equilibrium phase diagram respectively.

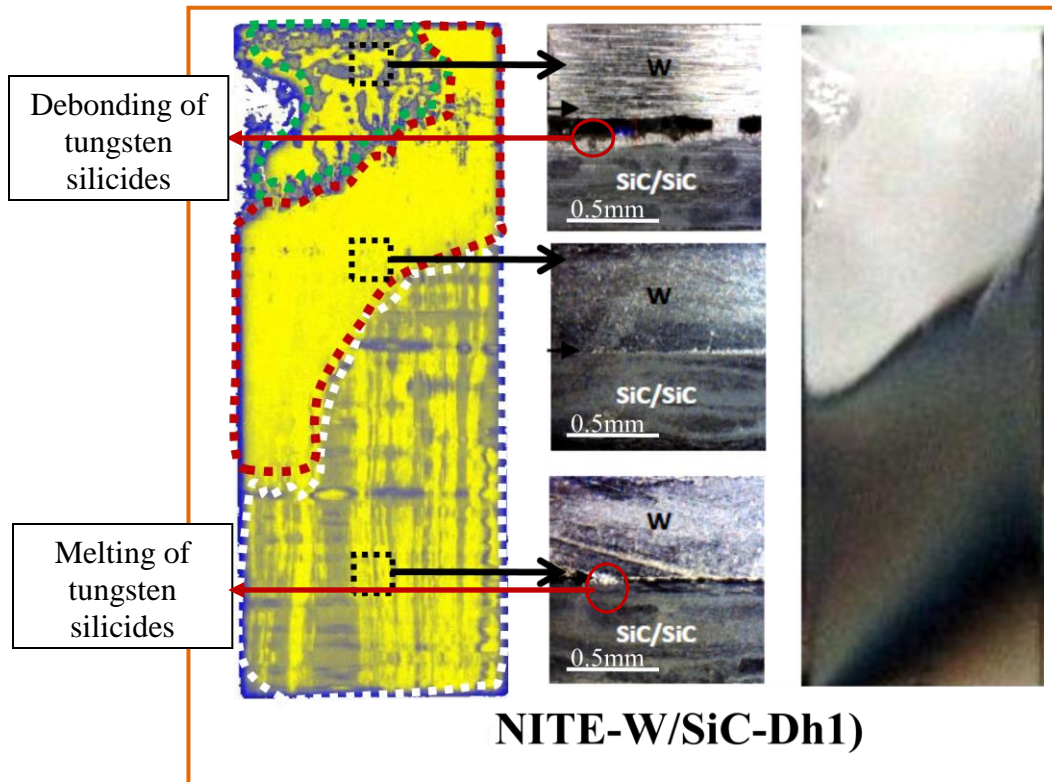


Fig.6.34.The damage analyses on the tile (NITE-W/SiC-Dh1) by C-Scanning image

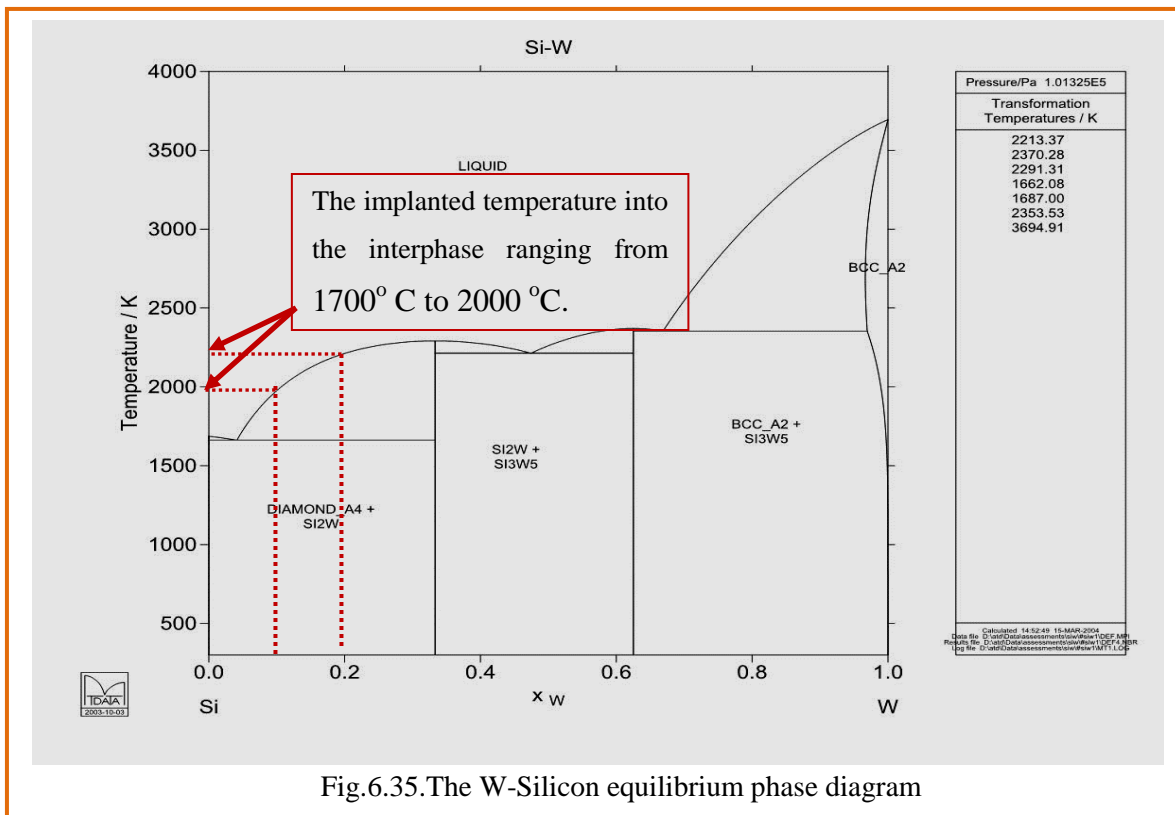


Fig.6.35.The W-Silicon equilibrium phase diagram

6-4-3-Deducing the implanted temperature by: tracking the diffusion of silicon in the interphase layer.

EPMA analysis provided us qualitative measurement of the diffused elements from SiC/SiC side to W side, before and after plasma exposure, in this section the tracking of silicon behavior into the interphase reaction layer will be used to deduce the temperature required to achieve such diffusion of silicon into tungsten silicides, where Arrhenius and Einstein equations were applied to calculate the temperature required to make diffusion of silicon into tungsten silicides, due to the plasma exposure. EPMA analysis of the tile (NITE-W/SiC-Dv1); before and after plasma exposure is shown in the Fig.6.36.

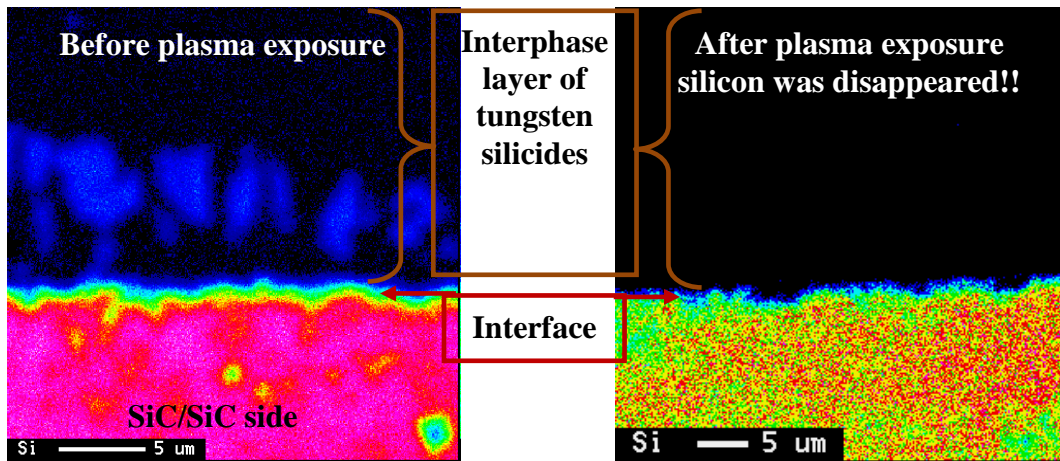


Fig.6.36. EPMA analysis of the tile (NITE-W/SiC-Dv1); before and after plasma exposure

$$D_2 = X^2 / 2t \dots\dots\dots \text{Einstein equation}$$

$$D_2 = D_1 \exp \left[-Qd / R \left(1/T_2 - 1/T_1 \right) \right] \dots\dots\dots \text{Arrhenius Equation}$$

Where D_1 is the diffusion coefficient m^2/s , of silicon in tungsten silicides due to plasma exposure, Qd is the activation energy of silicon in kJ/mol [5]. R is the general gas constant, $T_2(\approx 1870^\circ C)$ is the temperature of diffusion due to fabrication conditions[6]. D_2 is the diffusion coefficient m^2/s of silicon into tungsten silicides due to fabrication conditions, X is the displacement of silicon and t is the time of fabrication in seconds. By applying the above equation it was found that the temperature required for diffusing the silicon into tungsten silicides, due to plasma exposure was up to $1650^\circ C$.

6-4-4-Deducing the distribution of the temperature by: finite element method.

Prediction and analysis methods are key parameters to decrease the gap between long and short term design aspects of the high heat flux components; also it is effective tool to judge on the durability of the proposed material for high heat flux components, where we can simulate different operating conditions without producing large numbers of samples.

Finite elements method is highly considerable tool to conduct the numerical steady state thermal analysis. ANSYS code release 13 was used to conduct this study, by mechanical APDL application, where steady state thermal analysis can determine the temperature distribution and other thermal quantities under steady-state loading conditions. Steady-state loading condition is the situation, where heat storage effects varying over a period of time can be ignored.

The steady state thermal loading condition on the hybrid W-SiC/SiC system was conducted. Different thermal conductivity of each tungsten tile, due to the different rolling direction of the three fabricated tiles, the transverse thermal conductivity of SiC/SiC composite were used as physical material properties. Application of coupled field analysis was conducted to provide us the temperature distribution through the tile thickness due to the applied heat flux.

The model was constructed as 2D cross section of W/SiC-SiC, with dimension 5x1.5mm, where tungsten thickness is 0.7mm and SiC/SiC thickness is 0.8mm.

The thermal boundary conditions were selected as; heat flux acts on tungsten edge, the upper and lower edge of the model was completely isolated and the boundary condition of the SiC/SiC surface was selected to be as active cooled surface with a bulk temperature, and the mechanical boundary conditions were selected as free expandable tungsten face and the upper and lower edge were selected to be expandable, whereas the surface of SiC/SiC was selected to be fixed.

6-4-4-1-Building and loading of the model

The model was built to be a 2D cross section of a thermally connected Tungsten and SiC/SiC, with dimension of 10x1.5mm, tungsten thickness is 0.7mm and SiC/SiC thickness is 0.8mm. After geometric building of the model, the selection of the element type was conducted to be (PLANE223 coupled field solid), where this element has eight nodes with up to four degrees of freedom per node [7]. The geometry of the (PLANE223) is illustrating at **Fig...** after building the 2D cross section model, the loading and boundary conditions were selected to be a heat flux confronting the tungsten armor and the both of upper and lower edge of the tile and the back side of SiC/SiC were loaded to be zero heat flux, SiC/SiC side supposed to be a heat sink with film coefficient up to 100 and bulk temperature 100°C. The static boundary conditions of W face, upper and lower edge of the tile were selected to be expandable in directions X, Y, where SiC/SiC side was fixed in both X, Y directions. Material properties of tungsten (powder and horizontal, vertical) and SiC/SiC were: thermal conductivity, poisson ration and modulus of elasticity and coefficient of thermal expansion. The Tiles ID (NITE-W/SiC-S2), (NITE-W/SiC-Dh1), (NITE-W/SiC-Dv1) used tungsten with anisotropic thermal conductivity, where it was investigated by laser flash analysis, where 173 W/mK at 25°C, 90 W/mK, 110W/mK and was indicated at 1300°C for tungsten without rolling direction, parallel to rod axis (horizontal rolling direction) and perpendicular to plate (vertical rolling direction), respectively[8] (The selected materials properties are illustrating at **table.6.1.** [9]).

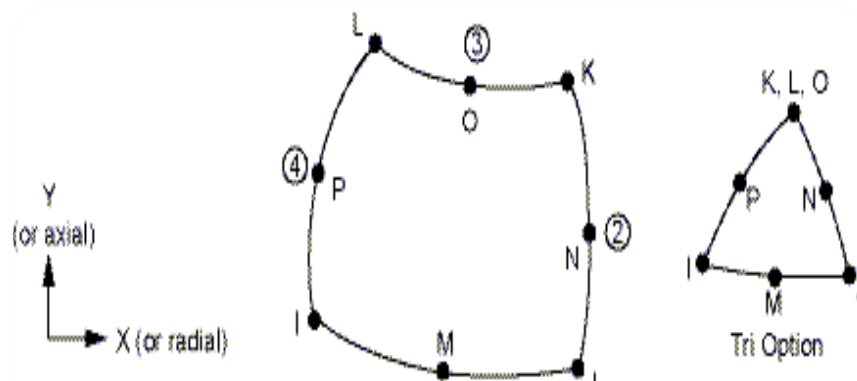


Fig.6.37.the geometry of the element (PLANE223)

Table.6.1. (The physical properties of tungsten and SiC/SiC)

Material property	SiC/SiC	W (without rolling direction)	W(with horizontal rolled direction)	W (with vertical rolled direction)
Thermal conductivity	34W/mK @ 200 ^o c, 26 W/mK @1000 ^o c (@ transverse direction)	173W/mK@25 ^o c	90W/mK at 1300 ^o c	110W/mK @1300 ^o c
Coefficient of thermal expansion	4.3	4.5	4.5	4.5
Poison ratio	0.21	0.28	0.28	0.28
Modulus of Elasticity	32Gpa@0^oc,11Gpa @740^oc,19 Gpa @750^oc	411Gpa	411Gpa	411Gpa

After preparing the model geometrically and boundary conditions, the heat flux; up to 10 Mw/m² was applied at the tungsten armor of the three tiles, to investigate; surface temperature, the thermal gradient through the thickness of each exposed tile, therefore we can investigate; if these temperatures will exceed the DBTT and recrystallization temperature of tungsten or not. The DBTT and recrystallization temperature of tungsten had been investigated to be 400^oc and 1300^oc respectively [10]. Loading and boundary conditions of the model are illustrated in the schematic view in Fig.6.38., where tungsten confronted the applied heat flux up to 10 Mw/m², and upper and lower edge of the tile were selected to be in adiabatic conditions, and the side of SiC/SiC worked as heat sink, with bulk temperature up to 100^oC. The results of the model of the three exposed tiles are illustrating in the Fig.6.39, and the temperature distribution from the surface through the thickness of the tile is illustrating in the Fig.6.40.

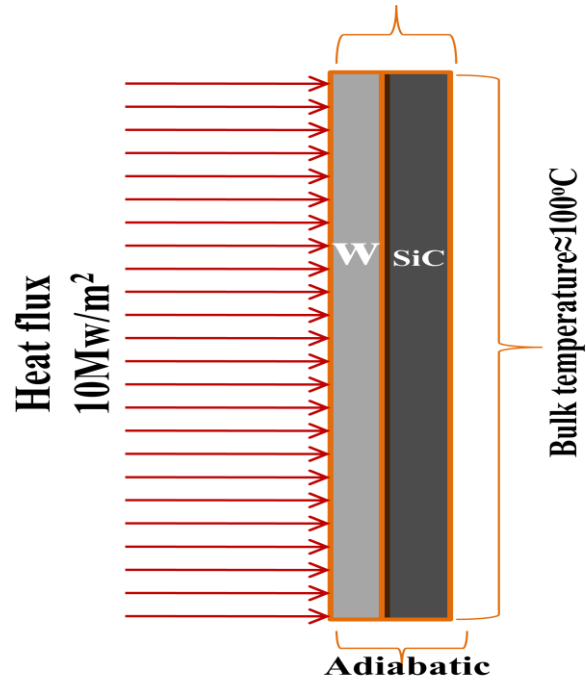


Fig.6.38. Loading and boundary conditions of the model

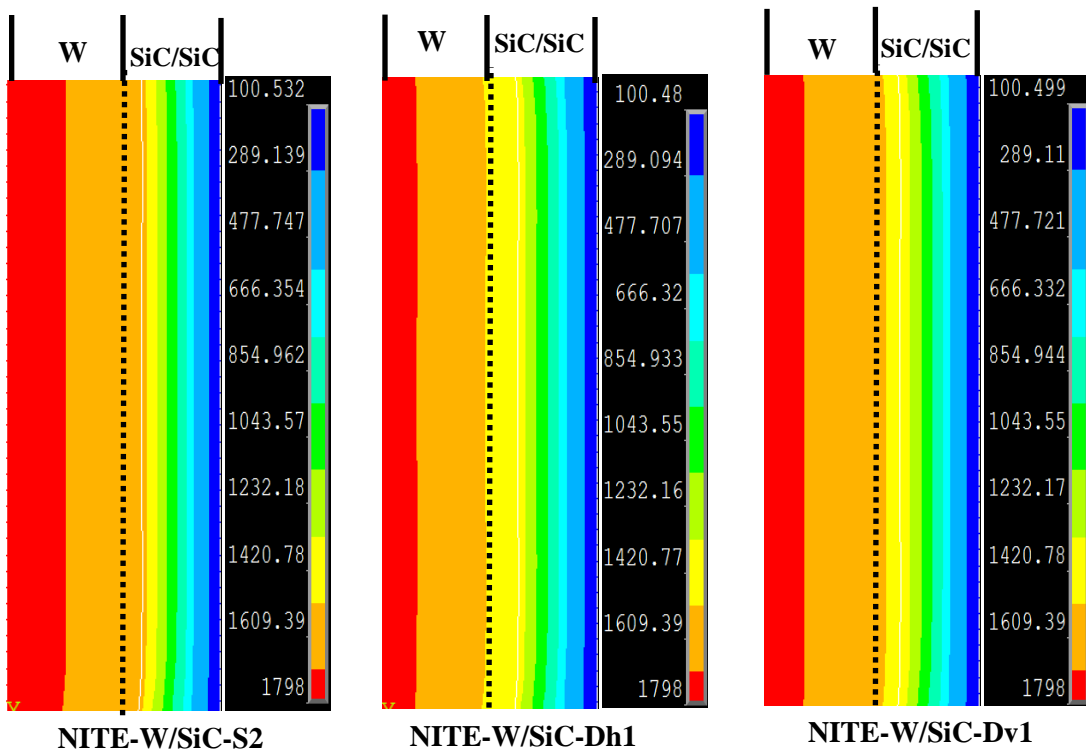


Fig.6.39. The results of the model of the three exposed tiles

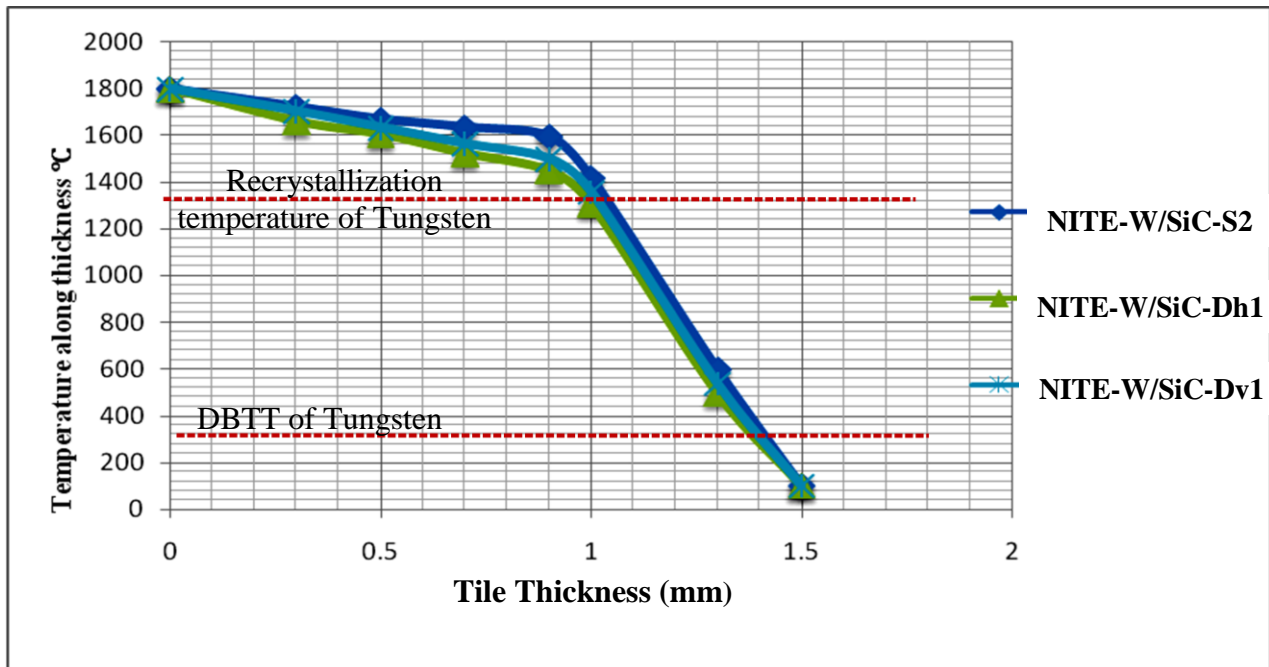


Fig.6.40.The temperature distribution from the surface through the thickness of the irradiated tiles.

The results of the model showed that; the maximum surface and interface temperatures of the tiles (NITE-W/SiC-S2), NITE-(W/SiC-Dh1) and (NITE-W/SiCDv1) were; (1798 °C, 1634 °C), (1789 °C, 1521 °C), (1798 °C, 1563 °C), respectively.

6-5-Discussion

The irradiated tiles were survived from catastrophic damage due to applied heat flux of 10 MW/m²; i.e. there was not complete debonding between tungsten and SiC/SiC along each tile length. Due to thermal effect of applied heat flux and plasma strike, there was degradation on tungsten surface and on the interface zone between tungsten and SiC/SiC also there was an observed degradation on SiC/SiC part .the analysis methods to investigate was ranged from visual test to macro and micro structure tests, where the visual test provided information of the conditions of the tiles around it's perimeter and on tungsten and SiC/SiC sides only. The macro and micro structures of the irradiated tiles provided a qualitative analysis of degradation of the exposed tiles, where the analysis of the three

exposed tiles showed that heat flux effect on tungsten surface caused different degradation due to different thermal conductivity of tungsten and different fabrication conditions of the tiles, the highly effected zones of the irradiated tiles were near the fused zones of the surface and near to the edges. The analysis by electron probe micro analyzer showed also that the behavior of diffusion of (W, Si, C) was not the same at the irradiated tiles due to different thermal conductivity of the tungsten surface.

The techniques used to deduce the temperature implanted to the interface provided us reliable data about the temperature distribution through the thickness of the irradiated tile where using technique by the Comparison between Micro structure evolution due to heat treatment of 1600 °c for 10 hours and the micro structure evolution due to plasma heat flux exposure provided reliable evidence that the implanted temperature to the interface of the W-SiC/SiC tile was not less than 1600 °c, this temperature exceeded the recrystallization temperature of the tungsten which had been investigated as 1300 °c and exceeded the temperature of DBTT of tungsten, which had been investigated as 400 ° c .

Deducing the implanted temperature by damage analysis, utilizing ultrasonic method was used by interpretation the meaning of the color contrast of the irradiated tiles, where the yellow zones with attenuation by blue colors referred to discontinuity at the interphase region, this discontinuity was investigated as complete debonding and melting of the interphase reaction layer, which its main composition was tungsten silicides, the analyses showed that tungsten silicides has an eutectic temperature with silicon percentage ranging from 10 to 20 ranging from 1700 °C to 2000 °C, respectively.

Deducing the implanted temperature by tracking the silicon diffusion into tungsten silicides, also was reliable technique by calculation the temperature; required to diffuse silicon into tungsten silicides, due to the heat flux load after divertor plasma exposure, where EPMA data showed that the silicon disappeared from the tungsten silicides interphase reaction layer in the tile (NITE-W/SiC-Dv1), which means that the silicon diffused from low

concentration region of silicon to high concentration region of silicon, which its conflicting with basics rules of diffusion laws , but this could be argued due to slightly segregation between tungsten and SiC/SiC side as shown in the Fig.6.22, beside the slight segregation between W and SiC/SiC, the calculated temperature required to diffuse silicon into tungsten silicides in the direction of SiC/SiC side was also a driving force to cause the diffusion of silicon, where the calculated temperature showed that the implanted temperature to cause such diffusion was up to 1650°C.

Deducing the temperature distribution of the three irradiated tiles by using the finite element method was reliable to show the temperature distribution from the surface of the irradiated tiles to the interface region, but due to the limitations of ANSYS code, and the insufficient data of the thermal conductivity of the interphase layer, it was not accurate temperature at the interphase region. The surface temperature of the irradiated tiles was average calculated as 1800°C and it was descending into the interface region to be almost 1550 °C.

6-6-Conclusion

Macro and micro structure investigation, due to the divertor plasma exposure test to 10 MW/m², showed that the fabricated tiles of the hybrid component of W-SiC/SiC survived from the catastrophic damage, i.e. there was not completely debonding between Tungsten and SiC/SiC around the tile thickness, the macro and micro structure analysis showed that the degradation of tungsten surface was only tiny scratches due to arc traces of plasma strike and neutron irradiation, beside the fused protrusion of tungsten on the edge of the tiles (NITE-W/SiC-S2), (NITE-W/SiC-Dh1) which it is evidence that the surface temperature exceeded the limit of melting point of the tungsten, i.e. it was greater than 3400 °C.

Micro structure analysis of the interface between tungsten and SiC/SiC showed that there were debonding regions and segregation zones between W and SiC/SiC, due to the implanted temperature, which was investigated; not less than 1600°C which it is greater

than the recrystallization temperature of Tungsten i.e. greater than 1300° C, and greater than the DBTT of tungsten (300°C). EPMA analysis showed that the behavior of silicon diffusion from SiC/SiC side to tungsten was changed, due to 10 MW/m² heat flux exposure.

References

- [1] ITER Final Design Report 1998, G 17 FDR 5 98-05-29 W 0.2, Design Description Document WBS 1.7, Divertor.
- [2] C.Ibbot, et al., Overview of the engineering design of the ITER divertor, Proceeding of 21st SOFT, Madrid, Spain, 2000.
- [3] A.Makhankov, et al., Development and optimization of tungsten armor geometry for ITER, Proceeding of 20th SOFT, Marseille, France, 1998.
- [4] V.Gagen-Torn, et al., Experimental complex for high heat flux materials interaction research, 18th SOFT, Germany, Karlsruhe, 1994, vol. 1, pp. 363-366.
- [5] Soumitra Roy, et al, diffusion in tungsten silicides, intermetallic 37 (2013) 83-87.
- [6] Hiroshi Kobayashi Yong, master thesis in Kyoto University, 2008.
- [7] Official site of ANSYS code, <www.ansys.com>.
- [8] M. Reith et al., Tungsten as structure DEMO divertor material, in: Proceedings of Annual Meeting on Nuclear Technology, Dresden, Germany, 2009.
- [9] G.E. Youngblood et al. J. Nucl.Mater., 307-311 (2002), pp. 1120-1125.
- [10] A.R. Raffray, R. Nygren, D.G. Whyte, S. Abdel Khalik, R. Doerner, F. Escourbiac Fusion Eng., 85 (2010), pp. 93-108.

Chapter-7

Future Work and Promising Achievements

7-Future Work and promising achievements

7-1-Introduction

This chapter is previewing the future work related to the investigation of the hybrid components of W-SiC/SiC, where five tiles of W-SiC/SiC were fabricated and were mounted inside the first wall of LHD, where the location of the tiles fabricated inside LHD not subjected to a high heat flux, but were subjected to plasma exposure with lower heat flux. The purpose of this study will investigate the environmental impact of the subjected tiles, due to the plasma contamination absorption on the surface of tungsten armor and the effect of irradiation for long time on the bonding region between W and SiC/SiC.

Also in this chapter; the fabrication of tungsten mono block with actively cooled tube of SiC/SiC will be showed, where the future work will subject the fabricated monoblock with actively cooled tube; to more high heat flux inside the electron beam test facility at the JAEA Electron Beam Irradiation Stand (JEBIS). The designed maximum heat flux inside JEBIS is up to 30Mw/m^2 .

7-2-First wall exposure test inside LHD

Five tiles of hybrid component W-SiC/SiC were fabricated, with dimension of $20 \times 10 \times 1 \text{ mm}^3$ (**Fig.7.1**), subsequently these tiles were mounted inside the first wall of LHD at different positions (**Fig.7.2**),(**Fig.7.3**) and subjected to total 5134 plasma shots, where the energy distribution of charge exchange (CX) neutral particles on the first wall in LHD was calculated at different ion density of plasma, **Fig.7.4** showing the energy distribution of charge exchange at different ion densities. The samples were taken ID related to their positions inside first wall, where the samples ID as follows: (1B, 2B, 2C, 1A, 2A).

①10×20×1.0mm
SiC側を研削して最終厚さを1.0mmに調整

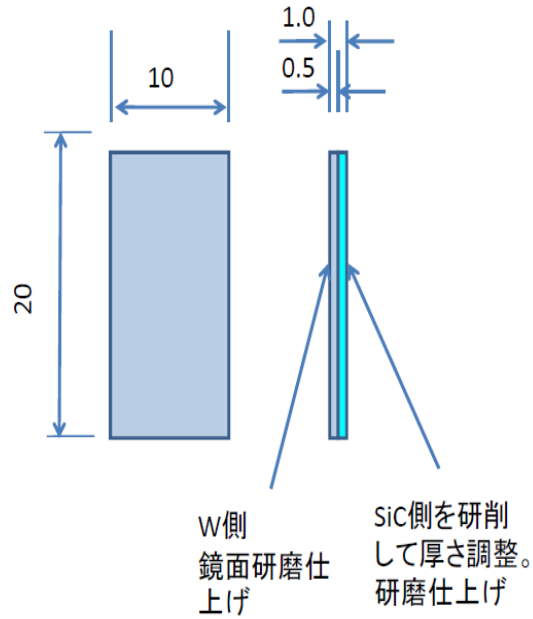


Fig.7.1.The dimension of the W-SiC/SiC tiles inside the first wall of

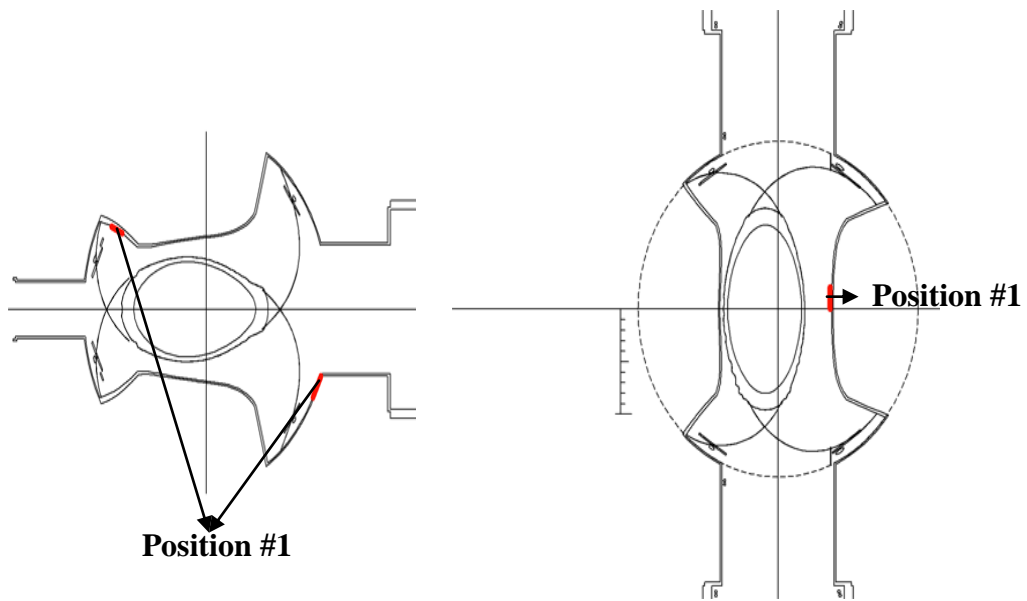


Fig.7.2.Schematic view of the positions of samples inside first wall of

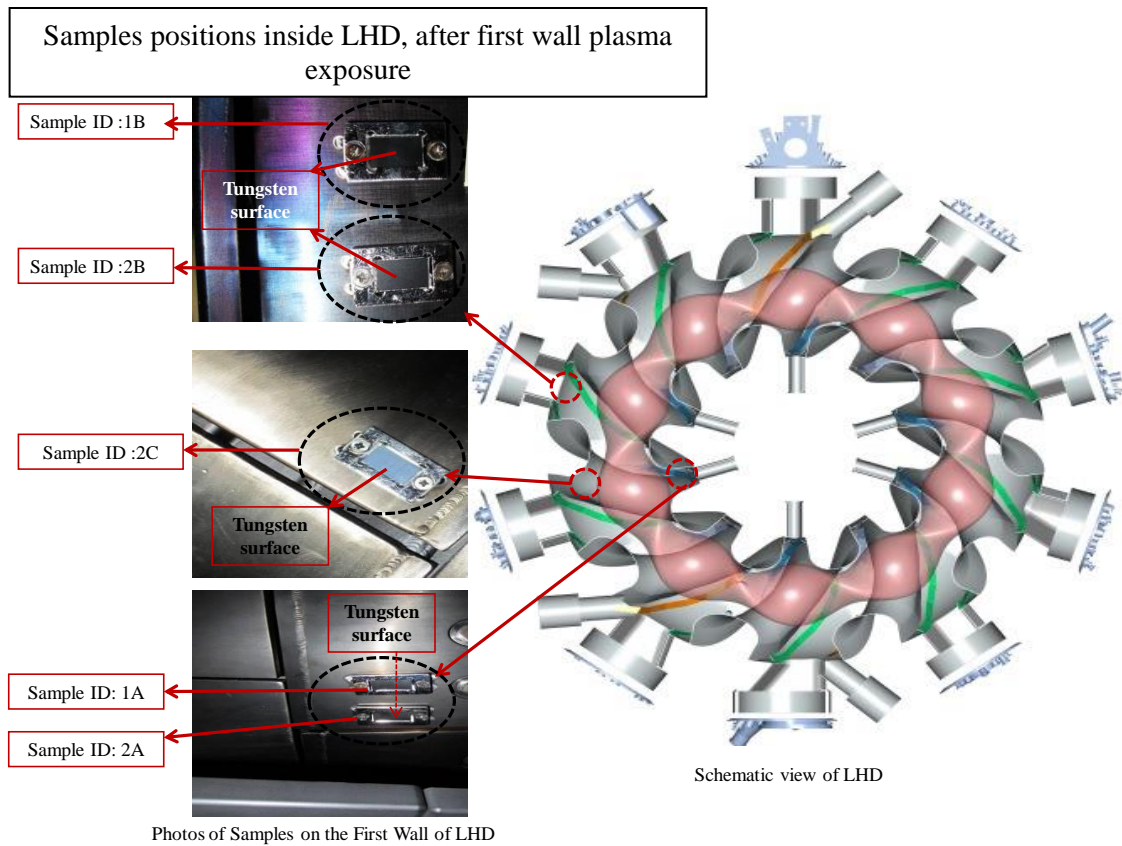


Fig.7.3.Schematic view of the sample inside first wall of LHD

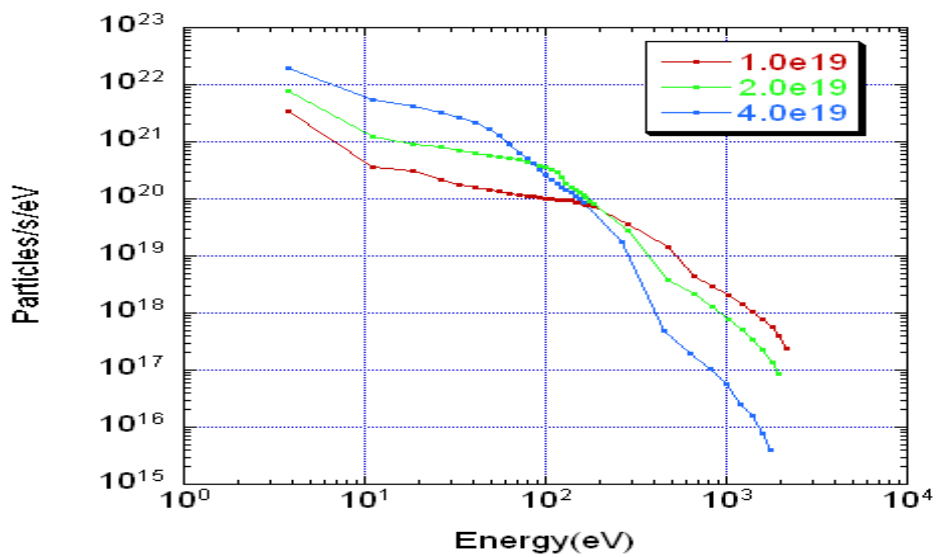


Fig.7.4.The energy distribution of charge exchange (CX) neutral particles on the first wall in LHD

7-2-1-Future investigation of plasma surface interaction

Reliable analysis of plasma-facing materials (PFMs) is indispensable to understand plasma-surface interactions (PSIs). Glow-discharge optical emission spectroscopy (GDOES) is a technique to measure depth profiles of constituent elements in a solid sample by detecting emissions from atoms accommodated in plasma by sputtering. The benefits of this technique are: [1-6].

- (1) PFMs used in fusion devices can be analyzed without modification (no ultra-high vacuum, large sample is acceptable),
- (2) High depth resolution (a few nanometers)
- (3) Very quick measurements (several minutes)

In PSI studies, we need to measure depth profiles of H, D, T and He. In the present study, the abilities of GDOES for isotopic measurements of hydrogen and detection of He have been examined. Schematic view of the GDOES is showing in the Fig.7.5.

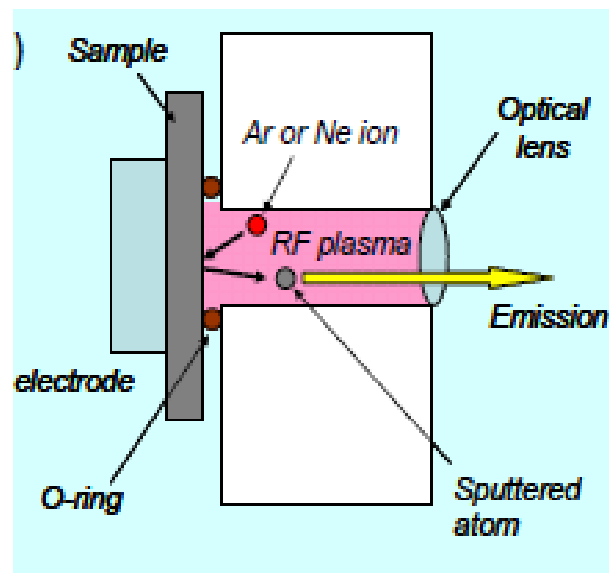


Fig.7.5.Schematic view of the GDOES.

7-3-Tungsten monoblock with actively cooled SiC/SiC tube.

Tungsten monoblock with actively cooled tube of SiC/SiC (**Fig.7.6**) was fabricated, where the bonding between SiC/SiC tube and inner surface of the hole in tungsten monoblock was accomplished by ceramic adhesive materials, then the SiC/SiC tube was attached with cooper tube to the SiC/SiC tube. It has been planning that the actual design of tungsten monoblock divertor system will be exposed to heat flux up to 30 Mw/m^2 inside JEBIS. Before the test inside the JAEA Electron Beam Irradiation Stand (JEBIS),hydraulic and thermal conductivity tests was conducted, but unfortunately the bonding between W and SiC/SiC was very poor and the thermal conductivity between tungsten and SiC/SiC tube was not convenient. Tungsten monoblock mockup is illustrating in **Fig.7.7**.

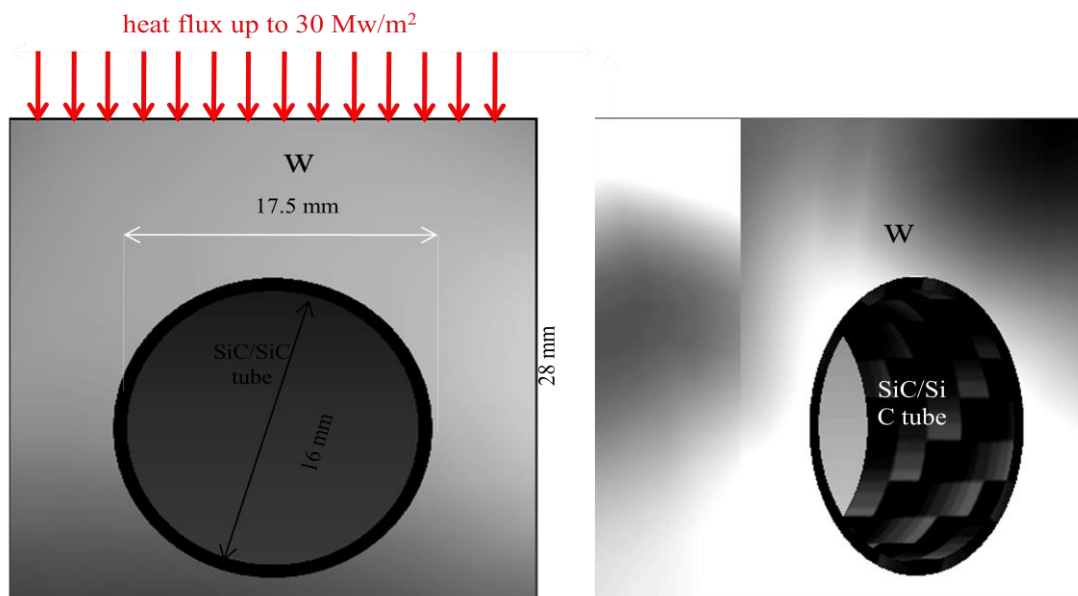


Fig.7.6. Schematic view of Tungsten monoblock with actively cooled tube of SiC/SiC



Fig.7.7. Schematic view of Tungsten monoblock mockup with actively cooled tube of SiC/SiC and cooper cooling tube

7-3-1 Challenges of fabrication technology for actively cooled mockup.

The test of the actively cooled tungsten monoblock before JEBIS test, illustrated that the bonding technology between W and SiC/SiC actively cooled needs modification, and direct contact between tungsten and SiC/SiC must be accomplished as the same in the case of fabrication of NITE W-SiC/SiC, where the direct contact in the case of 3D components needs modification of the hot press technology which is being modified inside Muroran institute of technology at FEEMA project, where hot isostatic press(HIP) is strongly recommended to achieve the soiled state diffusion bonding of this 3D components.

References.

- [1] R.Payling, An overview of GD-OES, in: R.Payling, D. Jones, A.Bengtson (Eds.), Glow Discharge Optical Emission Spectroscopy, John Wiley & Sons, Chichester,1997, pp. 20–47.
- [2] C.W.Magee, E.M.Botnick, Hydrogen depth profiling using SIMS – problems and their solutions, J. Vac. Sci. Technol. 19 (1981) 47–52
- [3] E.Markina, M. Mayer, H.T. Lee, Measurement of He and H depth profiles in tungsten using ERDA with medium heavy ion beams, Nucl.Instrum.Methods Phys. Res. B 269 (2011) 3094–3097.
- [4] W.Wang, M.Kobayashi, R.Kurata, S.Suzuki, N.Ashikawa, A.Sagara, et al., Temperature dependence of retention of energetic deuterium and carbon simultaneously implanted into tungsten, J. Nucl.Mater. 417 (2011) 555–558.
- [5] K.Watatsuma, Optical emission in the glow discharge source, in: R.Payling, D. Jones, A.Bengtson (Eds.), Glow Discharge Optical Emission Spectroscopy, John Wiley & Sons, Chichester, 1997, pp. 348–435.
- [6] T.Nelis, R.Payling, Glow Discharge Optical Emission Spectroscopy: A Practical Guide RSC Analytical Spectroscopy Series, Royal Society of Chemistry, Cambridge, 2004, p. 197.

Chapter-8

Summary

8-Summary

Based on the large scale production capability of NITE-SiC/SiC products at OASIS, Muroran Institute of Technology; the results from the 1st LHD divertor plasma exposure test, about 10MW/m² with 6 sec. shot. The first divertor plasma exposure test inside LHD was successfully accomplished, where the plasma control facilities and the plasma heating ancillaries succeeded to expose the test tiles to the required heat flux where the tentatively estimation of the plasma exposure was 10 Mw/m² as average heat flux. The mounting of the test sample at the location inside LHD was key parameter to expose to such estimated heat flux. Although there was not actively cooled conditions of the exposed tiles during the divertor plasma exposure test; the preliminary investigation of the picked up tiles of hybrid component of W/SiC/SiC showed that the tiles survived from the catastrophic damage i.e. there was not complete melting of the tungsten surface, and there was not a complete debonding along the circumference of the exposed tiles at the interface.

Damage analysis of dual layers tiles of Tungsten and SiC/SiC after plasma exposure inside LHD by means of Ultra sonic methods showed reliable and clear evaluation of bonding layer at the interface between tungsten and SiC/SiC, where two types of presentation data showed and evaluated the diffusion bonding layer, by C-scanning images, B-scanning images, where C-scanning showed partial and complete bonding interface beside the thick and integral bonding interface ,such variant in the diffusion bonding interface is due to the variable temperature distribution inside the reactor ,thus we could speculate the temperature distribution on the surface of each tile by referring to the temperature of diffusion bonding of fabrication, B-Scanning images gave a reliable view about the profile of each interface of each tile. Ultra sonic method can be used as quality control method to evaluate the tiles inside the reactor in the future during the operation with sufficient degree of reliability.

Macro and micro structure investigation, due to the divertor plasma exposure test to 10 MW/m², showed that the fabricated tiles of the hybrid component of W-SiC/SiC survived from the catastrophic damage, i.e. there was not completely debonding between Tungsten and SiC/SiC around the tile thickness, the macro and micro structure analysis showed that the degradation of tungsten surface was only tiny scratches due to arc traces of plasma strike and neutron irradiation, beside the fused protrusion of tungsten on the edge of the tiles (NITE-W/SiC-S2), (NITE-W/SiC-Dh1) which it is evidence that the surface temperature exceeded the limit of melting point of the tungsten, i.e. it was greater than 3400 °C.

Micro structure analysis of the interface between tungsten and SiC/SiC showed that there were debonding regions and segregation zones between W and SiC/SiC, due to implanted temperature, which was investigated to be greater than the recrystallization temperature of Tungsten i.e. greater than 1300° C, where the temperature was investigated to be not less than 1600 °c. EPMA analysis showed that the behavior of silicon diffusion from SiC/SiC side to tungsten, was changed, due to 10 MW/m² heat flux exposure.

The advantages of NITE-W-SiC/SiC divertor system are supported by the macro- and micro- structural control through NITE process, where single and two-step NITE processes have been applied. W-SiC/SiC hybrid component for divertor systems will bring further attractiveness of Fusion Power Energy under realistic domestic R & D scenario.

Due to the investigation of the heat flux durability of the hybrid components of W/SiC/SiC, it is strongly recommending to increase the W armor thickness to be not less than 1mm to be able to decrease the implanted temperate to the interphase region.

List of Publications the Scientific Conferences.

List of Publications

Three published articles were released from this work, the list as follows:

- Waleed.A.Mohrez, Hirotatsu. Kishimoto, Yutaka Kohno, S. Hirotaki, Akira Kohyama, **Behavior of W-SiC/SiC Dual Layer Tiles under LHD Plasma Exposure**, international journal of nuclear materials, 2013 .(available online at: <http://www.sciencedirect.com/>)
- Waleed.A.Mohrez, Hirotatsu. Kishimoto, Yutaka Kohno, S. Hirotaki, Akira Kohyama, **Effect of 10 MW/m² plasma exposure on W-SiC/SiC dual layer tiles**, international journal of fusion engineering and design, 2013(available on line at: <http://www.sciencedirect.com/>)
- W. A. Mohrez, Hirotatsu Kishimoto, Akira kohyama, Yutaka Kohno “**Damage Analysis of Plasma Exposed W-SiC/SiC HHFC Materials By Means of Ultra Sonic Testing Method**”, Al-Azhar University Engineering Journal, ISSN (1110-6409), Vol 7, No2, December 2012

Scientific Conferences

- 1- Alazhar Engineering International Conference (AEIC 2012), 25-27 December 2012, Cairo, Egypt, verbal presentation of the theme:” **Damage Analysis of Plasma Exposed W-SiC/SiC HHFC Materials By Means of Ultra Sonic Testing Method**”.
- 2- International conference of nuclear materials (NuMat2012), 22-25 October 2012, Osaka, Japan, poster presentation of a theme: “**Behavior of W-SiC/SiC Dual Layer Tiles under LHD Plasma Exposure**”.
- 3- International symposium of fusion technology (SOFT27th), 24-28 September 2012, Liege, Belgium, poster presentation of a theme title: “**Effect of 10MW/m² Plasma Exposure on W-SiC/SiC Dual Layer Tiles**”.